Louisiana State University
LSU Digital Commons

LSU Historical Dissertations and Theses | Graduate School

1967

Lateral and Angular Structure of Electromagnetic Cascades.

William Vernon Jones
Louisiana State University and Agricultural & Mechanical College

Follow this and additional works at: https://digitalcommons.lsu.edu/gradschool_disstheses

Recommended Citation
Jones, William Vernon, "Lateral and Angular Structure of Electromagnetic Cascades." (1967). *LSU Historical Dissertations and Theses*. 1254.
https://digitalcommons.lsu.edu/gradschool_disstheses/1254

This Dissertation is brought to you for free and open access by the Graduate School at LSU Digital Commons. It has been accepted for inclusion in LSU Historical Dissertations and Theses by an authorized administrator of LSU Digital Commons. For more information, please contact gradetd@lsu.edu.

This dissertation has been
microfilmed exactly as received 67-8785

JONES, William Vernon, 1935-
LATERAL AND ANGULAR STRUCTURE OF
ELECTROMAGNETIC CASCADES.

Louisiana State University, Ph.D., 1967
Physics, nuclear

University Microfilms, Inc., Ann Arbor, Michigan

LATERAL AND ANGULAR STRUCTURE OF ELECTROMAGNETIC CASCADES

A Dissertation

Submitted to the Graduate Faculty of the
Louisiana State University and
Agricultural and Mechanical College
in partial fulfillment of the
requirements for the degree of
Doctor of Philosophy

in

The Department of Physics and Astronomy

by
William Vernon Jones
B.S., University of Tulsa, 1963
January, 1967

ACKNOWLEDGEMENTS

The author wishes to express his sincere appreciation to Dr. R. W. Huggett for assuming the many obligations of his major professor, for his interest and guidance throughout this course of study and for providing laboratory technicians to assist in performing the experimental measurements. He is deeply indebted to Dr. K. Pinkau for the suggestion of this research project and for his many other suggestions which greatly implemented this work. He is very grateful to Dr. R. Holynski for his advice and assistance during all aspects of the research. He is also grateful to Dr. W. Enge for discussions in the early stage of the work.

The author greatly appreciated the assistance of Dr. B. B. Townsend and his staff of the LSU Computer Research Center and the extended use of their facilities. He would also like to express his thanks to the Institute of Nuclear Research in Crocow, Poland for the use of their emulsion plates.

The author is extremely grateful for the National Defense Education Act Title IV Fellowship which made his graduate studies possible and for financial assistance from the National Science Foundation grant to Dr. Huggett and Dr. Pinkau. He also owes his gratitude for financial assistance received from the Dr. Charles E. Coates Memorial Fund of the LSU Foundation donated by George H. Coates for the preparation of this manuscript.

TABLE OF CONTENTS

LIST OF TABLES

LIST OF FIGURES

ABSTRACT

Simultaneous measurements of the radial position and angular orientation of electrons in ten high energy electromagnetic cascades which were initiated by single γ-rays have been made. Six cascades having energies in the range 845 - 2000 BeV which were developed in a large pure emulsion stack were measured up to the radial distance 2.1×10^{-2} r.l. from the cascade axis. Four cascades which were developed in a lead-emulsion sandwich stack were measured up to the radial distance 7.4×10^{-2} r.l. and these cascades had energies in the range 178 - 720 BeV. Numerical calculations of the angular distributions from cascade theory have been performed within approximation B and within the core approximation. A method has been presented for utilizing the energy determination from the angular distribution to establish the correct effective radiation length of a heavy sandwich stack.

The integral radial and angular distributions which were obtained experimentally have been compared with the predictions of cascade theory under approximation B and the core approximation. No clear deviation of the experimental results from the radial core approximation was found over the range of energies and distances which were measured, but approximation B was found to underestimate

the total number of particles. It was shown that the radial range must extend up to approximately 7×10^{-2} r.l. for the cascades measured in the sandwich stack in order to permit the measurement of all particles having angles even as small as those in the range up to 4-5°. The radial distance 2.1×10^{-2} r.l. measured for the cascades in the pure emulsion stack did not allow the measurement of all particles even at 1-2°. The energy determination using only small angles from the angular distribution of particles in the sandwich stack agreed with the standard method of using the radial distribution. Therefore, it was concluded that the cascade theory is internally consistent under the core approximation and that the "wavelength" of the particular sandwich stack that was used was sufficiently small so that the arrangement could be considered to be a homogeneous mixture of lead and emulsion.

I. INTRODUCTION

Direct measurements of the energy of ultra high energy particles ($\gtrsim 10^{11}$ eV) poses one of the most difficult and most important problems in the field of high energy physics. Bubble chambers, spark chambers and various counter systems can be used for energy determinations with an accuracy of a few percent in the range of accelerator energies (1 - 30 BeV). These techniques can in principle be used for much higher energies by increasing the dimensions of bubble chambers, Cherenkov counters, etc., and/or the strength of electromagnetic fields used in association with these detectors. With the advent of rapidly increasing technology such as that involved with superconducting magnets, it has been or will be possible to make the necessary extension of present techniques so that the energies of ultra high energy particles can be determined. However, the expense involved increases rapidly with the particle energy to be measured.

The energies of ultra high energy particles (electrons and γ-rays) can be measured in a much less expensive manner and with reasonable accuracy via the electromagnetic cascade. There is apparently no upper limit to the energy range over which this method can be used. However, for very high energies, such large particle densities may be encountered that it is necessary to go

to large distances from the cascade axis to distinguish individual particle tracks, or to be in a range of density so that one is able to use a photometric densitometer.[1]

A disadvantage to the electromagnetic cascade method of energy determination is that the energy is not derived from first principles, but instead is derived from the electromagnetic cascade theory. In addition to this, the actual measurement process is somewhat slow and tedious, and the technique is limited to determining the energy of only electrons and γ-rays.

There are many current problems in the field of high energy physics where it is necessary to know as accurately as possible the energy of an electromagnetic cascade. Determinations of the energy of cascades from γ-rays created in π^0 decay are being used to study the transverse momenta of secondary particles in high energy interactions. Since the transverse momentum p_t of a secondary particle is a Lorentz invariant quantity, it is a convenient parameter to use in analysis of individual jet events and in studying the theoretical mechanism of multiple meson production. A determination of p_t obviously necessitates accurate measurements of both the energy and angle of emission of the secondary particle.

Investigations of the dynamics of π^0-meson production in ultra high energy collisions are being done in experiments designed to measure the multiplicities, energies, and angles of individual

---

[1] P. K. Malhotra, P. G. Shukla, S. A. Stephens, B. Vijaylakshmi, J. Boult, M. G. Bowler, P. H. Fowler, H. L. Hackforth, J. Keereetaveep, V. M. Mayes and S. N. Tovey, Nuovo Cimento 40A, 385 (1965).

γ-rays. Such measurements are planned in the mountain experiment which is now under development by LSU in collaboration with the Max Planck Institute.[2] In these measurements, the energy determination of electromagnetic cascades from the γ-rays of π^o decay are essential in the determination of the total energy E_{π^o} going into the γ-rays and therefore for an evaluation of the inelasticity coefficient. Also, knowledge of the cascade energy is necessary for the evaluation of the energy and p_t distributions.

The accurate measurement of the electromagnetic cascade energy in experiments investigating the cosmic ray primary energy spectrum is also very important because any experimental bias in the energy determination would affect the slope of the γ-ray spectrum and hence the slope of the primary spectrum. The γ-ray spectrum has been a controversial issue for several years. Apart from a general discrepancy in the slope, some of the experimental evidence[3] indicates that the spectrum steepens around energies of 10^{12} eV. Other investigations[4] indicate there may be more than one change of slope of the spectrum, or perhaps the true spectrum may indeed be curved.

---

[2]Supported by the National Science Foundation. The principal investigators are R. W. Huggett, Louisiana State University and K. Pinkau, Max Planck Institute and consulting professor for Louisiana State University.

[3]J. Duthie, P. H. Fowler, A. Kaddoura, D. H. Perkins, and K. Pinkau, Nuovo Cimento 24, 122 (1962).

[4]M. Akashi, Z. Watanabe, A. Misaki, I. Mito, Y. Oyama, S. Tokunaga, T. Ogata, Y. Tsuneoka, S. Dake, K. Yokoi, S. Hasegawa, J. Nishimura, K. Niu, T. Taira, A. Nishio, Y. Fujimoto, and N. Ogita, Suppl. Progr. Theoret. Phys. (Kyoto) 32, 1 (1964).

Such changes of the spectrum if real imply changes in the nature of the interactions or are related to the composition and energy spectrum of the primary radiation. The latter interpretation is presently the most favored one. In any case, the spectrum itself needs to be well established.

The above examples are just a few of many cases where it is necessary to know the primary energy of electromagnetic cascades. They are given to show the necessity of being able to measure this energy with the highest possible accuracy.

Prior to the development of the three-dimensional cascade theory,[5] the energies of electromagnetic cascades were estimated by performing multiple scattering measurements on individual cascade electrons and comparing the results with approximation A in the one-dimensional cascade theory.[6] Such individual scattering measurements are not practical for extremely high energy cascades which often contain several hundred particles. Even for relatively low energy cascades, scattering measurements are very tedious and sometimes impossible because of the dip angle of the cascade or distortion of the emulsion.

Recent high energy cascade measurements have relied only upon the comparison of experimental results with the theoretical calculations of the integral radial distribution from the

---

[5] K. Kamata and J. Nishimura, Suppl. Progr. Theoret. Phys. (Kyoto) 6, 93 (1958).

[6] See Chap. II. for a discussion of the various approximations used in the cascade theory.

three-dimensional cascade theory. The theoretical calculations[7] utilized an approximation which required that the radius R be small compared to unity when expressed in units of the radiation length (r.l.). This is called the "core approximation" since it is valid only near the core of the cascade.

The results of the three-dimensional cascade theory, as described in Chap. II, show that within the limitation of the core approximation ($R \ll 1$) the number of particles within a distance R of the cascade axis is a function only of the product E_0R. Therefore, an attempt was made to obtain sufficient information about E_0, the primary energy of the cascade, merely by determining the radial distribution of the cascade electrons at given distances from the origin.[8] This first attempt compared the cascade energy predicted by the three-dimensional theory with the energy obtained from scattering measurements on the individual cascade electrons. The attempt was successful in showing that the shape of the theoretical distribution was correct, but there was a discrepancy in the predicted number of particles. This discrepancy was attributed to the inadequacy of the Landau approximation used in obtaining the theoretical curves.[9]

---

[7] J. Nishimura and J. Kidd, Suppl. Nuovo Cimento 1, 1039 Appendix II (1964).

[8] K. Pinkau, Phil. Mag. 2, 1389 (1957).

[9] K. Kamata and J. Nishimura, Suppl. Progr. Theoret. Phys. (Kyoto) 6, 93 (1958).

A later attempt to check experimentally the accuracy of the three-dimensional cascade theory was reported by the Japanese collaboration.[10] Measured in this collaboration was the distance between the two cores of three double-core cascades, each of which could be interpreted as the result of a single π^o-meson decay. Thus, it was possible to obtain the angle of divergence of the two γ-rays for the three individual π^o-meson decays. Then the core approximation curves were used to determine the energy of each γ-ray. Using this energy determination and the kinematics of π^o-decay, it was possible to calculate the expected value for the opening angle of the γ-rays. A comparison of the measured values of the opening angles with the calculated values showed good agreement and indicated that there was no systematic error in the cascade function over the range of energies and distances which were investigated. The energies of the individual γ-rays for the three double-core cascades used in checking the theoretical distributions ranged from 50 to 300 BeV. Also, it appears from the published data that cascade particles were counted within a distance of about 7×10^{-3} r.l. from the cascade axis.

Another check of the core approximation was reported by the emulsion group at the University of Bristol.[11] This group made a

---

[10] O. Minakawa, Y. Nishimura, M. Tsuzuki, H. Yamanouchi, Y. Fujimoto, S. Hasegawa, J. Nishimura and K. Niu, Suppl. Nuovo Cimento 11, 125 (1959).

[11] P. H. Fowler, D. H. Perkins and K. Pinkau, Proceedings of the Moscow Cosmic Ray Conference, Moscow, 1960, edited by V. I. Zatsepin and B. A. Khrenov, Vol. 2, p. 302.

comparison of experimental results with the core approximation curves after determining the cascade energy by individual scattering measurements on the cascade electrons. They also made two independent estimates of the cascade energy from the kinematics of π^0-decay. Good agreement was found over their range of measurements which were made up to a distance of about 10^{-2} r.l. from the cascade axis for energies in the range 130 - 1100 BeV.

In summary, experimental evidence seems to support the use of the core approximation up to distances of $\sim 10^{-2}$ r.l. from the cascade axis over the energy range 10^{11} - 10^{12} eV. However, as discussed in detail in Sec. II.3, this radial distance is just the point where the core approximation is theoretically predicted to begin to deviate from the true electron distribution.

One of the main objectives of this experiment is to find the experimental radial distribution of cascade particles up to a significantly greater distance from the axis than has previously been reported in order to check the core approximation. It should be emphasized that in obtaining the experimental distributions up to the larger distances, the core approximation is accepted as being valid up to its proven range of validity (10^{-2} r.l.), and this range is used to determine the primary energy of a cascade. Any deviation from the core approximation can then be found by comparing the experimental distribution $N(<R)$ vs E_0R up to the maximum distances of R which are measured with the theoretical curves predicted by the core approximation.

The experimental <u>angular</u> distribution of the particles in ultra high energy electromagnetic cascades have not previously

been measured. However, in this experiment, the radial position and angular orientation of the cascade particles are measured simultaneously. Because of the relation between the radial and angular coordinates, it is possible in principle to check any deviation of the experimental radial distribution from the core approximation curves by using the angular distribution. This could be accomplished by finding the angle where the experimental angular distribution deviates from the theoretical angular distribution in the core approximation and then determining an effective radius for the angle where the deviation occurs. Since fairly large values of R correspond to relatively small angles θ, the angular distribution may actually show a more pronounced deviation from the core approximation than the radial distribution.

The angular distribution is distinct from the radial distribution in that it is insensitive to the particular geometrical arrangement of the cascade producing material. If, for example, the cascade producing material is arranged in layers, the angular distribution of the cascade particles at any point will depend only on the distance from the cascade origin expressed in radiation lengths. However, the radial distribution which is a result of the scattering process and diffusion under the angle attained in the scattering process is dependent on the arrangement of the absorber. This is clear because the particles will diffuse outward in any less dense material or space between the producing layers.

Most detectors[12] employed in investigations involving measurements of high energy electromagnetic cascades have consisted of alternate layers of lead or tungsten and nuclear emulsion. Such stacks are called "sandwich stacks". The question has remained open whether the "wavelength" of the arrangements were sufficiently small compared to the radiation length so that the absorber could be treated as a homogeneous medium. Obviously, a comparison of the angular distribution (which is not dependent on the arrangement) and the radial distribution (which is dependent on the arrangement) with each other and with the corresponding theories should reveal any inconsistencies.

In complete analogy to energy determinations from the radial distribution, the primary energy E_o of an electromagnetic cascade can be determined from its angular distribution. The theoretical angular distributions $N(< \theta)$ vs $E_o\theta$ are presented in Appendix III for several distances from the cascade origin. The value of E_o can be obtained by comparing the experimental distribution $N(< \theta)$ vs θ with the theoretical distribution $N(< \theta)$ vs $E_o\theta$ in exactly the same manner as is described for the radial distribution in Sec. IV.1. By using the value of E_o obtained from the angular distribution, the effective radiation length of a sandwich stack having any particular geometrical arrangement can then be found by fitting the theoretical distribution $N(< R)$ vs E_oR, where R is expressed in radiation lengths, to the experimental distribu-

---

[12] See, for example, Refs. 1, 3, and 4.

tion $N(< R)$ vs R with R expressed in microns. Since E_o is known from the angular distribution, the number of microns per radiation length can be determined.

Another problem closely related to the validity of cascade theory at high energies, and therefore to the interpretation of cosmic ray data up to the highest energies in the extensive air shower region, is the transition of the cascade distribution curves from the region of validity of the core approximation to the region of predicted validity of approximation B.[13] Theoretically, at large R, the shape of the distribution predicted by approximation B should be independent of primary energy and should yield information on the total number of particles at any depth. Determination of the angular and radial distributions at large distances from the cascade axis would therefore be a check on the validity of approximation B.

From the considerations given above, it appears to be of great importance to measure the positions and angles of electrons in high energy electromagnetic cascades which are observed in pure emulsion blocks and in lead-emulsion sandwich stacks that have been exposed to the cosmic radiation.

At the present time Louisiana State University has acquired about 40% (32 liters) of the original 80 liters of the Brawley

---

[13] See Chap. 11 for a discussion of the cascade theory under approximation B.

pure emulsion stack.[14] This stack consisted of 500 sheets of Ilford K-5 nuclear emulsion, each having the dimensions 45 x 60 x 0.06 cm. This stack was launched from Brawley, California in 1961 and was recovered after having flown approximately thirty hours.

In addition to the pure emulsion from the Brawley stack, several emulsion plates have been borrowed from the Institute of Nuclear Research in Cracow, Poland. These plates are part of the SSS lead-emulsion sandwich stack[15] which was irradiated in Italy in 1961. This stack consisted of 140 Ilford G-5 nuclear emulsion plates each having dimensions 25 x 25 x 0.06 cm and 70 lead plates each 2 mm in thickness. The stack was constructed so that two emulsion plates were placed between adjacent lead plates. The radiation length of the stack was calculated to be 8.1 mm by assuming a homogeneous mixture of lead and emulsion. The SSS stack was irradiated for only about five hours. Therefore, the number of background tracks is considerably less in the SSS stack than in the Brawley stack. This is an important advantage when measurements are made far from the cascade axis where the ratio of the background tracks to cascade tracks may be relatively high.

---

[14] F. Abraham, J. Gierula, R. Levi Setti, K. Rybicki, C. H. Tsao, W. Wolter, R. L. Fricken and R. W. Huggett, "Multiple Meson Production by Heavy Nuclei of Cosmic Origin and Their Fragmentation Products at Energies Above 10^{12} eV." (To be published in Phys. Rev.)

[15] J. Babecki, R. Holynski, S. Krzywdzinski, A. Peeva, K. Rybicki and W. Wolter, Nukleonika 9, 271 (1964).

The radial and angular distributions of six electromagnetic cascades from the Brawley stack having energies in the range 845 - 2000 BeV have been measured. The same distributions were measured for four cascades from the SSS stack in the energy range 178 - 720 BeV. These measurements permitted a check of the core approximation up to distances seven times larger than previously reported. Also, approximation B could be checked up to the maximum distances measured. The simultaneous measurement of radii and angles of the cascade particles provided a check on the internal consistency of the cascade theory within the core approximation and gave the possibility for establishing the effective radiation length for the lead-emulsion sandwich stack.

II. THEORETICAL SUMMARY

1. The Physical Processes Involved in the Development of an Electromagnetic Cascade

When a high energy electron passes through matter, most of its energy is spent in the radiation of high energy photons. These secondary photons either undergo materialization into electron-positron pairs or Compton collisions which in turn produce electrons with energies comparable to that of the photon. These new electrons radiate more photons which again materialize or produce Compton electrons. At every new step the number of particles increase and their average energy decreases. As the process goes on, an increasing number of particles fall below the limiting energy where the collision losses become important until eventually the energy of the primary electron is completely dissipated.

The phenomena qualitatively outlined above is called a "cascade shower," or more specifically an "electromagnetic cascade." Obviously, an electromagnetic cascade can be initiated by a high energy photon as well as a high energy electron.

The physical processes which are involved in the development and eventual dissipation of an electromagnetic cascade are the radiation and collision processes of the electrons and the interaction processes of photons with matter. The latter processes include pair production, Compton scattering, and the photoelectric effect.

Most of the energy lost by electrons undergoing collisions while traversing matter is spent in exciting atoms or ejecting electrons of small energy from the atoms and is thus considered as dissipated. However, the energy lost by radiation is fairly uniformly distributed among secondary photons of all energies from nearly zero up to the energy of the primary particle. The fractional energy loss per radiation length, $-\frac{1}{U}(\frac{dE}{dt})$, is plotted as a function of the instantaneous total energy U of the electron in Fig. 1. The figure compares the loss due to collision and radiation for the two absorbers air and lead. It is seen from the curves that only the radiation loss is important for energies above $\sim 10^9$ eV in the case of air and $\sim 10^8$ eV in the case of lead.

In discussing the interactions of high energy photons with matter, the photoelectric effect can be omitted since this process becomes less frequent with increasing photon energy and is almost non-existent at cosmic ray energies. Thus, the only important interactions of the photons in discussing electromagnetic cascades are Compton scattering and pair production.

Shown in Fig. 2 is the total probability per radiation length for Compton scattering (μ_{Com}) and for pair production (μ_{pair}) as a function of the energy E of the photon for two absorbers, air and lead. The figures show that only the pair production process is of importance for energies above $\sim 10^9$ eV in the case of air and $\sim 10^8$ eV in the case of lead.

From the above discussion it is seen that the physical phenomena mainly responsible for the development of high energy electromagnetic cascades ($> 10^{11}$eV) are the radiation and pair production processes

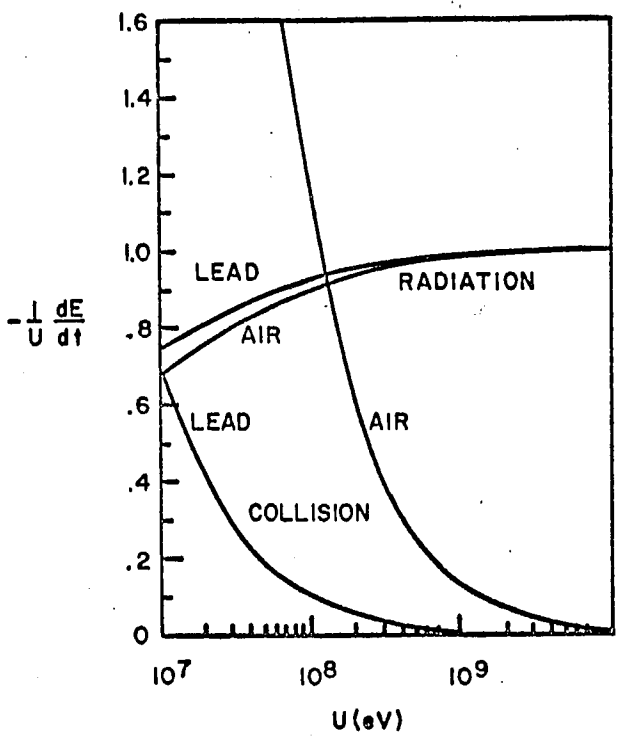

Fig. 1. Fractional energy loss per radiation length for electrons, $-\frac{1}{U}\frac{dE}{dt}$, caused by collision and radiation. The curves are given for two absorbers, air and lead. From B. Rossi, High Energy Particles (Prentice-Hall, Inc., Englewood Cliffs, N.J., 1952) p. 52.

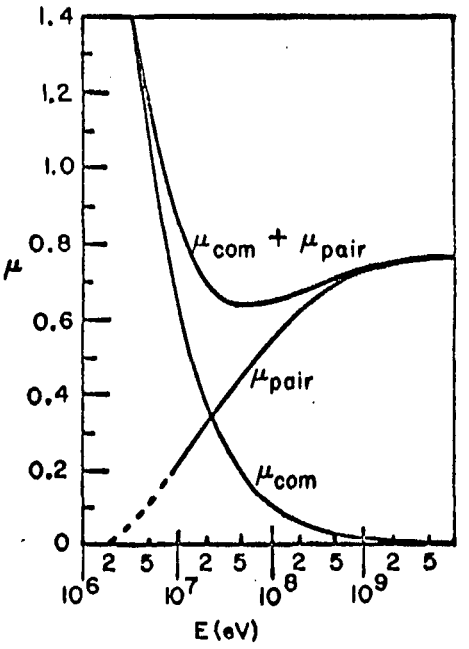

(a)

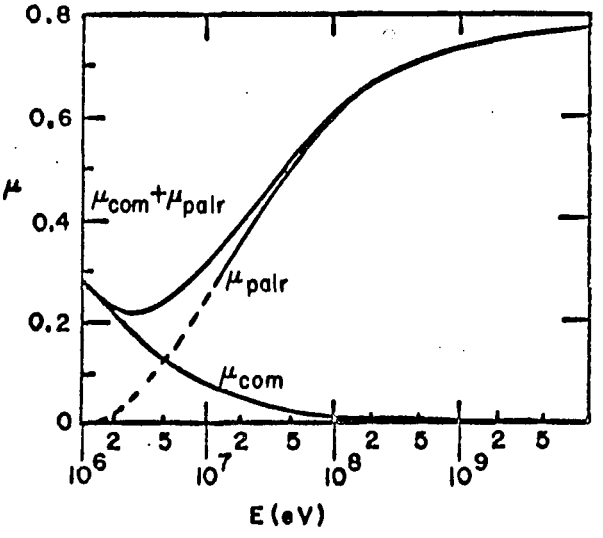

(b)

Fig. 2. The total probability per radiation length for Compton scattering (μ_{com}), for pair production (μ_{pair}), and for either effect ($\mu_{com} + \mu_{pair}$). Part "a" is for air and part "b" is for lead. From Rossi, High Energy Particles (Prentice-Hall, Inc., Englewood Cliffs, N.J., 1952) p. 84.

in the electric field of the nuclei of the absorber. Consequently, cascade theory derived by considering only these processes is satisfactory in the solution of many problems. The other processes must be considered if the theory is to extend to the energy range where radiation and pair production processes are no longer the most important ones.

2. Summary of the Development of Cascade Theory

Under the assumption that the ordinary laws of quantum electrodynamics can be extrapolated to cosmic ray energies, a quantitative theory of the electromagnetic interactions of cosmic rays with matter has been developed.[16] The results have proven to be extremely useful in the explanation of some very complex cosmic ray phenomena. In particular, the theory of the electromagnetic cascade has been developed to the point where most of its fundamental features are quite well known.

In the early days of shower theory the problem was considered as one-dimensional in the respect that the longitudinal development and lateral spread of showers were treated as two separate problems. More specifically, the dependence of the functions describing the shower on the thickness t of the matter traversed was first determined by neglecting the path increase due to the angular spread of the shower particles. The lateral spread around the axis and the angular distribution of the shower particles were then investigated

---

[16] This theory is a result of the combined efforts of many workers in the field. For complete references and a comprehensive survey see B. Rossi and K. Greisen, Rev. Mod. Phys. 13, 240 (1941).

by making use of the information obtained from the solution of the longitudinal development. This separation is justified only if attention is restricted to the behavior of high energy particles where the angles of emission of secondary electrons and photons are small and also where the scattering of the electrons is negligible.

Since the phenomena mainly responsible for the generation of showers are radiation processes and pair production, it is convenient in cascade theory to measure thickness in "radiation lengths". This unit of length for a given medium is equal to the mean distance through which an electron must pass for its energy to be reduced by the radiation process to 1/e of its original value. The radiation length X_o for a given material is defined by the equation

$$\frac{1}{X_o} = 4\alpha\frac{N}{A} Z^2 r_e^2 \ln(183Z^{-\frac{1}{3}}) \quad . \qquad (11.2.1)$$

This unit of length contains the material characteristics of a given absorber. Therefore, when expressed in radiation lengths, the theoretical expressions for the probabilities of radiation and pair production are practically independent of atomic number in the limit of high energies. The symbols used in the definition of X_o are the usual ones. That is, N is Avogadro's number, A is the mass number, Z is the atomic number, α is the fine structure constant ($\alpha = 1/137$), and r_e is the classical radius of the electron. The above expression for X_o has been calculated by considering only the effect of the electric field of nuclei and disregarding the electric fields of atomic electrons. The effect of the electrons can be included by simply changing Z^2 into $Z^2 + Z = Z(Z+1)$ in the definition of X_o.

Most of the results of cascade theory refer to the average behavior of the showers. One usually wants to know the average number of electrons (or photons) with energy greater than E that emerge from a layer of absorber with thickness t. The "fluctuation" problem[17] is concerned with estimating the probability of a given deviation from this average behavior. Even the discussion of the average behavior of a shower represents a difficult mathematical problem, and consequently the solutions are invariably given under specified approximations.

In cascade theory "approximation B" is the standard approximation. In this approximation the Compton effect is neglected, the rate of energy loss by collision is taken to be a constant, and the asymptotic formulas of complete screening for radiation and pair production are used. The constant ϵ is called the critical energy. An electron having energy ϵ is brought to rest as a result of collision losses in one radiation length. The special case of approximation B when collision energy loss is neglected is known as "approximation A."

The emission of photons by electrons is connected with the deflection of their trajectories in the electric field of nuclei. The distance from the nucleus at which radiation phenomena occur plays an essential role in the development of the theory. It turns out[18] that the radiation processes of electrons take place at distances from the nucleus that are large compared with the nuclear radius, and thus the nucleus can be considered as a point charge.

---

[17] L. Janossy and H. Messel, Proc. Phys. Soc. (London) A 63, 1101 (1959).

[18] B. Rossi, High Energy Particles, (Prentice-Hall, Inc., Englewood Cliffs, N.J., 1952), Chap. 5, p. 214.

However, the screening effect of the outer electrons is often important. This effect has been calculated,[19] and the theory indicates that the influence of screening on a radiation process in which an electron having kinetic energy E produces a photon with energy E' is determined by the quantity

$$\gamma_r = 100 \frac{mc^2}{E+mc^2} \frac{v}{1-v} Z^{-\frac{1}{3}} \quad , \qquad (II.2.2)$$

where v is the ratio $E'/(E+mc^2)$ and m is the rest mass of the electron. The screening is greater for smaller values of γ_r. For $\gamma_r \gg 1$ screening can be neglected. The term "complete screening" is used for the case $\gamma_r \to 0$. If the primary electron energy E is large enough, screening may be considered as complete for all energies of the emitted photons.

The influence of screening in the pair production process in which a photon of energy E materializes into an electron and positron with the positron having kinetic energy E' is determined by the quantity

$$\gamma_p = 100 \frac{mc^2}{E} \frac{1}{v(1-v)} Z^{-\frac{1}{3}} \quad , \qquad (II.2.3)$$

where $v = \frac{E' + mc^2}{E}$ is the fractional energy of the positron. Again, the case where $\gamma_p \to 0$ is referred to as "complete screening" and for large energies of the primary photon the screening may be considered as complete.

---

[19] H. A. Bethe and W. Heitler, Proc. Roy. Soc. A146, 83 (1934).

By considering the various production and absorption phenomena that take place in an infinitesimal layer dt of the absorber, one may obtain a set of equations, known as the diffusion equations, which describe the variation with thickness in the number of electrons and photons of each energy interval. The derivation[20] of the diffusion equations is outlined below. Attention has been restricted to the high energy region in which the assumptions of approximation B are valid. In the equations, all thicknesses are measured in radiation lengths.

The following notation and definitions are introduced:

(a) Differential electron spectrum, $\pi(E,t)dE$: average number of electrons (positive and negative) at the thickness t with energy between E and E + dE.

(b) Differential photon spectrum, $\gamma(W,t)dW$: average number of photons at the thickness t with energy between W and W + dW.

(c) Integral electron spectrum, $\Pi(E,t)$: average number of electrons with energy larger than E at the thickness t.

$$\Pi(E,t) = \int_E^\infty \pi(E',t)dE' \qquad (11.2.4)$$

(d) Integral photon spectrum, $\Gamma(W,t)$: average number of photons with energy larger than W at the thickness t.

$$\Gamma(W,t) = \int_W^\infty \gamma(W',t)dW' \qquad (11.2.5)$$

In the electron-photon (electromagnetic) cascade, the number of electrons with energy between E and E+dE undergoes a change in a

---

[20] B. Rossi and K. Greisen, Rev. Mod. Phys. 13, 240 (1941).

thickness dt of the absorber because of the following effects:

(a) Photons with energy W larger than E produce electrons (both positive and negative) in the energy range (E,dE). The number produced is

$$dEdt\cdot 2\int_E^\infty \gamma(W,t)\psi(\frac{E}{W})\frac{dW}{W} = dEdt\cdot 2\int_0^1 \gamma(\frac{E}{u},t)\psi(u)\frac{du}{u} \quad , \qquad (II.2.6)$$

where u = E/W. The differential pair creation probability per radiation length for a photon of energy W to produce one electron pair in which the positron has fractional energy between u and u+du is for complete screening

$$\psi'(W,E)dW = \psi(\frac{E}{W})\frac{dW}{W} \quad ,$$

and

$$\psi(u)du = [u^2 + (1-u)^2 - \frac{2}{3} - 2b)u(1-u)]du \quad , \qquad (II.2.7)$$

with $b = \dfrac{1}{18\ \ln(183Z^{-\frac{1}{3}})}$.

(b) The electrons with energy in the interval (E,dE) may leave this interval by radiating part of their energy while electrons with energy E' larger than E may enter the interval by radiation loss. The net change in their number is given by

$$dEdt[-\int_0^E \pi(E,t)\phi(\frac{W}{E})\frac{dW}{E} + \int_E^\infty \pi(E',t)\phi(1-E'/E)\frac{dE'}{E}] = \qquad (II.2.8)$$

$$dEdt\int_0^1[-\pi(E,t) + \frac{1}{1-v}\pi(\frac{E}{1-v})]\phi(v)dv \quad ,$$

where

$$\phi(v)dv = [1 + (1-v)^2 - (1-v)(\frac{2}{3} - 2b)]\frac{dv}{v} \qquad (II.2.9)$$

is the complete screening differential radiation probability per radiation length for an electron of energy E to emit a photon with fractional energy between v and v+dv. Note that in the first integral v = E/W, while in the second integral v = 1 - E/E'.

(c) An electron loses an amount of energy ϵdt in a thickness dt by the collision process. Therefore, as a result of collision, $\pi(E+dE)\epsilon dt$ electrons enter the interval (E,dE) and $\pi(E)\epsilon dt$ electrons leave this interval. The net change in their number is

$$[\pi(E+dE) - \pi(E)]\epsilon dt = \epsilon \frac{\partial \pi}{\partial E} dE dt \quad . \qquad (II.2.10)$$

Similarly, the number of photons with energy between W and W+dW in the thickness dt undergoes changes because of the following effects:

(a) Electrons with energy E larger than W radiate photons in the energy interval (W,dW). This number is

$$dW dt \int_W^\infty \pi(E,t)\phi\left(\frac{W}{E}\right)\frac{dE}{E} = dW dt \int_0^1 \pi\left(\frac{W}{v},t\right)\phi(v)\frac{dv}{v} \quad , \qquad (II.2.11)$$

where $\phi(v)dv$ is as already defined and v = W/E.

(b) Photons initially in the interval (W,dW) are absorbed by pair production. Their number is

$$dW dt \gamma(W,t)\sigma_o \quad ,$$

where σ_o is the total probability per radiation length for pair production as defined by

$$\sigma_o = \int_{m/w}^{1-m/w} \psi(u)du = 7/9 - b/3 \quad . \qquad (II.2.12)$$

Consequently, the diffusion equations which give the variation in the number of electrons and photons, respectively, in an electromagnetic cascade under approximation B are obtained by combining the above effects to give

$$\frac{\partial \pi}{\partial t} = 2\int_0^1 \gamma\left(\frac{E}{u}, t\right)\psi(u)\frac{du}{u} + \tag{II.2.13}$$

$$\int_0^1 \left[\frac{1}{1-v}\pi\left(\frac{E}{1-v}, t\right) - \pi(E,t)\right]\phi(v)dv + \epsilon\frac{\partial \pi}{\partial E}$$

$$\frac{\partial \gamma}{\partial t} = \int_0^1 \pi\left(\frac{W}{v}, t\right)\phi(v)\frac{dv}{v} - \sigma_0\gamma(W,t) \quad . \tag{II.2.14}$$

The diffusion equations under approximation A are immediately obtainable from these by taking $\epsilon = 0$ in the one term where it appears in the expression for $\frac{\partial \pi}{\partial t}$.

It should be noted that the diffusion equations do not explicitly contain any quantity that depends on the properties of the matter in which the shower propagates. This is a direct consequence of expressing distances in radiation lengths. As long as this unit of length is used and energies are measured in terms of the critical energy, the shower theory under approximation B gives exactly the same result for all materials.

It is also noteworthy that the cross sections for radiation and pair production do not depend explicitly on the energy of the particle, but only on the ratio of the energy of the secondary particle to that of the incident particle. Consequently, the integrals are in such form that the Mellin transformation may be used to obtain

the solution of the cascade equations. The problem under approximation A can be solved completely. The inclusion of the collision loss in approximation B merely adds a term to the diffusion equations for approximation A, but this requires that the solution be approximate in that higher order terms are neglected. However, this solution is believed to be good for energies not smaller than about twice the critical energy.

The determination of the energy distribution of electrons and photons having energies small compared with the critical energy constitutes a very difficult mathematical problem. In this low energy region the asymptotic expressions for pair production and radiation probabilities cannot be used, and the Compton effect as well as the production of secondary electrons by collision must be taken into consideration. The result is that the equations become so involved that it is impractical to attempt an analytical solution. Therefore, no general expressions exist for the low energy end of the spectrum and such problems are treated individually by numerical methods.

The results of the one-dimensional cascade theory under approximations A and B for the integral electron spectrum are given in the form of graphs in Figs. 3 and 4, respectively. The expressions for the spectra depend only on the thickness t and the ratio of the initial energy to the energy of the observed shower particles. For a given value of this ratio, the intensity of the spectrum increases at first with increasing t, goes through a maximum and then decreases again.

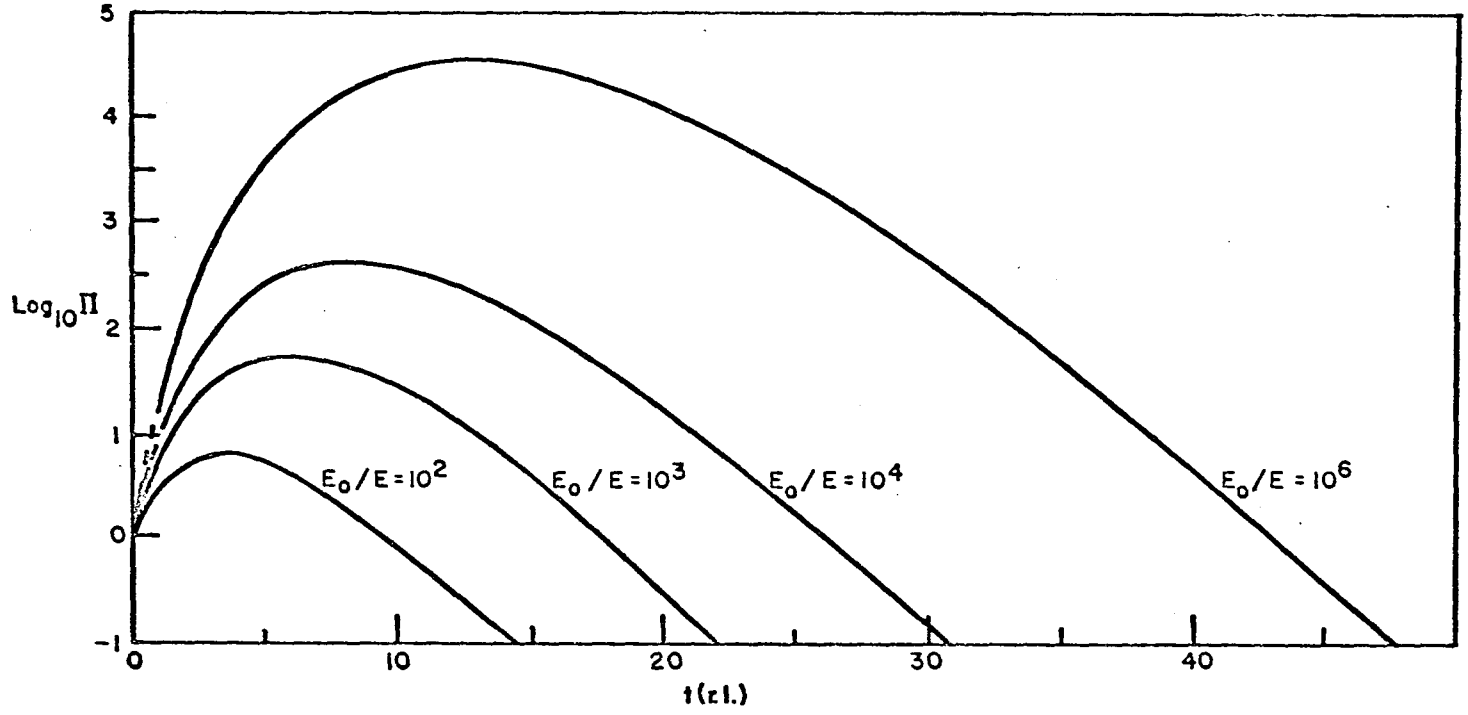

Fig. 3. The total number $\Pi(E_0,E,t)$ of electrons having energy greater than E in a shower initiated by an electron of energy E_0 as a function of the depth t in an absorber. Computed for various values of E_0/E according to approximation A. From B. Rossi, High Energy Particles (Prentice-Hall, Inc., Englewood Cliffs, N.J., 1952) p. 249.

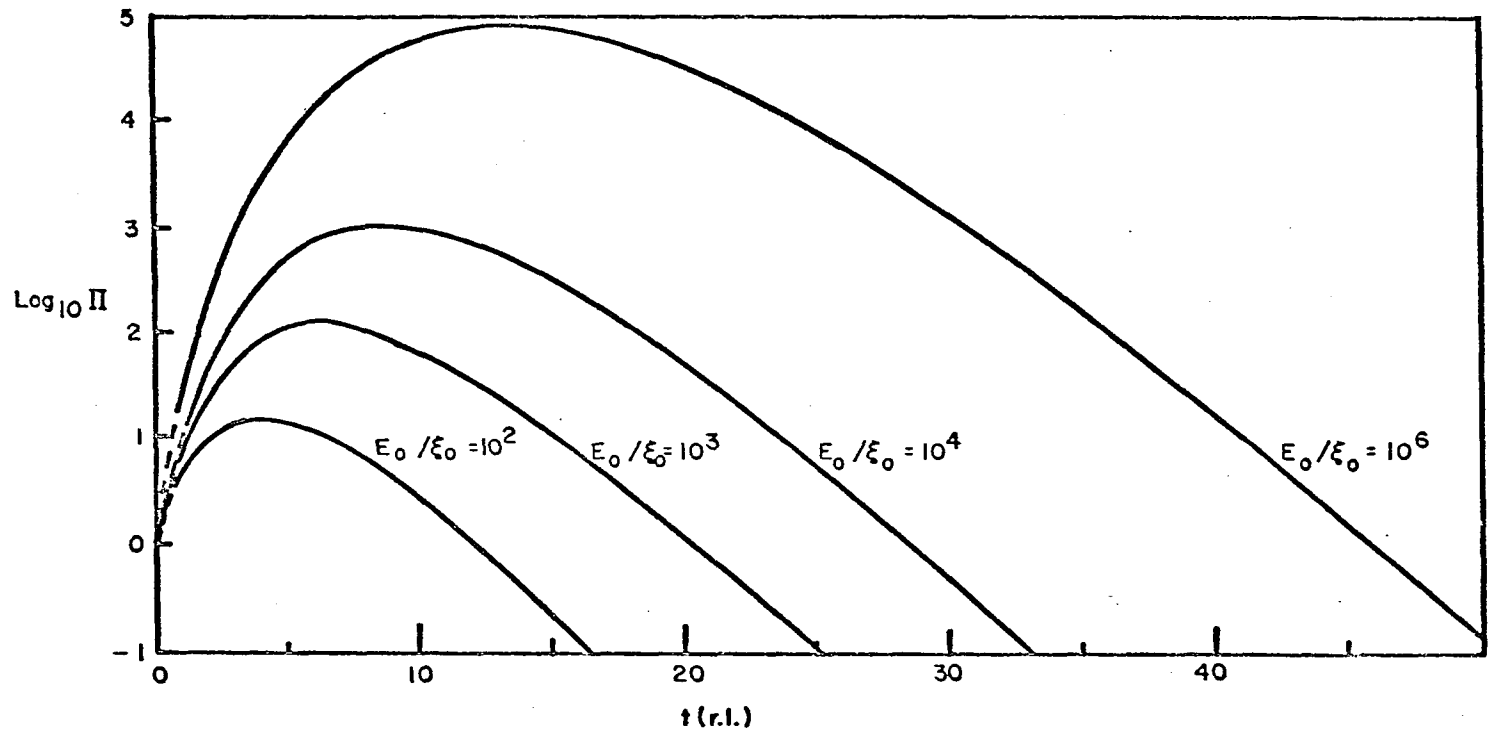

Fig. 4. The total number $\Pi(E_0,0,t)$ of electrons in a shower initiated by an electron of energy E_0 as a function of the depth t in an absorber. Computed for various values of E_0/ϵ_0 under approximation B. From B Rossi, High Energy Particles (Prentice-Hall, Inc., Englewood Cliffs, N.J., 1952) p. 258.

To meet the needs of improved experimental techniques, Kamata and Nishimura[21,22] developed the three-dimensional cascade theory. This three-dimensional theory was constructed from the one-dimensional theory and the theory of Coulomb scattering. The lateral spread of a cascade due to deflections arising from the radiation and pair creation processes are known to be negligible when compared with the contribution of Coulomb scattering, except at the beginning of the shower development. Therefore, they are neglected.

Following Kamata and Nishimura, one can consider the lateral and angular variation of electrons to be the result of Coulomb scattering in a thickness dt of an absorber. One can define $\sigma(\vec{\theta})\, d\vec{\theta}$ to be the probability that an electron is scattered through an angle between $\vec{\theta}$ and $\vec{\theta} + d\vec{\theta}$ while traveling the given thickness dt. The variation of the number of electrons in the spatial and angular intervals $(\vec{r}, d\vec{r})$ and $(\vec{\theta}, d\vec{\theta})$ is caused by:

(a) An electron at a position $(\vec{r}, d\vec{r})$ traveling at an angle $\vec{\theta}$ with the cascade axis will be laterally displaced $\vec{\theta}dt$ in the thickness dt. Therefore, an electron at $\vec{r}$ at the depth t will be at $\vec{r} + \vec{\theta}dt$ at the depth t + dt. Thus,

$$\begin{aligned} \pi(t + dt, \vec{r}, \vec{\theta}) &= \pi(t, \vec{r} - \vec{\theta}dt, \vec{\theta}) \\ &= \pi(t, \vec{r}, \vec{\theta}) - \vec{\theta}dt\frac{\partial \pi}{\partial r} \ . \end{aligned} \tag{II.2.15}$$

---

[21] J. Nishimura and K. Kamata, Progr. Theoret. Phys. (Kyoto) 7, 185 (1952).

[22] K. Kamata and J. Nishimura, Suppl. Progr. Theoret. Phys. (Kyoto) 6, 93 (1958).

(b) An electron traveling in the direction $(\vec{\theta}', d\vec{\theta}')$ at the depth t will be scattered by Coulomb scattering into the interval $(\vec{\theta}, d\vec{\theta})$ while the electrons originally in the interval $(\vec{\theta}, d\vec{\theta})$ will be scattered out of this interval. The net variation caused by scattering is given by

$$dt\left[\int_{-\infty}^{\infty}\sigma(\vec{\theta}-\vec{\theta}')\pi(\vec{\theta}')d\vec{\theta}' - \int_{-\infty}^{\infty}\sigma(\vec{\theta}')\pi(\vec{\theta})d\vec{\theta}'\right] . \qquad (11.2.16)$$

Since a photon does not suffer Coulomb scattering, only a statement exactly similar to (a) above applies to the variation in the number of photons in an interval $(\vec{\theta}, d\vec{\theta})$ after traversing a thickness dt of absorber.

Adding these expressions to the one-dimensional diffusion equations given earlier, we have for the basic diffusion equations in the three-dimensional cascade theory under approximation B:

$$\frac{\partial\pi}{\partial t} + \vec{\theta}\frac{\partial\pi}{\partial r} = \int_{-\infty}^{\infty}\sigma(\vec{\theta}-\vec{\theta}')\ \pi(\vec{\theta}')d\vec{\theta}' - \int_{-\infty}^{\infty}\sigma(\vec{\theta}')\ \pi(\vec{\theta})d\vec{\theta}'$$

$$+ 2\int_0^1\gamma\left(\frac{E}{u},t\right)\psi(u)\frac{du}{u} + \int_0^1\left[\frac{1}{1-v}\pi\left(\frac{E}{1-v},t\right) - \pi(E,t)\right]\phi(v)dv + \epsilon\frac{\partial\pi}{\partial E} \qquad (11.2.17)$$

$$\frac{\partial\gamma}{\partial t} + \vec{\theta}\frac{\partial\gamma}{\partial r} = \int_0^1\pi\left(\frac{w}{v},t\right)\phi(v)\frac{dv}{v} - \sigma_0\gamma(w,t) \qquad (11.2.18)$$

As before, approximation A is immediately obtained from these equations by taking $\epsilon = 0$.

Kamata and Nishimura[23] obtained a solution to these equations both with and without the use of the Landau approximation. This

---

[23] Ibid.

approximation amounts to expanding the function $\pi(t,\vec{\theta}'+\vec{\theta})$ in a Taylor series of $\vec{\theta}'$ so that the variation in the number of shower particles in the interval $(\vec{\theta}, d\vec{\theta})$ due to scattering can be expressed by

$$dt\{\int_{-\infty}^{\infty}\int[\pi(\vec{\theta}) + \vec{\theta}'\vec{\nabla}_{\theta}\pi(\vec{\theta}) + \frac{(\vec{\theta}')^2}{2!}\ \nabla^2{}_{\theta}\pi(\vec{\theta})$$

$$+ \ . \ . \ . \ ]\sigma(\vec{\theta}')d\vec{\theta}' - \int_{-\infty}^{\infty}\pi(\vec{\theta})\sigma(\vec{\theta}')d\vec{\theta}'\} \ . \qquad (11.2.19)$$

The first term in the series is canceled by the second integral, while the second term vanishes because of axial symmetry of the scattering probability. The third term is proportional to the mean square angle of the scattering which can be represented by $\frac{1}{2}(\frac{E_s}{E})^2$, where E_s = 21 MeV is the so-called scattering energy.

Large deflections of a particle passing through an absorber are more likely to occur in single collisions, while small deflections are generally caused by many collisions. The result of single collisions is referred to as "single scattering", the result of a small number of collisions as "plural scattering", and the result of a large number of collisions as "multiple scattering".

The Landau approximation corresponds to the theory of multiple scattering for a singly charged particle. The contributions of plural and single scattering are not included, since the higher moments of the Rutherford cross section are neglected. Therefore, the cascade distributions so derived will be in error at large angles and distances. The distributions under the Landau approximation do not completely agree with the more exact ones obtained without this

approximation even in the limit of small angles and distances.

The solution without the Landau approximation is based on Moliere's scattering theory[24] for a singly charged particle which does include the contributions of single and plural scattering. Extensive studies[25] reveal that these effects give not only a major contribution in the region of large deflection angles and distances but also appreciable contribution even in the limit of small angles and distances. The solutions of the cascade equations without the Landau approximation are believed to represent well the lateral and angular spread of the electromagnetic cascade.

The lateral and angular structure functions are rather complicated expressions and will not be reproduced here. They may be found in Ref. 22 where they are derived both with and without the Landau approximation.

Theoretical lateral cascade distributions were first calculated[26] using the three-dimensional cascade theory with the Landau approximation. These distributions did not agree with experimental results because of the inadequacy of this approximation, but they did show that $N(<R)$ depended only on the product $E_o R$. This was a milestone in the application of the theory since it presented the possibility of obtaining the primary energy of a cascade by simply counting the number of electrons within some circle about the cascade axis.

---

[24] H. A. Bethe, Phys. Rev. 89, 1256 (1953).

[25] H. S. Snyder and W. T. Scott, Phys. Rev. 76, 220 (1949).

[26] K. Pinkau, Phil. Mag. 2, 1389 (1957).

Later calculations[27,28] using the cascade theory without the Landau approximation were in good agreement with experimental results. However, the transition curves so derived are valid only for small values of R since they were obtained under the approximation that R be small compared to unity. (R is expressed in units of radiation length.)

The results of the calculation of the lateral distribution of electrons for a cascade initiated by an electron pair are given in the form of transition curves in Fig. 5a. The curves show the number of electrons located within a circle of radius R about the cascade axis as a function of the depth t in the absorber for various values of the parameter $E_o R$. The same results are shown in Fig. 5b as a function of $E_o R$ with t as a parameter.

3. Limitation to the Core Approximation

It has been anticipated that the cascade distributions calculated within the framework of the core approximation ($R \ll 1$) may have been used beyond their range of validity to determine the primary energy of electromagnetic cascades.[29] To emphasize this fact,

---

[27] J. M. Kidd, Nuovo Cimento 27, 57 (1963).

[28] P. H. Fowler, D. H. Perkins, and K. Pinkau, Proceedings of the Moscow Cosmic Ray Conference, Moscow, 1960, edited by V. I. Zatsepin and B. S. Khrenov, Vol. 2, p. 302.

[29] K. Pinkau, Proceedings of International Conference on Cosmic Rays, Jaipur, India, 1963, edited by R. R. Daniel, P. J. Lavakave, M. G. K. Menon, S. Navanan, N. W. Nerurkar, Yash Pal, and B. V. Sreekantan (The Commercial Printing Press, Limited, Bombay, India, 1964), Vol. 5, p. 555.

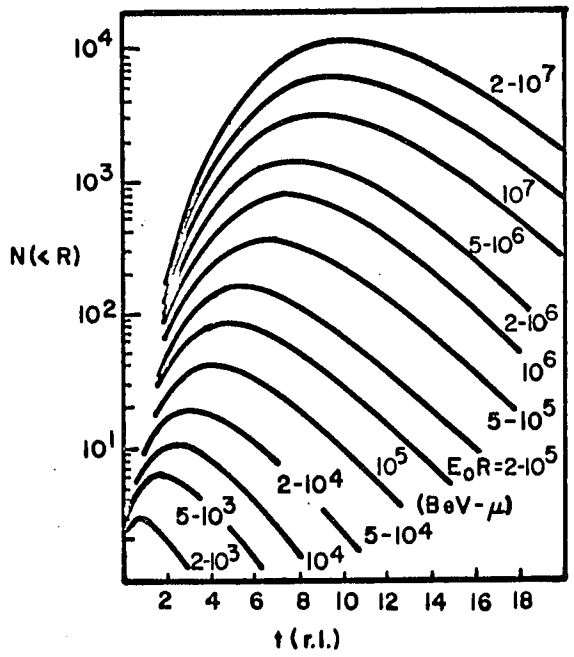

Fig. 5a. Transition curves for a cascade initiated by an electron pair. The curves are calculated with the core approximation for G-5 emulsion. From Kidd, Nuovo Cimento 27, 57 (1963).

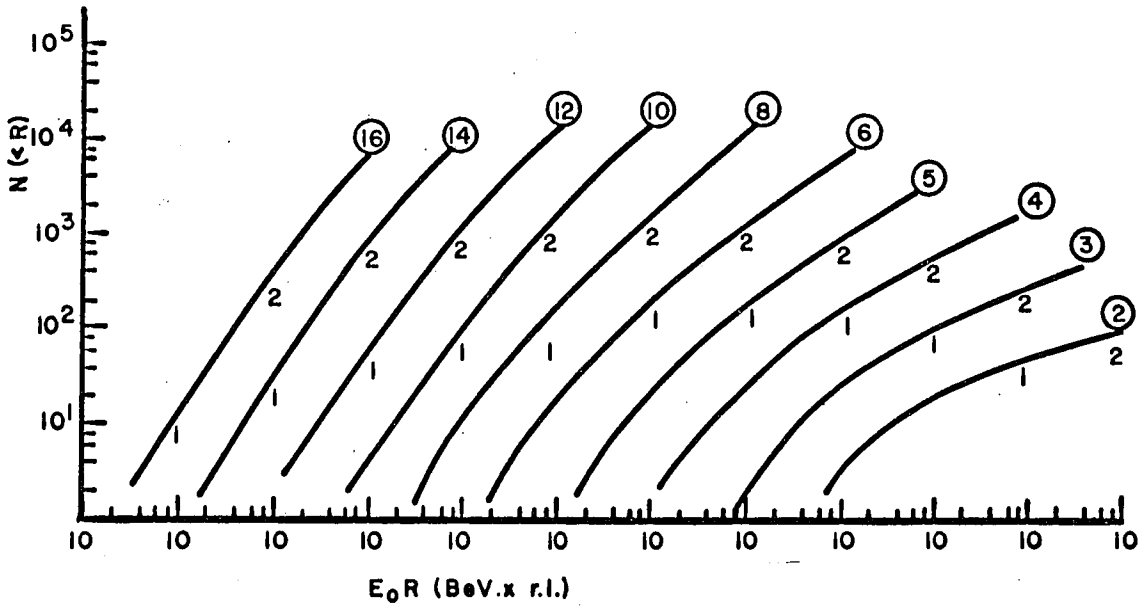

Fig. 5b. Curves of N(<R) vs E_0R within the core approximation. The radiation lengths t from the origin are given in circles while the powers of ten to be used are given beside the individual curves. From Pinkau, Nuovo Cimento 33, 221 (1964).

Pinkau[30] has performed calculations on the equations of the three-dimensional cascade theory for the case where R is not small compared to unity. For simplicity, his argument is based on the cascade theory derived within the Landau approximation.

The integral electron distribution in the Landau approximation is obtained by integrating the lateral structure function $\Pi_e(E_o, E, r, t)$ given by Kamata and Nishimura[31] as discussed in the preceding section. This distribution, which gives the number of electrons contained within a circle of radius R about the cascade axis, is given by the integral

$$N(<R) = -\frac{1}{4\pi^2}\int_{-i\infty}^{+i\infty}\int ds\,dp\ \left(\frac{E_o}{\epsilon}\right)^s \left(\frac{\epsilon R}{E_s}\right)^{-2p} \left(\frac{1}{-p}\right) \Gamma(p+1)\,\Gamma(s+2p)\,M_e(p,-s-2p,s,t)\ , \tag{11.3.1}$$

for the limiting case where the energy E of the electrons approaches zero.

The integral over s represents the total number of particles at the depth t in the longitudinal development of the cascade. The parameter s is commonly called the "shower age" parameter since before the maximum development of the cascade $s < 1$, while $s = 1$ at the maximum and $s > 1$ after the maximum development. The remaining integral over p represents the lateral spread of the cascade.

---

[30] K. Pinkau, Nuovo Cimento 33, 221 (1964).

[31] K. Kamata and J. Nishimura, Suppl. Progr. Theoret. Phys. (Kyoto) 6, 93 (1958).

For large values of R, $p \to 0$ while $p \to -\frac{s}{2}$ in the limit $R \to 0$.

The above equation may be evaluated by using the double saddle point method of solution.[32] The core approximation makes use of the fact that in the limit as $R \to 0$ the integral expression for $N(<R)$ can best be evaluated by considering just the pole $p = -\frac{s}{2}$ of the gamma function. It is possible to estimate the values of R for which this approximation is valid by determining the shape of the distribution at the other extreme limit of large R. Since this latter approximation applies to regions of the cascade far from the core, it is called the "approximation for large radii."

The results of Pinkau's calculations show that the solutions of Eq. (II.3.1) that are valid for large R must be upper limits to the distribution of electrons predicted by an exact solution. The solutions for large R are made with the assumption that $E_o/\epsilon \to \infty$ where $\epsilon = \epsilon_o$, the critical energy, if approximation B is considered and $\epsilon = E_c$, the lower energy limit, if approximation A is considered. These approximations are called "approximation B for large radii" and "approximation A for large radii", respectively.

The region of validity of the core approximation can be estimated from Pinkau's calculations by comparing the electron distributions predicted by the core approximation with the distributions predicted by the approximations for large radii. If the latter distributions predict particle numbers smaller than the core approximation, then the core approximation has apparently ceased to be

---

[32] K. Pinkau, Ph.D. Thesis, Appendix I, University of Bristol, England, 1958 (unpublished).

valid, because the approximations for large radii give upper limits to the total number of particles.

The distributions predicted by approximations A (curve "A") and B (curve "B") for large radii are shown superimposed on the curves for the core approximation (curve "C") in Fig. 6. The values E_c = 50 MeV and ϵ_0 = 10 MeV have been used. In order to present specific examples to show the dependence on the primary energy of the cascade and the distance from the origin, the plots are made for primary energies of 100, 1000, and 10 000 BeV at distances of 5 and 10 r.l.

The core approximation apparently ceases to be valid at radii which are near the crossing points of curves "A" and "B" with "C". The curves imply that the region of validity of the core approximation is smaller for the shorter radiation lengths and decreases with increasing energy.

It should be noted that very dense cores of the higher energy cascades present measurement difficulties, and an experimenter may be required to investigate somewhat distant regions from the core where the track density is smaller. Consequently, one is more likely to go beyond the predicted region of validity of the core approximation as the cascade energy increases.

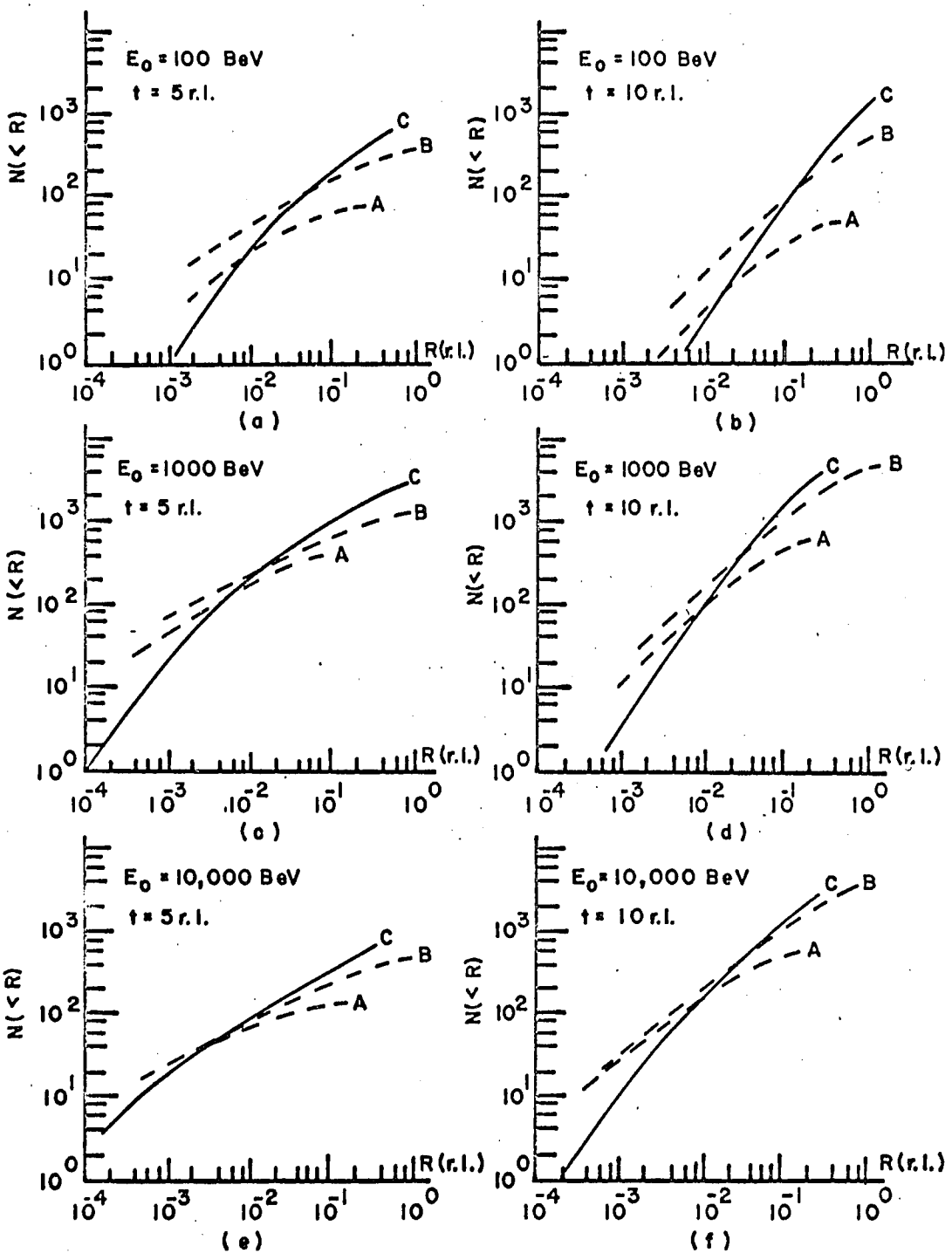

Fig. 6. Integral radial distributions predicted by the core approximation (curves C), and the approximation A (curves A) and B (curves B) for large radii. The distributions are presented for three values of the primary energy E_o and two distances t from the cascade origin. From Pinkau, Nuovo Cimento 33, 221 (1964).

III. EXPERIMENTAL PROCEDURE

1. Selection of Cascades for Measurement

The cascades investigated in this experiment are found in that part of the Brawley stack which is in the L.S.U. laboratory or in the SSS sandwich stack. Visual scanning for electromagnetic cascades was performed on the emulsion plates of both stacks by placing them over a uniformly illuminated light box and looking for the cascades, which appear as a dark streak in the emulsion, with the unaided eye.

Each electromagnetic cascade observed during the visual scanning was traced back to its origin or point of entry into the stack. Various types of events were found by this process, but the analysis described herein concerns only those events classified as pure electromagnetic in origin.

An electromagnetic cascade found in an emulsion stack which has been exposed at the top of the atmosphere may be the result of an interaction of the cosmic rays with the nuclei of the atmosphere above the emulsion stack or with the nuclei in the emulsion stack itself.

Each interaction of the primary cosmic radiation with a nucleus of the earth's atmosphere produces, among other particles, a number of π^0 - mesons. The π^0 - mesons decay with a half life of $\sim 10^{-16}$ sec. into two γ-rays. Most of the γ-rays resulting from such decay,

which initiate an electromagnetic cascade in the emulsion block, enter the detector before materializing. However, some may materialize in the atmosphere above the detector and either one or two cascades will develop from the conversion electrons upon entering the stack. The former process is called the direct component and the latter is called the cascade component of the gamma radiation.

The primary cosmic radiation may produce jets inside the detector which are accompanied by π^0 - mesons. The γ-rays from the subsequent π^0 -decay will materialize before their spatial separation becomes appreciable and give rise to overlapping electromagnetic cascades of possibly different energy. Also, secondary interactions may result in additional pions which are mixed with the cascade. The resolution of such a complex shower development into its components is impractical, and such cascades were rejected from the group which was considered in this experiment.

Since the distance from the cascade origin can only be measured with certainty from the first electron pair, this experiment also rejected the cascade component and considered only the direct component of the gamma radiation. To insure that the cascades to be measured were indeed of the direct component, the Brawley cascades were required to fulfill the following criteria:

1. The origin of the first pair was located within about two conversion lengths from the edge of the stack.[33]

---

[33] K. Pinkau, Nuovo Cimento 3, 1156 (1956).

2. The origin of the first pair was found and scanning of the adjacent area showed no accompanying parallel tracks which might be connected with a low multiplicity nuclear interaction.

3. The origin of the first bremsstrahlung pair was located a reasonable longitudinal distance from the origin of the primary pair ($\sim$ 1 cm) and had a small lateral displacement from that pair ($< 3\ \mu$).[34]

4. The cascade had only one apparent core.

5. Scanning of the immediate area around the cascade showed no secondary interactions.

The cascades in the SSS lead-emulsion sandwich stack could not be continually observed throughout their development since much of the development was in the lead plates. Consequently, all of the above criteria were not always used for this stack. Each of these cascades was traced back toward its origin by observing the cascade in each emulsion plate where it could be found. These observations showed that each cascade had only one apparent core. When the cascade could no longer be found in an emulsion plate, calculations were performed by using the dip angle of the cascade to be sure that the cascade could not reach the next adjacent lead plate before exiting the stack. In this manner, the origin of the cascade was located within a lead plate. To calculate the distance t from the origin where measurements were made, the origin was assumed to be in the center of this lead plate. This assumption is consistent with the

---

[34]E. Lohrmann, Phys. Rev. 122, 1908 (1961).

first criterion given above. To satisfy the second criterion, the first emulsion plate in which the cascade could be found after entering the stack was scanned for parallel tracks. By calculating the distance traveled in each lead and each emulsion plate from the dip angle of the cascade, and by knowing the number of lead and emulsion plates between the assumed origin and the position of measurement, the distance t in radiation lengths was calculated using 5.7 mm/r.l. for lead and 28.3 mm/r.l. for emulsion.

2. Technique of Measurements

The object of making the cascade measurements was to obtain the spatial position and angular orientation of each cascade particle relative to the cascade axis.* Fig. 17 shows a schematic picture of the cascade as it appeared in the emulsion and its relation to the positions of measurement.

Three measurements were made on each Brawley cascade at distances from the origin which corresponded to 5, 7, and 9 r.l. This range was selected because the maximum development of the cascades for the energies under consideration ($\sim 10^{12}$ eV) occurs about 7 r.l. from the origin. Below 5 r.l. the fluctuations in development become increasingly important and troublesome, while above 9 r.l. the cascades become so diffuse that it is

---

*The details of measurements are given in Appendix I.

difficult to distinguish any apparent core. The positions of measurement on the SSS cascades were restricted by the development of the cascades in the lead plates. Therefore, the measurements were made such that each was separated from an adjacent measurement by one lead plate and yet was as close as possible to 5, 7, and 9 r.l.

The volume of measurement at each radiation length consisted of 15 adjacent fields of view of the microscope focused from the glass to air surface of the emulsion plate.

In order to get the best possible experimental results, each field of view was read by two different observers. Any disagreement in the results of the two readings was checked by a third observer before the readings were accepted as final data to be used in the calculation of coordinates for the particles of the cascade.

Because the emulsion is very sensitive to changes in temperature and humidity, extreme caution was exercised to assure that these remained as stable as possible. In addition to this precaution, the light source of the microscope was turned on automatically by a time clock two hours before measurements were made to minimize the microscope "drift." Under the best of conditions these factors are present to some extent, and therefore the coordinates of easily recognizable tracks were recorded in each field of view and used as calibration points. These calibration tracks were checked periodically to prevent relative displacement of the cascade track coordinates and assure good agreement between the two readings of each field of view.

The actual measurements were performed by using a Koristka R4 microscope which has a vernier scale to permit determination of the absolute depth of the field of measurement in the emulsion. The microscope was equipped with a square "box" graticule having 100 scale divisions per side.* See Fig. 18. For each cascade track which crossed the horizontal centerline of the graticule, three spatial coordinates were obtained for each of the two points where it crossed the sides of the graticule. These two positions for each track permitted the calculation of the spatial position and angular orientation of the track relative to the cascade axis.

The apparent core of the cascade was located midway between the glass and air surface of the emulsion plate. This permitted measurements to be made at approximately equal distances above and below the core. All cascade tracks, irrespective of angle, were measured over a lateral spread of $\gtrsim 600\ \mu$ to either side of the apparent core. Since the undeveloped emulsion is approximately $600\ \mu$ in thickness, these lateral measurements extend to about twice as far from the core as the respective glass and air surfaces of the emulsion. See Fig. 7. Thus, while one could obtain exact distributions of the tracks up to distances of about $300\ \mu$ from the core, larger distances required some correction. The needed correction was calculated from the ratio of the area in

*The box graticule was furnished by W. Enge of Institut fur Reine und Angewandte Kernphysik der Christian-Albrechts-Universitat Kiel in Kiel, Germany.

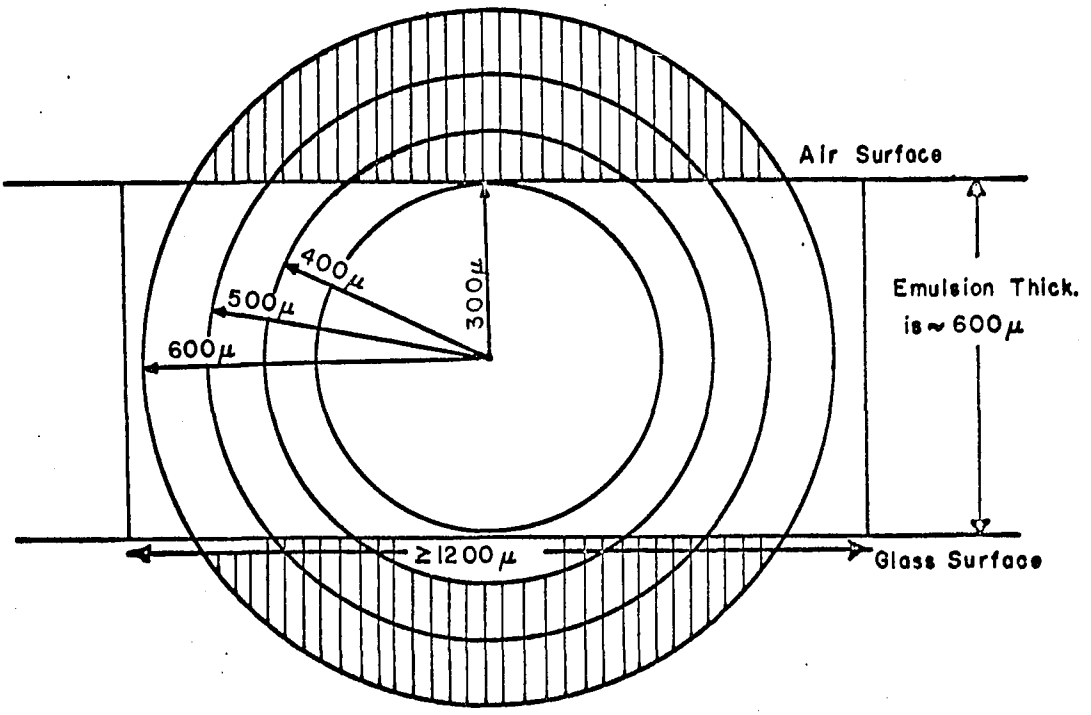

Fig. 7. Schematic diagram showing needed correction for cascade particle distributions for the lateral distance R greater than $\sim 300\ \mu$ from the cascade axis. The lateral spread in measurements was $\gtrsim 1200\ \mu$ or about twice the thickness of an emulsion plate which was $\sim 600\ \mu$. The diagram represents the target plane (with the cascade axis near the center) of a cascade at a fixed position of measurement. Corrections are needed for the shaded area of the target plane which was outside the range of measurements.

that part of an annular ring in which measurements were made to the entire area of the ring. This technique of correction amounts to assuming azimuthal symmetry of tracks about the cascade axis.

There are three cases to consider in making the corrections, since the axis of the cascade may not have been located exactly at the midpoint between the glass and air surfaces of the emulsion plate. Let the shorter of the two distances from the axis to the glass and air surfaces be represented by "a" and the larger distance by "b". It is desired to know the lateral and angular distributions of all cascade particles within a distance R of the cascade axis. If $R \leq a$, no correction is needed. For $R > a$ the needed correction increases with increasing R.

If n is the number of particles actually measured in part of an annular ring having radii R_1 and R_2, then the number of particles N which would have been measured in the entire ring is given by

$$N = \frac{2\pi n}{\varphi} ,$$

where

$$\varphi = 2\pi, \qquad \text{if } r \leq a$$

$$= 2\left[\pi - \cos^{-1}\left(\frac{a}{r}\right)\right], \qquad \text{if } a < r \leq b$$

$$= 2\left[\pi - \cos^{-1}\left(\frac{a}{r}\right) - \cos^{-1}\left(\frac{b}{r}\right)\right], \quad \text{if } r > b$$

The symbol r is the average of the radii R_1 and R_2 of the ring. The correction is better the smaller the differences between R_1 and R_2, and this difference was taken to be 50μ in actually performing the corrections.

3. Background Analysis

When a given volume of nuclear emulsion has been exposed near the top of the earth's atmosphere for a prolonged period of time, many primary cosmic rays as well as secondary particles resulting from high energy nuclear interactions in the atmosphere above the volume will leave tracks in the emulsion. (The total number of tracks is dependent among other things on the time and altitude of exposure.) In addition, many secondary particles from interactions in the emulsion itself will spread out in all directions and leave tracks. The result is that a somewhat random distribution of tracks will exist throughout the volume of emulsion.

In electromagnetic cascade measurements, one is interested in observing only the electrons and positrons connected with the cascade. However, it is impossible to differentiate between electron tracks and the tracks of other singly charged particles such as muons, pions, and protons if the energies of the particles are high. For relatively low energies the grain density depends on the velocity of the particle as well as its charge, but for high energies the grain density reaches a plateau value which is independent of the velocity of the particle. Tracks in emulsion which have grain densities around this plateau value for singly charged particles will hereafter be called minimum tracks. If during the course of measurements one observes all minimum tracks, it is certain that the measurements would include particles which are not electrons or positrons. Any particle which is not directly connected with a cascade is classified as a background particle.

In the measurements performed on the electromagnetic cascades in this experiment, each minimum track was measured in order to obtain its spatial and angular orientation relative to the cascade axis. The technique of the measurements is discussed in Sec. III.2. with details given in Appendix I. In such measurements, it is impossible to select individual tracks as belonging to the background or to the cascade. In order to determine the background level, the field of view of the microscope was located in a region of the emulsion which was $\gtrsim 1$ cm from the axis of a cascade and measurements were done exactly as for a cascade. The background measurements for the Brawley stack were made in three different positions of the emulsion stack. These three independent sets of background data yielded a total of more than 2000 tracks from which could be derived average values for the lateral and angular distribution of the background noise. Four such independent sets of background data were obtained for the SSS stack. From this data there were more than 1500 tracks from which to obtain the average background distributions.

For high energy cascades, the ratio of cascade particles to background particles is large as long as attention is restricted to regions near the core. As the lateral distance from the core is increased, the ratio of signal to noise decreases and fluctuations in the randomly distributed background become increasingly important. The ratio of signal to noise for individual cascades also depends on the energy of the cascade and the distance from the origin at which measurements are made. In this experiment, the background was predominant over the cascade for particles having large angles with respect to the cascade axis.

In measurements of the background as well as the cascades, an attempt was made to measure all particles regardless of angle over a lateral spread of $\sim$ 1200 μ. However, the measurement of all particles was limited because of inefficiency in observing tracks which were inclined at a large angle with respect to the emulsion surface. This angle of inclination with the emulsion surface is known as the dip angle of the track.

As described in Appendix I, an averaging procedure was used to determine the cascade axis, relative to which the spatial and angular coordinates of all the cascade particles were calculated. This method was not used in calculating the coordinates for the background particles because small fluctuations in spatial or angular orientation of the background tracks could cause large deviations in the location of the axis. Instead, the coordinate system used in making measurements* of either cascades or background was fixed as the coordinate system for the background calculations. Since the axis of each measured cascade was inclined at some angle with the emulsion surface, the background data was calculated for the background "axis" inclined at several different angles. The dip angle of the background "axis" could then be matched with the axis of any cascade. This technique of calculation tends to correct for any loss in cascade tracks which had a large dip angle.

Since the background was predominant over the cascades for large angles, the cascade distributions are presented only up to the

---

*See Appendix I.

maximum angle with respect to the cascade axis where the number of cascade particles above the background could be reliably established. This maximum angle is $\sim 20^{o}$ and coincides with the maximum angle wherein it is reasonable to assume that all tracks were measured. This limiting angle can be deduced from Fig. 8. The figure shows the integral angular distribution of background tracks for different dip angles of the background "axis". Curves are given for both the Brawley stack and the SSS stack at R = 600 μ.

It is seen from the curves for the Brawley background that there is little difference between the number of particles as calculated relative to an "axis" which has dip angle 0^{o} or dip angle 10^{o}. Since the curves extend up to angles of 20^{o} with respect to the "axis", this implies that practically all particles were measured which had an angle $\lesssim 30^{o}$ with respect to the emulsion surface. This limit in angular measurement is also evident from the curve for the "axis" inclined at 20^{o} with respect to the emulsion surface, since the latter curve begins to deviate from the former curves for angles greater than $\sim 10^{o}$ with respect to the background "axis". Similar results can be obtained from the SSS data.

Of the six cascades measured in the Brawley stack, the average dip angle was $\sim 10^{o}$. The cascades measured in the SSS stack had dip angles in the range $\sim 12\text{-}15^{o}$. These dip angles must be deducted from the angle ($\lesssim 30^{o}$) wherein it can be assumed that practically all tracks have been measured to determine the maximum angle with respect to the cascade axis which could be used in the radial and angular distributions and still be sure that practically all particles were included. Using the average dip angle of the cascades in

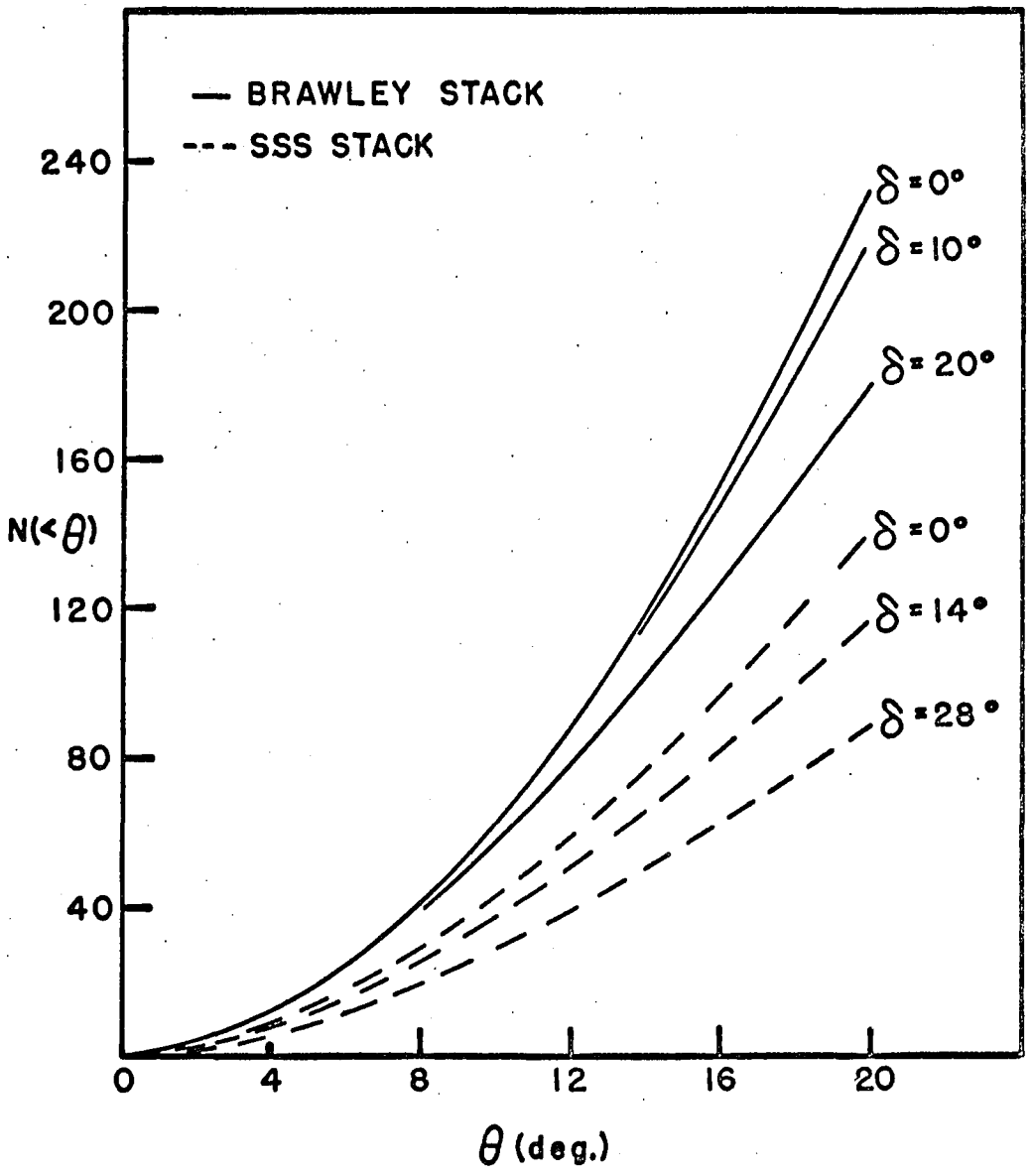

Fig. 8. Average number of background tracks $N(<\theta)$ as a function of θ. The plot is made for different values of the dip angle δ of the background "axis" at R = 600 μ. The solid and broken lines show the background in the Brawley stack for δ = 0, 10 and 20° and in the SSS stack for δ = 0, 14 and 28°, respectively. The background in the Brawley stack is about twice that in the SSS stack when distances are measured in microns. In terms of radiation lengths, the SSS background is lower by a factor of ~ 6.

the Brawley stack, this maximum angle has been taken to be 20°. This angular cutoff was used for all the cascades which have been measured, regardless of their dip angle.

In all respects other than the determination of the axis, exactly the same calculations were performed on the background data as on the data which had the cascades superimposed on background. Therefore, for any distribution of coordinates which was desired, the corrections for background noise could be made by a simple subtraction of the average background from the cascade superimposed on background.

IV. RESULTS

1. Presentation of Experimental Results

From the initial cascade measurements, the projected coordinates y, z, θ_y, and θ_z for each electron in the cascade were determined for the coordinate system having the x axis coincident with the cascade axis (See Appendix I). From these projected coordinates, the space coordinates R and θ which give the lateral displacement and angular orientation of each track relative to the cascade axis, respectively, were calculated. Shown in tables I and II are the distributions of the number of cascade particles having lateral displacements less than R versus the number having angles less than θ. These distributions are given for each position of measurement for the ten cascades which were measured.

Table I contains the integral radial and angular distributions of electrons for the six cascades measured in the Brawley stack, while Table II contains the same distributions for the four cascades measured in the SSS stack. From these tables, one can obtain directly the integral radial distribution at a fixed angular cutoff by reading across the correct row. The integral angular distribution for a fixed radius is obtained by reading down the proper column. The differential distributions can be obtained by subtracting adjacent rows and columns. It should be noted that the results given are the differences between two integral

TABLE 1

N(<R) vs N(<θ) for Brawley Cascades

Brawley Cascade No. 1044 t = 5 r.l.

R r.l.		1.77×10^{-3}	3.53×10^{-3}	5.30×10^{-3}	7.07×10^{-3}	8.83×10^{-3}	1.06×10^{-2}	1.24×10^{-2}	1.41×10^{-2}	1.59×10^{-2}	1.77×10^{-2}	1.94×10^{-2}	2.12×10^{-2}
θ tan	μ deg	50	100	150	200	250	300	350	400	450	500	550	600
1.75×10^{-2}	1.0	27	56	66	74	82	87	93	93	95	94	94	100
3.49×10^{-2}	2.0	44	95	118	140	159	171	187	195	197	201	206	210
5.24×10^{-2}	3.0	54	111	150	181	211	235	255	264	269	279	285	296
6.98×10^{-2}	4.0	55	119	160	196	230	256	277	289	295	307	313	328
8.73×10^{-2}	5.0	56	124	168	210	246	271	293	307	312	325	341	355
1.05×10^{-1}	6.0	56	128	172	216	252	281	306	321	330	345	358	372
1.22×10^{-1}	7.0	57	129	173	220	256	289	315	330	338	352	364	380
1.40×10^{-1}	8.0	57	128	175	222	259	291	316	333	340	353	365	378
1.57×10^{-1}	9.0	57	130	179	227	266	300	325	343	348	361	375	387
1.75×10^{-1}	10.0	57	132	182	230	269	303	329	353	360	374	386	400
1.92×10^{-1}	10.9	57	132	184	233	272	307	332	355	363	378	391	403
2.27×10^{-1}	12.8	57	131	185	238	276	315	338	359	367	389	405	415
2.62×10^{-1}	14.7	57	131	185	240	281	324	346	364	369	392	406	411
2.97×10^{-1}	16.6	56	130	185	243	282	328	349	367	369	392	410	413
3.32×10^{-1}	18.4	56	129	184	245	284	329	353	370	376	398	419	424
3.67×10^{-1}	20.2	56	129	183	244	286	334	357	373	375	400	417	423

Brawley Cascade No. 1044 t = 7 r.l.

1.75×10^{-2}	1.0	32	45	59	71	83	92	103	107	110	112	114	117
3.49×10^{-2}	2.0	74	113	152	178	221	242	271	292	304	307	320	333
5.24×10^{-2}	3.0	81	130	180	216	268	301	334	362	379	385	404	422
6.98×10^{-2}	4.0	85	140	190	229	286	321	357	388	419	424	448	468
8.73×10^{-2}	5.0	85	140	190	236	297	336	377	409	443	452	480	505
1.05×10^{-1}	6.0	89	146	199	249	310	351	396	432	470	478	509	534
1.22×10^{-1}	7.0	89	146	202	254	318	360	405	442	482	489	522	551
1.40×10^{-1}	8.0	89	145	202	255	320	365	411	450	492	498	537	565
1.57×10^{-1}	9.0	90	148	204	264	328	374	421	463	504	510	549	583
1.75×10^{-1}	10.0	90	148	204	265	331	378	426	468	509	519	559	595
1.92×10^{-1}	10.9	90	148	205	268	335	382	430	476	517	526	571	611
2.27×10^{-1}	12.8	92	150	209	272	341	388	440	493	532	538	582	627
2.62×10^{-1}	14.7	92	150	212	274	344	391	443	496	534	541	583	641
2.97×10^{-1}	16.6	91	152	215	278	349	396	449	504	541	553	592	653
3.32×10^{-1}	18.4	92	153	218	283	354	402	454	507	548	559	600	666
3.67×10^{-1}	20.2	92	152	216	280	352	402	457	513	550	571	608	676

TABLE I (Continued)

Brawley Cascade No. 1044 t = 9 r.l.

R r.l.		1.77 X10^{-3}	3.53 X10^{-3}	5.30 X10^{-3}	7.07 X10^{-3}	8.83 X10^{-3}	1.06 X10^{-2}	1.24 X10^{-2}	1.41 X10^{-2}	1.59 X10^{-2}	1.77 X10^{-2}	1.94 X10^{-2}	2.12 X10^{-2}
θ tan \ μ deg		50	100	150	200	250	300	350	400	450	500	550	600
1.75X10^{-2}	1.0	11	33	55	72	76	82	85	86	86	90	92	98
3.49X10^{-2}	2.0	26	71	118	153	168	184	199	224	241	247	257	267
5.24X10^{-2}	3.0	35	91	151	194	224	250	270	300	227	348	359	378
6.98X10^{-2}	4.0	36	94	162	208	245	273	302	339	368	401	423	446
8.73X10^{-2}	5.0	36	100	172	222	260	292	327	369	399	437	460	490
1.05X10^{-1}	6.0	37	104	177	229	268	306	343	386	421	461	487	523
1.22X10^{-1}	7.0	37	106	180	234	272	311	351	396	436	477	502	540
1.40X10^{-1}	8.0	37	106	181	236	275	317	357	401	441	485	509	550
1.57X10^{-1}	9.0	37	106	180	236	279	322	362	411	452	496	520	579
1.75X10^{-1}	10.0	37	106	181	237	281	325	367	417	458	504	526	587
1.92X10^{-1}	10.9	37	107	183	239	285	331	374	428	469	513	538	601
2.27X10^{-1}	12.8	38	109	185	244	290	336	379	434	478	529	558	617
2.62X10^{-1}	14.7	38	110	187	247	295	342	385	441	493	545	574	635
2.97X10^{-1}	16.6	37	110	188	252	300	345	398	455	511	566	601	665
3.32X10^{-1}	18.4	37	109	186	249	300	348	399	453	510	567	611	672
3.67X10^{-1}	20.2	37	110	187	252	308	357	415	468	520	579	631	687

Brawley Cascade No. 1068 t = 5 r.l.

1.75X10^{-2}	1.0	14	26	36	41	41	44	44	44	44	43	43	46
3.49X10^{-2}	2.0	23	46	62	78	83	91	97	104	110	110	109	111
5.24X10^{-2}	3.0	23	49	68	89	96	106	115	125	134	135	141	143
6.98X10^{-2}	4.0	24	50	70	91	99	108	118	129	138	141	146	150
8.73X10^{-2}	5.0	24	50	70	91	100	109	121	133	142	149	158	166
1.05X10^{-1}	6.0	25	51	71	96	106	116	130	145	154	161	170	177
1.22X10^{-1}	7.0	25	51	72	97	108	120	137	152	160	167	180	186
1.40X10^{-1}	8.0	25	50	73	97	113	124	142	157	164	172	183	194
1.57X10^{-1}	9.0	25	50	72	97	114	125	142	161	170	179	194	207
1.75X10^{-1}	10.0	25	50	72	96	113	124	142	159	175	183	197	208
1.92X10^{-1}	10.9	25	50	71	95	112	123	141	161	177	186	203	213
2.27X10^{-1}	12.8	25	50	73	99	117	128	145	164	179	185	204	215
2.62X10^{-1}	14.7	25	51	74	100	119	131	151	167	181	182	207	213
2.97X10^{-1}	16.6	24	51	75	102	122	134	154	169	181	183	211	217
3.32X10^{-1}	18.4	24	50	74	104	129	146	165	180	192	200	225	232
3.67X10^{-1}	20.2	24	49	73	104	127	145	166	186	203	217	247	249

TABLE I (Continued)

Brawley Cascade No. 1068 t = 7 r.l.

R r.l.		1.77 X10⁻³	3.53 X10⁻³	5.30 X10⁻³	7.07 X10⁻³	8.83 X10⁻³	1.06 X10⁻²	1.24 X10⁻²	1.41 X10⁻²	1.59 X10⁻²	1.77 X10⁻²	1.94 X10⁻²	2.12 X10⁻²
θ μ tan deg		50	100	150	200	250	300	350	400	450	500	550	600
1.75X10⁻²	1.0	13	26	35	38	46	52	52	52	52	51	54	54
3.49X10⁻²	2.0	30	64	89	104	118	129	134	142	147	156	162	164
5.24X10⁻²	3.0	37	76	109	129	145	162	173	183	192	204	212	222
6.98X10⁻²	4.0	37	79	117	138	156	177	190	204	213	231	242	251
8.73X10⁻²	5.0	40	83	122	148	168	190	209	225	236	254	266	279
1.05X10⁻¹	6.0	41	85	124	151	172	195	218	234	247	263	277	293
1.22X10⁻¹	7.0	41	87	126	153	176	199	225	240	255	278	293	307
1.40X10⁻¹	8.0	41	86	126	153	176	203	230	246	262	284	298	317
1.57X10⁻¹	9.0	41	87	127	156	181	211	238	253	268	288	304	322
1.75X10⁻¹	10.0	41	88	129	157	186	215	245	264	280	298	313	334
1.92X10⁻¹	10.9	42	90	130	157	186	213	242	264	279	299	311	337
2.27X10⁻¹	12.8	43	94	138	165	194	222	251	277	293	318	335	366
2.62X10⁻¹	14.7	43	93	137	164	194	221	252	280	294	319	335	360
2.97X10⁻¹	16.6	42	97	142	171	202	231	262	296	317	343	356	387
3.32X10⁻¹	18.4	42	97	142	171	200	231	263	300	324	353	369	404
3.67X10⁻¹	20.2	42	96	142	173	207	244	279	316	337	362	382	417

Brawley Cascade No. 1068 t = 9 r.l.

1.75X10⁻²	1.0	8	17	22	29	38	40	49	55	61	62	65	71
3.49X10⁻²	2.0	11	33	42	55	71	78	89	101	108	112	116	121
5.24X10⁻²	3.0	13	39	54	70	90	107	120	134	148	158	166	174
6.98X10⁻²	4.0	15	42	58	74	97	116	130	152	166	177	185	194
8.73X10⁻²	5.0	17	44	66	86	99	130	144	172	190	202	214	230
1.05X10⁻¹	6.0	17	44	65	87	111	134	150	181	203	215	227	245
1.22X10⁻¹	7.0	18	45	67	90	115	139	154	184	213	227	242	259
1.40X10⁻¹	8.0	18	45	71	94	122	148	164	198	230	245	260	279
1.57X10⁻¹	9.0	18	45	70	94	122	148	166	201	233	249	264	282
1.75X10⁻¹	10.0	18	45	69	93	121	145	164	205	240	261	276	292
1.92X10⁻¹	10.9	18	47	71	94	122	145	163	206	242	264	282	308
2.27X10⁻¹	12.8	18	47	73	96	124	145	165	212	250	276	296	321
2.62X10⁻¹	14.7	19	47	74	99	126	150	175	221	259	293	309	340
2.97X10⁻¹	16.6	18	48	78	102	129	156	183	231	274	307	326	359
3.32X10⁻¹	18.4	18	47	81	105	133	161	187	238	289	321	342	377
3.67X10⁻¹	20.2	18	47	81	108	140	169	198	251	309	341	361	397

TABLE I (Continued)

Brawley Cascade No. 1032 t = 5 r.l.

R r.l.		1.77 X10^{-3}	3.53 X10^{-3}	5.30 X10^{-3}	7.07 X10^{-3}	8.83 X10^{-3}	1.06 X10^{-2}	1.24 X10^{-2}	1.41 X10^{-2}	1.59 X10^{-2}	1.77 X10^{-2}	1.94 X10^{-2}	2.12 X10^{-2}
θ tan	μ deg	50	100	150	200	250	300	350	400	450	500	550	600
1.75X10^{-2}	1.0	19	28	31	43	44	47	48	50	50	51	51	51
3.49X10^{-2}	2.0	38	67	81	102	121	133	141	145	154	163	170	169
5.24X10^{-2}	3.0	42	78	94	119	140	156	169	174	187	199	205	204
6.98X10^{-2}	4.0	42	78	96	122	146	166	181	190	204	215	221	224
8.73X10^{-2}	5.0	42	79	100	127	152	173	189	200	212	224	231	233
1.05X10^{-1}	6.0	43	80	101	128	152	174	191	201	216	225	232	234
1.22X10^{-1}	7.0	43	80	102	131	155	179	199	211	228	242	250	262
1.40X10^{-1}	8.0	43	79	103	134	159	185	206	223	247	260	266	285
1.57X10^{-1}	9.0	44	80	105	137	162	189	209	226	251	267	275	298
1.75X10^{-1}	10.0	44	81	106	140	165	191	213	230	256	273	283	307
1.92X10^{-1}	10.9	44	81	106	139	165	194	215	231	257	277	288	311
2.27X10^{-1}	12.8	44	80	108	142	167	197	217	232	261	278	288	313
2.62X10^{-1}	14.7	44	79	107	146	171	200	220	232	269	284	294	320
2.97X10^{-1}	16.6	43	78	107	146	171	201	221	234	269	284	298	326
3.32X10^{-1}	18.4	43	77	108	148	172	202	223	241	275	289	297	330
3.67X10^{-1}	20.2	43	76	107	148	173	202	225	245	282	296	301	323

Brawley Cascade No. 1032 t = 7 r.l.

1.75X10^{-2}	1.0	10	28	38	51	56	65	73	77	77	78	78	78
3.49X10^{-2}	2.0	29	73	113	144	162	180	196	209	209	216	223	222
5.24X10^{-2}	3.0	33	85	135	171	195	216	235	251	254	262	272	271
6.98X10^{-2}	4.0	34	92	145	186	214	237	256	277	283	294	307	305
8.73X10^{-2}	5.0	36	97	152	195	226	251	271	296	300	312	329	328
1.05X10^{-1}	6.0	37	103	158	202	234	262	281	308	320	334	351	358
1.22X10^{-1}	7.0	37	103	161	210	243	274	293	323	336	359	376	388
1.40X10^{-1}	8.0	37	103	162	212	245	277	298	329	348	371	390	401
1.57X10^{-1}	9.0	37	103	164	217	251	282	304	337	354	382	405	420
1.75X10^{-1}	10.0	37	104	165	218	254	284	312	344	362	394	419	432
1.92X10^{-1}	10.9	37	104	165	217	255	284	315	349	371	404	432	447
2.27X10^{-1}	12.8	37	105	167	220	258	286	320	357	379	412	446	465
2.62X10^{-1}	14.7	37	106	172	227	268	294	331	369	397	428	461	481
2.97X10^{-1}	16.6	36	107	174	228	272	299	336	378	407	443	474	499
3.32X10^{-1}	18.4	37	107	177	231	274	303	343	384	417	462	493	511
3.67X10^{-1}	20.2	37	106	176	233	275	308	249	392	425	467	497	507

TABLE I (Continued)

Brawley Cascade No. 1032 t = 9 r.l.

R r.l.		1.77×10^{-3}	3.53×10^{-3}	5.30×10^{-3}	7.07×10^{-3}	8.83×10^{-3}	1.06×10^{-2}	1.24×10^{-2}	1.41×10^{-2}	1.59×10^{-2}	1.77×10^{-2}	1.94×10^{-2}	2.12×10^{-2}
θ tan	μ deg	50	100	150	200	250	300	350	400	450	500	550	600
1.75×10^{-2}	1.0	7	13	22	26	32	38	43	44	46	48	48	53
3.49×10^{-2}	2.0	18	40	64	86	103	118	128	139	152	163	162	175
5.24×10^{-2}	3.0	21	48	85	118	137	161	177	192	209	228	226	241
6.98×10^{-2}	4.0	22	52	91	127	148	173	190	209	226	244	244	267
8.73×10^{-2}	5.0	22	54	95	137	162	187	206	225	245	267	274	302
1.05×10^{-1}	6.0	22	55	95	138	163	189	208	230	251	273	280	313
1.22×10^{-1}	7.0	23	57	97	141	165	194	213	236	255	283	290	327
1.40×10^{-1}	8.0	23	57	99	142	166	194	212	236	256	282	294	332
1.57×10^{-1}	9.0	23	57	98	143	168	198	216	247	266	290	308	349
1.75×10^{-1}	10.0	23	57	98	142	167	195	216	246	266	289	309	347
1.92×10^{-1}	10.9	23	59	100	145	172	199	221	250	272	294	317	357
2.27×10^{-1}	12.8	23	58	100	149	177	206	231	264	288	310	337	373
2.62×10^{-1}	14.7	23	57	100	150	180	209	233	266	294	310	343	377
2.97×10^{-1}	16.6	22	56	100	149	182	211	235	266	297	316	355	391
3.32×10^{-1}	18.4	24	58	104	153	185	219	242	274	318	341	383	427
3.67×10^{-1}	20.2	24	57	104	153	184	216	240	272	318	343	386	424

Brawley Cascade No. 1101 t = 5 r.l.

1.75×10^{-2}	1.0	11	17	22	30	32	36	41	43	43	42	42	44
3.49×10^{-2}	2.0	30	46	57	77	87	100	114	119	124	126	126	130
5.24×10^{-2}	3.0	34	52	66	91	104	121	136	143	152	160	162	169
6.98×10^{-2}	4.0	34	55	70	101	120	144	159	173	183	192	196	205
8.73×10^{-2}	5.0	34	55	72	103	125	149	166	180	191	202	213	223
1.05×10^{-1}	6.0	35	57	74	106	128	153	170	188	199	209	220	234
1.22×10^{-1}	7.0	36	59	76	99	132	160	177	194	204	215	228	241
1.40×10^{-1}	8.0	36	59	77	99	134	163	180	198	207	217	234	244
1.57×10^{-1}	9.0	38	61	80	112	137	165	183	200	212	223	240	253
1.75×10^{-1}	10.0	38	63	82	113	138	167	186	205	217	227	239	256
1.92×10^{-1}	10.9	38	64	82	114	142	173	190	208	223	234	247	262
2.27×10^{-1}	12.8	39	66	86	118	146	179	201	227	240	254	270	282
2.62×10^{-1}	14.7	39	65	85	115	145	181	203	227	250	262	283	291
2.97×10^{-1}	16.6	39	65	85	115	143	177	197	223	242	252	270	273
3.32×10^{-1}	18.4	40	67	87	117	148	185	205	229	252	261	282	282
3.67×10^{-1}	20.2	41	71	90	120	152	192	212	235	259	273	302	298

TABLE I (Continued)

Brawley Cascade No. 1101 t = 7 r.l.

R r.l.		1.77×10^{-3}	3.53×10^{-3}	5.30×10^{-3}	7.07×10^{-3}	8.83×10^{-3}	1.06×10^{-2}	1.24×10^{-2}	1.41×10^{-2}	1.59×10^{-2}	1.77×10^{-2}	1.94×10^{-2}	2.12×10^{-2}
θ tan / μ deg		50	100	150	200	250	300	350	400	450	500	550	600
1.75×10^{-2}	1.0	28	43	53	60	66	70	73	74	76	75	78	78
3.49×10^{-2}	2.0	50	79	104	118	131	141	147	154	162	165	168	167
5.24×10^{-2}	3.0	59	91	123	143	158	174	186	191	202	207	214	216
6.98×10^{-2}	4.0	60	97	133	159	174	194	212	219	231	238	244	248
8.73×10^{-2}	5.0	62	101	141	169	184	204	225	239	255	265	270	278
1.05×10^{-1}	6.0	63	105	146	178	195	215	237	252	270	278	289	298
1.22×10^{-1}	7.0	63	105	147	179	195	219	241	257	276	285	298	305
1.40×10^{-1}	8.0	63	104	148	179	197	221	242	260	280	289	300	308
1.57×10^{-1}	9.0	63	104	147	178	197	222	245	264	285	296	310	319
1.75×10^{-1}	10.0	64	105	148	178	197	221	245	262	285	294	311	331
1.92×10^{-1}	10.9	64	106	148	180	200	223	245	263	288	304	326	344
2.27×10^{-1}	12.8	65	107	152	185	205	229	253	271	297	315	336	354
2.62×10^{-1}	14.7	65	107	153	185	205	232	255	275	304	329	348	367
2.97×10^{-1}	16.6	64	106	153	186	212	236	260	281	308	332	350	369
3.32×10^{-1}	18.4	64	106	153	185	212	234	257	276	317	336	362	379
3.67×10^{-1}	20.2	64	107	154	184	211	232	263	280	319	343	362	377

Brawley Cascade No. 1101 t = 9 r.l.

1.75×10^{-2}	1.0	23	50	58	73	82	85	89	95	103	104	109	118
3.49×10^{-2}	2.0	34	82	107	133	154	161	167	180	207	217	227	240
5.24×10^{-2}	3.0	38	95	127	165	194	209	220	243	280	293	307	331
6.98×10^{-2}	4.0	38	101	139	176	207	228	245	272	318	332	354	382
8.73×10^{-2}	5.0	38	103	142	186	221	246	262	291	338	356	379	409
1.05×10^{-1}	6.0	39	107	146	190	225	252	269	301	348	369	393	426
1.22×10^{-1}	7.0	40	109	148	195	232	264	286	320	366	390	416	448
1.40×10^{-1}	8.0	42	111	153	200	238	274	297	333	378	404	428	464
1.57×10^{-1}	9.0	42	111	153	200	238	276	297	333	381	407	431	465
1.75×10^{-1}	10.0	42	111	152	199	238	278	302	336	383	417	444	483
1.92×10^{-1}	10.9	42	111	153	202	242	282	305	340	386	421	451	488
2.27×10^{-1}	12.8	42	110	153	202	243	285	308	344	395	435	466	503
2.62×10^{-1}	14.7	42	109	153	202	246	291	314	353	406	447	478	512
2.97×10^{-1}	16.6	42	111	155	205	251	293	315	356	410	448	484	523
3.32×10^{-1}	18.4	42	111	154	205	252	295	322	358	418	457	491	535
3.67×10^{-1}	20.2	42	111	154	205	254	297	329	370	431	476	508	548

TABLE I (Continued)

Brawley Cascade No. 1150 t = 5 r.l.

R r.l.		1.77 X10⁻³	3.53 X10⁻³	5.30 X10⁻³	7.07 X10⁻³	8.83 X10⁻³	1.06 X10⁻²	1.24 X10⁻²	1.41 X10⁻²	1.59 X10⁻²	1.77 X10⁻²	1.94 X10⁻²	2.12 X10⁻²
θ tan	μ deg	50	100	150	200	250	300	350	400	450	500	550	600
1.75X10⁻²	1.0	22	40	61	67	75	79	83	86	88	87	89	89
3.49X10⁻²	2.0	27	50	77	87	98	109	114	117	119	120	128	127
5.24X10⁻²	3.0	34	71	101	117	133	149	154	161	166	174	183	193
6.98X10⁻²	4.0	36	78	109	127	146	163	169	180	188	195	204	216
8.73X10⁻²	5.0	38	82	114	132	151	169	174	184	196	208	218	232
1.05X10⁻¹	6.0	38	82	113	131	151	170	177	185	200	212	226	240
1.22X10⁻¹	7.0	38	84	116	134	154	175	183	191	204	218	231	246
1.40X10⁻¹	8.0	38	83	117	135	158	179	186	193	207	220	232	248
1.57X10⁻¹	9.0	38	83	117	135	159	181	187	195	215	228	239	253
1.75X10⁻¹	10.0	38	83	116	134	158	181	190	196	218	232	244	261
1.92X10⁻¹	10.9	38	84	116	134	158	181	188	198	221	239	251	269
2.27X10⁻¹	12.8	38	84	116	134	158	183	193	202	223	248	262	279
2.62X10⁻¹	14.7	38	83	115	138	162	191	200	210	235	258	274	296
2.97X10⁻¹	16.6	37	83	114	139	168	198	208	220	244	268	278	309
3.32X10⁻¹	18.4	37	83	116	144	177	208	218	227	256	281	292	325
3.67X10⁻¹	20.2	38	83	115	144	177	208	220	227	259	286	298	336

Brawley Cascade No. 1150 t = 7 r.l.

1.75X10⁻²	1.0	13	19	28	34	36	40	45	48	52	51	51	51
3.49X10⁻²	2.0	21	39	57	71	76	88	98	109	123	128	131	133
5.24X10⁻²	3.0	24	44	68	86	95	116	129	142	157	162	164	171
6.98X10⁻²	4.0	25	46	73	96	108	128	143	158	178	182	184	190
8.73X10⁻²	5.0	26	47	75	98	112	134	149	165	187	194	195	200
1.05X10⁻¹	6.0	26	47	75	99	115	139	156	174	200	208	209	214
1.22X10⁻¹	7.0	26	49	79	104	119	147	164	181	206	213	213	217
1.40X10⁻¹	8.0	26	50	81	105	120	148	167	185	209	218	217	222
1.57X10⁻¹	9.0	26	50	80	107	122	151	169	187	214	221	222	228
1.75X10⁻¹	10.0	26	50	79	105	122	152	170	188	214	221	221	230
1.92X10⁻¹	10.9	26	51	81	107	124	154	170	190	215	222	222	231
2.27X10⁻¹	12.8	26	51	82	107	124	153	171	189	214	220	221	230
2.62X10⁻¹	14.7	26	50	80	108	126	155	171	189	215	221	222	230
2.97X10⁻¹	16.6	25	49	79	109	127	156	172	189	214	219	222	231
3.32X10⁻¹	18.4	25	49	80	109	127	155	172	188	214	221	221	230
3.67X10⁻¹	20.2	25	49	80	109	125	154	171	189	214	221	221	230

TABLE I (Continued)

Brawley Cascade No. 1045 t = 4 r.l.

R r.l.		1.77 X10⁻³	3.53 X10⁻³	5.30 X10⁻³	7.07 X10⁻³	8.83 X10⁻³	1.06 X10⁻²	1.24 X10⁻²	1.41 X10⁻²	1.59 X10⁻²	1.77 X10⁻²	1.94 X10⁻²	2.12 X10⁻²
θ tan \ μ deg		50	100	150	200	250	300	350	400	450	500	550	600
1.75X10⁻²	1.0	15	38	45	53	59	66	70	75	77	78	78	78
3.49X10⁻²	2.0	33	73	89	105	124	135	144	155	162	169	168	169
5.24X10⁻²	3.0	41	84	102	121	143	166	176	191	206	214	212	219
6.98X10⁻²	4.0	43	89	107	125	152	182	197	217	233	242	242	249
8.73X10⁻²	5.0	44	91	110	133	162	194	213	236	250	259	266	274
1.05X10⁻¹	6.0	46	96	115	140	168	204	224	251	269	276	283	293
1.22X10⁻¹	7.0	47	97	119	145	172	209	231	258	277	289	299	308
1.40X10⁻¹	8.0	48	97	120	147	174	211	234	264	284	297	308	316
1.57X10⁻¹	9.0	48	98	120	149	175	213	235	264	285	302	313	320
1.75X10⁻¹	10.0	48	98	119	147	173	209	233	262	282	301	310	315
1.92X10⁻¹	10.9	48	98	120	149	176	212	235	264	284	302	312	322
2.27X10⁻¹	12.8	51	102	124	157	184	220	246	276	295	318	328	336
2.62X10⁻¹	14.7	51	102	125	158	187	223	253	285	305	326	339	350
2.97X10⁻¹	16.6	51	103	128	167	198	237	272	304	321	343	349	360
3.32X10⁻¹	18.4	52	104	131	174	204	244	277	312	333	360	368	370
3.67X10⁻¹	20.2	52	103	130	174	205	245	279	319	339	368	378	372

Brawley Cascade No. 1045 t = 6 r.l.

1.75X10⁻²	1.0	16	34	44	56	64	69	73	76	78	77	84	84
3.49X10⁻²	2.0	39	68	92	116	138	153	167	176	182	193	205	207
5.24X10⁻²	3.0	45	77	106	137	166	186	207	220	233	252	262	275
6.98X10⁻²	4.0	45	79	109	140	172	192	213	230	245	265	276	290
8.73X10⁻²	5.0	47	82	113	145	184	204	227	246	267	289	301	315
1.05X10⁻¹	6.0	48	84	118	150	189	212	238	259	279	304	319	331
1.22X10⁻¹	7.0	48	85	119	152	192	217	243	263	283	314	327	341
1.40X10⁻¹	8.0	48	85	121	154	195	219	248	267	285	318	332	348
1.57X10⁻¹	9.0	48	85	120	154	193	219	248	268	285	316	331	349
1.75X10⁻¹	10.0	48	86	121	153	194	220	248	270	286	320	340	359
1.92X10⁻¹	10.9	49	87	122	154	195	219	247	271	286	321	341	362
2.27X10⁻¹	12.8	49	86	121	153	195	220	246	273	291	326	351	376
2.62X10⁻¹	14.7	49	86	122	156	198	222	250	275	293	331	357	388
2.97X10⁻¹	16.6	48	89	124	162	207	234	260	285	305	340	363	396
3.32X10⁻¹	18.4	49	92	128	167	213	244	268	300	321	355	387	420
3.67X10⁻¹	20.2	49	91	128	167	214	244	266	302	323	364	399	426

TABLE I (Continued)

Brawley Cascade No. 1045 t = 8 r.l.

R r.l.		$1.77_{X10^{3}}$	$3.53_{X10^{3}}$	$5.30_{X10^{3}}$	$7.07_{X10^{3}}$	$8.83_{X10^{3}}$	$1.06_{X10^{2}}$	$1.24_{X10^{2}}$	$1.41_{X10^{2}}$	$1.59_{X10^{2}}$	$1.77_{X10^{2}}$	$1.94_{X10^{2}}$	$2.12_{X10^{2}}$
θ tan \ μ deg		50	100	150	200	250	300	350	400	450	500	550	600
$1.75X10^{-2}$	1.0	6	24	35	41	57	64	66	69	71	70	70	70
$3.49X10^{-2}$	2.0	14	47	70	96	125	135	144	156	165	167	169	173
$5.24X10^{-2}$	3.0	16	55	86	118	152	166	176	193	205	213	219	226
$6.98X10^{-2}$	4.0	18	59	93	129	167	187	199	222	236	242	253	262
$8.73X10^{-2}$	5.0	18	59	94	135	173	195	208	233	247	256	268	279
$1.05X10^{-1}$	6.0	19	60	96	138	178	202	219	243	259	266	281	293
$1.22X10^{-1}$	7.0	19	61	97	145	187	212	230	255	274	281	294	311
$1.40X10^{-1}$	8.0	19	61	99	146	191	217	236	259	279	286	297	313
$1.57X10^{-1}$	9.0	19	61	98	146	192	219	240	264	283	291	302	320
$1.75X10^{-1}$	10.0	19	61	97	145	191	217	237	263	283	297	312	331
$1.92X10^{-1}$	10.9	19	61	97	145	192	217	237	262	280	296	313	337
$2.27X10^{-1}$	12.8	19	61	96	143	193	219	241	270	291	305	330	352
$2.62X10^{-1}$	14.7	20	62	98	145	198	226	254	285	310	322	352	381
$2.97X10^{-1}$	16.6	19	62	97	147	201	230	257	289	314	322	353	375
$3.32X10^{-1}$	18.4	19	61	96	146	200	231	259	294	317	324	369	388
$3.67X10^{-1}$	20.2	20	61	98	148	201	234	265	306	323	332	375	399

TABLE II

N(<R) vs N(<θ) for SSS Cascades

SSS Cascade No. 51 t = 4.2 r.l.

R r.l.		3.09 X10⁻³	6.17 X10⁻³	9.26 X10⁻³	1.23 X10⁻²	1.85 X10⁻²	2.47 X10⁻²	3.09 X10⁻²	3.70 X10⁻²	4.32 X10⁻²	4.94 X10⁻²	5.56 X10⁻²	6.17 X10⁻²	6.79 X10⁻²	7.41 X10⁻²
θ tan	μ deg	25	50	75	100	150	200	250	300	350	400	450	500	550	600
1.75X10⁻²	1.0	15	29	37	39	44	51	53	53	57	59	59	58	58	58
3.49X10⁻²	2.0	37	66	88	95	116	134	141	147	152	155	157	161	161	161
5.24X10⁻²	3.0	44	78	103	113	146	170	186	194	204	210	218	228	227	227
6.98X10⁻²	4.0	45	81	106	117	152	178	202	212	227	242	249	264	268	267
8.73X10⁻²	5.0	48	85	110	121	158	186	216	229	242	262	273	291	298	296
1.05X10⁻¹	6.0	48	86	111	123	162	194	225	242	257	283	295	320	331	329
1.22X10⁻¹	7.0	48	87	110	124	164	196	227	244	260	285	300	325	336	342
1.40X10⁻¹	8.0	48	88	111	125	166	199	230	248	267	293	308	335	345	350
1.57X10⁻¹	9.0	49	88	112	126	167	203	237	255	275	302	317	343	354	364
1.75X10⁻¹	10.0	49	88	112	127	170	206	240	258	280	307	321	349	361	372
1.92X10⁻¹	10.9	49	87	113	128	171	208	241	261	285	313	326	353	367	377
2.27X10⁻¹	12.8	49	87	114	128	172	208	243	263	286	314	329	357	374	381
2.62X10⁻¹	14.7	49	88	117	131	176	212	247	267	293	320	337	363	381	384
2.97X10⁻¹	16.6	49	89	118	131	176	211	247	269	296	321	336	361	376	383
3.32X10⁻¹	18.4	49	89	118	130	174	211	246	269	297	329	342	372	385	391
3.67X10⁻¹	20.2	49	89	118	130	173	210	243	265	291	322	339	370	381	388
		SSS Cascade No. 51 t = 5.9 r.l.													
1.75X10⁻²	1.0	29	60	68	77	91	99	103	107	108	110	110	109	114	114
3.49X10⁻²	2.0	33	76	94	115	145	171	181	195	200	207	207	211	216	216
5.24X10⁻²	3.0	34	79	102	128	175	224	250	271	286	302	304	312	316	319
6.98X10⁻²	4.0	34	85	112	141	193	251	289	317	338	363	372	389	401	406
8.73X10⁻²	5.0	34	85	115	145	202	262	306	337	363	397	408	443	460	464
1.05X10⁻¹	6.0	34	85	117	148	210	277	326	362	397	442	456	495	516	520
1.22X10⁻¹	7.0	34	85	118	150	215	282	334	372	412	458	471	512	536	547
1.40X10⁻¹	8.0	34	85	118	150	216	283	336	374	416	463	476	521	544	554
1.57X10⁻¹	9.0	34	85	118	150	217	285	338	378	422	472	487	533	555	564
1.75X10⁻¹	10.0	34	85	119	152	219	287	340	383	428	477	495	544	564	572
1.92X10⁻¹	10.9	34	84	119	152	219	288	343	388	436	486	505	557	581	591
2.27X10⁻¹	12.8	34	84	120	152	223	291	346	391	441	494	513	568	598	605
2.62X10⁻¹	14.7	34	85	122	155	225	293	348	397	448	503	526	578	611	614
2.97X10⁻¹	16.6	34	85	122	154	224	291	348	398	451	512	541	593	624	625
3.32X10⁻¹	18.4	34	85	122	154	226	295	354	403	456	519	548	598	635	640
3.67X10⁻¹	20.2	34	85	122	155	227	296	356	405	458	521	548	604	644	650

TABLE II (Continued)

SSS Cascade No. 51 t = 7.5 r.l.

R r.l.		3.09 X10^{-3}	6.17 X10^{-3}	9.26 X10^{-3}	1.23 X10^{-2}	1.85 X10^{-2}	2.47 X10^{-2}	3.09 X10^{-2}	3.70 X10^{-2}	4.32 X10^{-2}	4.94 X10^{-2}	5.56 X10^{-2}	6.17 X10^{-2}	6.79 X10^{-2}	7.41 X10^{-2}
θ tan	μ deg	25	50	75	100	150	200	250	300	350	400	450	500	550	600
1.75X10^{-2}	1.0	10	21	34	45	56	64	69	70	70	70	72	71	71	71
3.49X10^{-2}	2.0	31	62	105	136	180	210	235	245	252	253	259	261	261	261
5.24X10^{-2}	3.0	39	80	131	171	232	278	313	330	343	347	356	373	372	378
6.98X10^{-2}	4.0	39	83	141	184	256	316	364	390	403	414	431	449	448	458
8.73X10^{-2}	5.0	40	87	147	191	273	338	393	427	449	465	484	503	515	539
1.05X10^{-1}	6.0	40	87	149	194	281	358	420	456	489	513	537	565	592	621
1.22X10^{-1}	7.0	42	89	151	199	293	373	443	482	520	552	587	615	641	681
1.40X10^{-1}	8.0	43	91	153	202	301	385	459	501	550	589	630	659	690	737
1.57X10^{-1}	9.0	43	91	154	204	305	392	474	518	573	613	656	691	729	787
1.75X10^{-1}	10.0	43	91	154	204	305	393	479	525	582	625	669	707	742	810
1.92X10^{-1}	10.9	43	90	154	205	307	396	486	532	592	639	682	728	765	838
2.27X10^{-1}	12.8	43	91	155	205	312	403	501	548	610	659	704	747	800	879
2.62X10^{-1}	14.7	44	92	157	207	313	408	507	557	620	674	720	762	819	908
2.97X10^{-1}	16.6	44	92	157	208	317	412	513	565	629	685	733	776	835	937
3.32X10^{-1}	18.4	44	92	157	208	318	414	515	565	633	691	740	784	841	942
3.67X10^{-1}	20.2	44	92	157	209	320	417	519	569	641	699	754	808	864	968

SSS Cascade No. 51 t = 9.3 r.l.

1.75X10^{-2}	1.0	3	7	15	19	25	29	38	40	40	43	43	44	44	44
3.49X10^{-2}	2.0	6	21	42	60	90	112	137	151	158	169	181	185	188	188
5.24X10^{-2}	3.0	6	26	48	66	103	135	170	193	209	230	248	256	263	266
6.98X10^{-2}	4.0	7	28	52	72	111	149	188	216	237	263	284	299	311	322
8.73X10^{-2}	5.0	8	29	55	78	122	161	203	237	260	293	318	337	354	369
1.05X10^{-1}	6.0	8	29	55	79	124	167	214	248	274	322	352	382	403	424
1.22X10^{-1}	7.0	8	29	55	81	129	174	223	260	290	342	375	414	440	460
1.40X10^{-1}	8.0	8	29	56	83	131	179	232	270	301	355	388	433	461	488
1.57X10^{-1}	9.0	9	31	58	86	133	182	235	274	306	364	397	441	468	501
1.75X10^{-1}	10.0	10	31	59	88	137	188	242	284	318	378	412	458	491	525
1.92X10^{-1}	10.9	10	31	59	88	138	189	244	288	322	384	417	462	499	538
2.27X10^{-1}	12.8	10	32	60	88	141	192	247	291	325	386	425	471	514	561
2.62X10^{-1}	14.7	10	32	60	88	141	194	250	297	333	397	440	483	529	574
2.97X10^{-1}	16.6	10	32	60	87	142	195	252	301	333	401	446	494	540	595
3.32X10^{-1}	18.4	10	32	60	86	140	193	251	299	334	403	448	498	545	611
3.67X10^{-1}	20.2	10	33	60	88	143	197	255	305	338	406	451	505	552	616

TABLE II (Continued)

SSS Cascade No. 59 t = 3.7 r.l.

R r.l.		3.09 X10^{-3}	6.17 X10^{-3}	9.26 X10^{-3}	1.23 X10^{-2}	1.85 X10^{-2}	2.47 X10^{-2}	3.09 X10^{-2}	3.70 X10^{-2}	4.32 X10^{-2}	4.94 X10^{-2}	5.56 X10^{-2}	6.17 X10^{-2}	6.79 X10^{-2}	7.41 X10^{-2}
θ tan	μ deg	25	50	75	100	150	200	250	300	350	400	450	500	550	600
1.75X10^{-2}	1.0	15	24	29	32	39	39	39	39	39	39	39	38	38	38
3.49X10^{-2}	2.0	25	46	58	66	76	77	77	78	78	78	78	77	77	77
5.24X10^{-2}	3.0	28	53	67	76	86	88	91	91	91	90	90	89	88	88
6.98X10^{-2}	4.0	30	56	72	83	96	100	105	105	108	107	106	105	104	106
8.73X10^{-2}	5.0	30	56	73	83	99	104	111	113	115	114	113	111	110	114
1.05X10^{-1}	6.0	30	56	73	84	100	106	115	119	122	121	119	120	118	124
1.22X10^{-1}	7.0	30	56	72	84	100	105	114	117	123	121	118	118	116	122
1.40X10^{-1}	8.0	30	56	72	85	103	109	121	123	128	129	126	128	127	132
1.57X10^{-1}	9.0	30	56	72	85	103	111	122	125	129	135	132	133	131	138
1.75X10^{-1}	10.0	30	56	72	85	103	112	123	125	131	138	134	135	134	139
1.92X10^{-1}	10.9	30	56	73	87	105	114	124	129	134	140	137	141	139	144
2.27X10^{-1}	12.8	30	57	74	87	105	114	125	132	138	149	146	148	147	151
2.62X10^{-1}	14.7	30	57	74	87	104	112	125	132	140	150	149	148	145	151
2.97X10^{-1}	16.6	30	57	74	86	105	111	124	133	142	153	152	151	151	158
3.32X10^{-1}	18.4	30	57	75	86	104	113	125	132	143	156	161	159	159	168
3.67X10^{-1}	20.2	30	57	75	86	103	112	127	134	143	159	166	162	168	184

SSS Cascade No. 59 t = 5.2 r.l.

1.75X10^{-2}	1.0	25	37	44	50	55	58	59	60	60	60	60	59	59	59
3.49X10^{-2}	2.0	26	45	56	64	76	83	84	86	86	88	90	89	89	89
5.24X10^{-2}	3.0	32	60	78	93	114	132	143	148	151	153	157	161	160	163
6.98X10^{-2}	4.0	33	62	82	98	125	150	163	172	176	182	185	195	194	196
8.73X10^{-2}	5.0	33	62	84	99	131	159	174	185	187	193	198	212	213	214
1.05X10^{-1}	6.0	35	64	87	103	136	166	182	197	200	209	213	230	230	234
1.22X10^{-1}	7.0	35	66	90	107	146	177	199	215	221	230	238	254	257	260
1.40X10^{-1}	8.0	35	66	90	107	147	180	202	222	233	247	254	271	273	275
1.57X10^{-1}	9.0	35	66	90	108	149	186	207	229	241	256	265	281	288	288
1.75X10^{-1}	10.0	37	68	92	110	151	188	210	233	246	263	277	296	303	303
1.92X10^{-1}	10.9	37	67	92	110	151	188	210	237	251	273	286	306	320	318
2.27X10^{-1}	12.8	37	68	93	110	152	190	217	246	261	287	298	321	338	337
2.62X10^{-1}	14.7	37	68	93	110	152	189	216	248	268	295	306	326	341	338
2.97X10^{-1}	16.6	37	68	93	109	152	189	215	248	270	301	316	339	354	352
3.32X10^{-1}	18.4	37	68	93	108	151	189	217	250	273	307	330	352	366	369
3.67X10^{-1}	20.2	37	69	94	111	154	191	218	253	275	310	331	352	369	370

TABLE II (Continued)

SSS Cascade No. 59 t = 6.8 r.l.

R r.l.		3.09×10^{-3}	6.17×10^{-3}	9.26×10^{-3}	1.23×10^{-2}	1.85×10^{-2}	2.47×10^{-2}	3.09×10^{-2}	3.70×10^{-2}	4.32×10^{-2}	4.94×10^{-2}	5.56×10^{-2}	6.17×10^{-2}	6.79×10^{-2}	7.41×10^{-2}
θ tan \ μ deg		25	50	75	100	150	200	250	300	350	400	450	500	550	600
1.75×10^{-2}	1.0	2	10	15	17	25	26	27	28	28	28	28	29	29	32
3.49×10^{-2}	2.0	4	17	30	40	66	72	78	80	81	83	85	86	89	95
5.24×10^{-2}	3.0	7	20	36	52	83	99	111	116	121	122	128	132	136	142
6.98×10^{-2}	4.0	7	21	42	61	97	122	136	145	153	154	161	164	171	176
8.73×10^{-2}	5.0	7	21	45	69	109	137	158	172	185	187	200	209	219	225
1.05×10^{-1}	6.0	7	21	45	69	111	143	171	191	204	208	224	236	247	253
1.22×10^{-1}	7.0	7	21	44	70	115	151	183	202	218	223	238	257	268	274
1.40×10^{-1}	8.0	7	21	44	73	122	161	195	214	232	240	261	281	294	299
1.57×10^{-1}	9.0	7	21	45	74	124	164	201	222	239	247	270	292	306	310
1.75×10^{-1}	10.0	7	22	46	75	126	167	204	228	246	259	281	302	317	320
1.92×10^{-1}	10.9	7	21	46	75	128	171	212	238	260	275	300	327	352	356
2.27×10^{-1}	12.8	7	23	48	76	129	172	216	244	269	283	307	334	364	377
2.62×10^{-1}	14.7	7	23	48	77	131	177	224	254	280	300	325	354	285	399
2.97×10^{-1}	16.6	7	23	48	76	130	178	226	256	284	308	333	360	389	401
3.32×10^{-1}	18.4	7	23	48	75	128	178	227	257	288	311	343	370	399	414
3.67×10^{-1}	20.2	7	23	48	75	127	176	225	259	292	318	349	380	412	425

SSS Cascade No. 59 t = 8.3 r.l.

1.75×10^{-2}	1.0	6	11	11	15	17	19	20	21	22	24	24	23	23	23
3.49×10^{-2}	2.0	9	21	28	35	41	47	53	57	60	63	63	62	62	62
5.24×10^{-2}	3.0	11	30	39	48	63	76	89	96	105	118	124	125	127	127
6.98×10^{-2}	4.0	12	34	44	53	72	91	104	114	129	145	158	168	172	171
8.73×10^{-2}	5.0	12	34	45	58	83	105	123	140	159	179	196	205	209	207
1.05×10^{-1}	6.0	12	35	46	60	86	116	137	157	182	201	219	236	241	242
1.22×10^{-1}	7.0	13	36	47	62	90	123	149	172	202	227	248	267	278	280
1.40×10^{-1}	8.0	13	37	49	64	94	128	157	184	214	243	264	284	296	304
1.57×10^{-1}	9.0	13	37	49	64	93	129	157	187	219	249	272	291	308	317
1.75×10^{-1}	10.0	13	37	49	64	95	132	161	194	226	260	288	310	324	335
1.92×10^{-1}	10.9	13	36	49	65	97	135	164	201	235	270	298	320	336	347
2.27×10^{-1}	12.8	13	36	49	64	101	140	172	210	244	289	332	355	380	387
2.62×10^{-1}	14.7	13	37	50	65	103	144	176	215	249	296	339	368	394	400
2.97×10^{-1}	16.6	13	37	51	66	107	146	180	219	252	298	344	378	403	413
3.32×10^{-1}	18.4	13	37	51	65	106	146	185	226	265	311	358	392	419	436
3.67×10^{-1}	20.2	14	37	51	68	109	149	190	230	271	321	368	401	426	447

TABLE II (Continued)

SSS Cascade No. 133 t = 3.7 r.l.

R r.l.		3.09 X10^{-3}	6.17 X10^{-3}	9.26 X10^{-3}	1.23 X10^{-2}	1.85 X10^{-2}	2.47 X10^{-2}	3.09 X10^{-2}	3.70 X10^{-2}	4.32 X10^{-2}	4.94 X10^{-2}	5.56 X10^{-2}	6.17 X10^{-2}	6.79 X10^{-2}	7.41 X10^{-2}
θ tan	μ deg	25	50	75	100	150	200	250	300	350	400	450	500	550	600
1.75X10^{-2}	1.0	1	5	7	9	10	10	10	10	10	10	10	10	10	10
3.49X10^{-2}	2.0	5	14	19	23	25	25	25	25	26	26	26	26	26	26
5.24X10^{-2}	3.0	5	15	20	26	29	29	30	30	31	31	31	31	33	33
6.98X10^{-2}	4.0	8	19	24	31	35	35	36	37	40	40	40	41	44	43
8.73X10^{-2}	5.0	8	19	24	31	37	38	39	40	43	42	42	43	46	45
1.05X10^{-1}	6.0	8	19	24	31	38	39	41	42	45	45	44	45	47	46
1.22X10^{-1}	7.0	9	22	27	34	41	43	45	47	50	49	47	48	50	48
1.40X10^{-1}	8.0	9	22	27	34	41	43	46	49	51	50	48	48	52	49
1.57X10^{-1}	9.0	9	22	27	34	41	43	48	50	52	52	50	51	54	51
1.75X10^{-1}	10.0	9	22	27	34	41	43	48	50	51	50	48	49	54	50
1.92X10^{-1}	10.9	10	23	28	35	42	45	50	52	53	52	49	50	54	50
2.27X10^{-1}	12.8	10	23	28	35	43	48	52	53	55	57	53	52	56	58
2.62X10^{-1}	14.7	10	23	28	35	43	48	54	56	58	61	59	57	60	64
2.97X10^{-1}	16.6	10	23	28	35	43	49	56	58	59	62	61	58	62	64
3.32X10^{-1}	18.4	10	23	28	35	44	51	57	60	60	65	63	59	65	69
3.67X10^{-1}	20.2	10	23	28	34	44	49	54	56	60	65	66	62	68	75

SSS Cascade No. 133 t = 5.2 r.l.

1.75X10^{-2}	1.0	4	13	15	17	19	20	20	20	20	20	24	24	24	24
3.49X10^{-2}	2.0	5	16	20	23	31	33	34	35	35	35	39	39	39	39
5.24X10^{-2}	3.0	8	23	31	41	58	62	64	66	66	66	70	70	69	69
6.98X10^{-2}	4.0	11	26	35	48	69	74	76	79	80	80	84	83	83	82
8.73X10^{-2}	5.0	11	26	35	48	70	77	80	86	89	88	92	93	95	94
1.05X10^{-1}	6.0	11	26	35	49	72	82	88	95	98	98	103	104	105	104
1.22X10^{-1}	7.0	11	27	36	51	75	86	92	101	104	109	117	119	123	121
1.40X10^{-1}	8.0	11	27	37	52	77	89	99	110	113	120	128	129	133	133
1.57X10^{-1}	9.0	11	27	37	52	78	90	102	112	115	126	136	136	139	142
1.75X10^{-1}	10.0	11	27	37	52	78	90	102	114	117	130	144	147	153	154
1.92X10^{-1}	10.9	11	27	37	52	79	92	106	118	122	136	149	151	156	161
2.27X10^{-1}	12.8	11	27	37	52	79	92	107	120	124	140	154	158	162	172
2.62X10^{-1}	14.7	12	28	38	53	80	94	111	125	130	146	166	169	172	181
2.97X10^{-1}	16.6	12	28	38	53	79	95	112	129	135	151	170	175	178	189
3.32X10^{-1}	18.4	12	28	38	53	78	95	114	131	138	154	178	181	184	197
3.67X10^{-1}	20.2	12	28	38	52	78	94	114	130	137	152	181	183	187	200

TABLE II (Continued)

SSS Cascade No. 133 t = 6.7 r.l.

R r.l.		3.09×10^{-3}	6.17×10^{-3}	9.26×10^{-3}	1.23×10^{-2}	1.85×10^{-2}	2.47×10^{-2}	3.09×10^{-2}	3.70×10^{-2}	4.32×10^{-2}	4.94×10^{-2}	5.56×10^{-2}	6.17×10^{-2}	6.79×10^{-2}	7.41×10^{-2}
θ tan	μ deg	25	50	75	100	150	200	250	300	350	400	450	500	550	600
1.75×10^{-2}	1.0	4	11	11	16	25	27	29	30	31	31	31	31	31	31
3.49×10^{-2}	2.0	4	12	15	21	36	40	45	47	48	50	52	52	52	55
5.24×10^{-2}	3.0	6	17	21	28	52	63	70	75	78	81	83	83	85	87
6.98×10^{-2}	4.0	6	21	25	33	59	70	79	84	88	93	97	100	106	107
8.73×10^{-2}	5.0	6	21	25	34	63	76	86	92	96	100	104	107	113	114
1.05×10^{-1}	6.0	6	21	26	35	65	80	92	97	101	109	114	118	122	124
1.22×10^{-1}	7.0	6	22	27	36	66	81	92	101	105	114	118	122	126	127
1.40×10^{-1}	8.0	6	22	27	36	67	83	94	108	110	121	125	127	132	131
1.57×10^{-1}	9.0	6	22	28	37	69	85	98	112	118	129	137	139	142	145
1.75×10^{-1}	10.0	6	22	28	37	71	87	102	117	122	132	140	144	148	149
1.92×10^{-1}	10.9	6	22	28	37	71	87	102	119	127	136	145	150	155	156
2.27×10^{-1}	12.8	6	22	28	37	71	88	103	121	130	139	152	159	165	167
2.62×10^{-1}	14.7	6	23	29	39	74	92	108	126	136	144	160	165	175	176
2.97×10^{-1}	16.6	6	23	31	41	75	93	111	129	138	151	166	172	186	186
3.32×10^{-1}	18.4	6	24	32	42	75	93	112	132	142	154	168	174	197	199
3.67×10^{-1}	20.2	6	24	32	41	75	91	110	129	140	152	168	185	208	216

SSS Cascade No. 306 t = 4.9 r.l.

1.75×10^{-2}	1.0	5	11	14	14	15	17	19	19	19	19	19	18	21	21
3.49×10^{-2}	2.0	5	18	28	30	38	48	51	55	58	58	58	57	59	59
5.24×10^{-2}	3.0	6	19	32	37	50	63	69	76	80	79	81	80	81	81
6.98×10^{-2}	4.0	6	22	35	43	59	74	82	92	99	99	102	99	105	104
8.73×10^{-2}	5.0	6	22	35	44	64	78	88	99	106	109	114	112	116	114
1.05×10^{-1}	6.0	7	23	37	46	67	82	95	106	117	121	127	127	131	137
1.22×10^{-1}	7.0	7	23	36	47	68	84	98	110	123	126	135	136	139	147
1.40×10^{-1}	8.0	7	23	37	48	71	87	101	113	128	131	142	146	148	156
1.57×10^{-1}	9.0	7	23	38	49	73	90	103	115	132	136	151	154	155	162
1.75×10^{-1}	10.0	7	23	38	49	74	90	103	115	132	137	155	158	157	163
1.92×10^{-1}	10.9	7	22	38	49	75	91	103	116	133	139	156	158	156	160
2.27×10^{-1}	12.8	7	22	38	48	76	93	107	122	137	148	167	169	171	175
2.62×10^{-1}	14.7	7	22	38	48	77	93	111	132	148	161	182	184	194	200
2.97×10^{-1}	16.6	7	22	38	48	78	95	113	134	148	160	179	184	191	195
3.32×10^{-1}	18.4	7	23	39	48	77	97	115	137	154	166	183	190	201	215
3.67×10^{-1}	20.2	7	23	40	49	76	98	118	141	159	177	196	204	212	228

TABLE II (Continued)

SSS Cascade No. 306 t = 6.9 r.l.

R r.l.		3.09×10^{-3}	6.17×10^{-3}	9.26×10^{-3}	1.23×10^{-2}	1.85×10^{-2}	2.47×10^{-2}	3.09×10^{-2}	3.70×10^{-2}	4.32×10^{-2}	4.94×10^{-2}	5.56×10^{-2}	6.17×10^{-2}	6.79×10^{-2}	7.41×10^{-2}
θ tan	μ deg	25	50	75	100	150	200	250	300	350	400	450	500	550	600
1.75×10^{-2}	1.0	1	4	10	10	12	12	13	14	14	14	14	13	16	16
3.49×10^{-2}	2.0	3	7	19	23	26	30	32	34	34	36	40	41	44	44
5.24×10^{-2}	3.0	3	8	25	32	39	44	48	53	56	58	64	65	66	66
6.98×10^{-2}	4.0	3	8	27	35	43	50	54	62	66	70	75	79	83	82
8.73×10^{-2}	5.0	3	9	28	35	47	58	67	76	80	83	94	101	105	103
1.05×10^{-1}	6.0	3	10	31	38	50	61	72	85	88	94	104	111	114	112
1.22×10^{-1}	7.0	3	10	30	38	52	64	77	90	95	102	117	124	127	127
1.40×10^{-1}	8.0	3	10	30	40	56	69	86	100	108	117	134	140	142	141
1.57×10^{-1}	9.0	3	10	30	40	55	69	85	99	106	118	137	144	145	146
1.75×10^{-1}	10.0	3	10	30	40	57	70	88	103	110	123	145	156	161	160
1.92×10^{-1}	10.9	3	9	30	40	59	72	91	106	116	131	151	165	168	169
2.27×10^{-1}	12.8	3	9	31	40	62	75	95	111	124	141	160	175	179	178
2.62×10^{-1}	14.7	3	9	31	42	64	76	96	112	127	141	161	174	178	175
2.97×10^{-1}	16.6	3	9	32	42	64	76	96	111	125	140	158	173	181	184
3.32×10^{-1}	18.4	3	9	32	41	62	76	96	109	122	136	154	179	190	198
3.67×10^{-1}	20.2	3	9	33	41	62	76	95	109	128	143	161	196	205	220

distributions i.e., the integral background distribution has been subtracted from the integral distribution of the cascade superimposed on background. Consequently, as a result of fluctuations in the background and/or the cascade, a small decrease in the integral number of particles is possible. This occurs occasionally at large angles and distances where the number of cascade particles is small.

The experimental radial and angular distributions of the cascades which have been measured are compared with the theoretical predictions of the core approximation and approximation B in Figs. 9-15. Part "a" of each figure displays the number of cascade particles $N(< R)$ having lateral displacements less than R from the cascade axis as a function of $E_o R$. Part "b" of each figure shows the number of cascade particles $N(< \theta)$ having angles less than θ with respect to the cascade axis as a function of $E_o \theta$. The curves for the radial core approximation (curves C) were taken from Kidd[35] while the curves for the angular core approximation (curves C') were taken from Appendix III. The curves of approximation B for the radial distribution (curves B) and the angular distribution (curves B') were calculated by determining the total number of particles from Fig. 5.13.3 of Rossi[36] and using the normalized radial and angular distributions given, respectively, by Fig. 7 of Pinkau[37] and Appendix II.

---

[35] J. Kidd, Nuovo Cimento 27, 57 (1963).

[36] B. Rossi, High Energy Particles (Prentice-Hall, Inc., Englewood Cliffs, N.J., 1952) p. 69.

[37] K. Pinkau, Nuovo Cimento 33, 221 (1964).

Brawley cascades 1068, 1032 and 1101 had approximately the same energies. Therefore, in order to decrease fluctuations, the distributions of these cascades were averaged and are presented in the figures as one cascade. For the same reason, SSS cascades 133 and 306 are presented as a single cascade.

The primary energy E_0 of each cascade was determined from the radial distribution by comparing the experimental points with the core approximation curves. Only the experimental points within $\sim 10^{-2}$ r.l. of the cascade axis were taken into consideration, since this is the region where the core approximation curves have previously been shown to be reliable.

In making the comparison, a transparent overlay containing the core approximation curves $N(<R)$ vs E_0R plotted to the same scale as the experimental points was simultaneously fitted by eye to the experimental distributions $N(<R)$ vs R at all the measured depths from the origin. The matching of the curves in this manner is done with some ambiguity. However, the agreement in the energy estimation by two different observers was better than 95%. The radiation lengths near the maximum of the longitudinal development ($\sim$ 6-7 r.l.) were given the larger weight, since these should have the smaller fluctuations. The primary energy of the cascade was then given by the ratio of the E_0R scale of the core approximation curves to the R scale of the experimental distributions. The energies of the cascades as determined from the radial distributions are shown in column 2 of Table III.

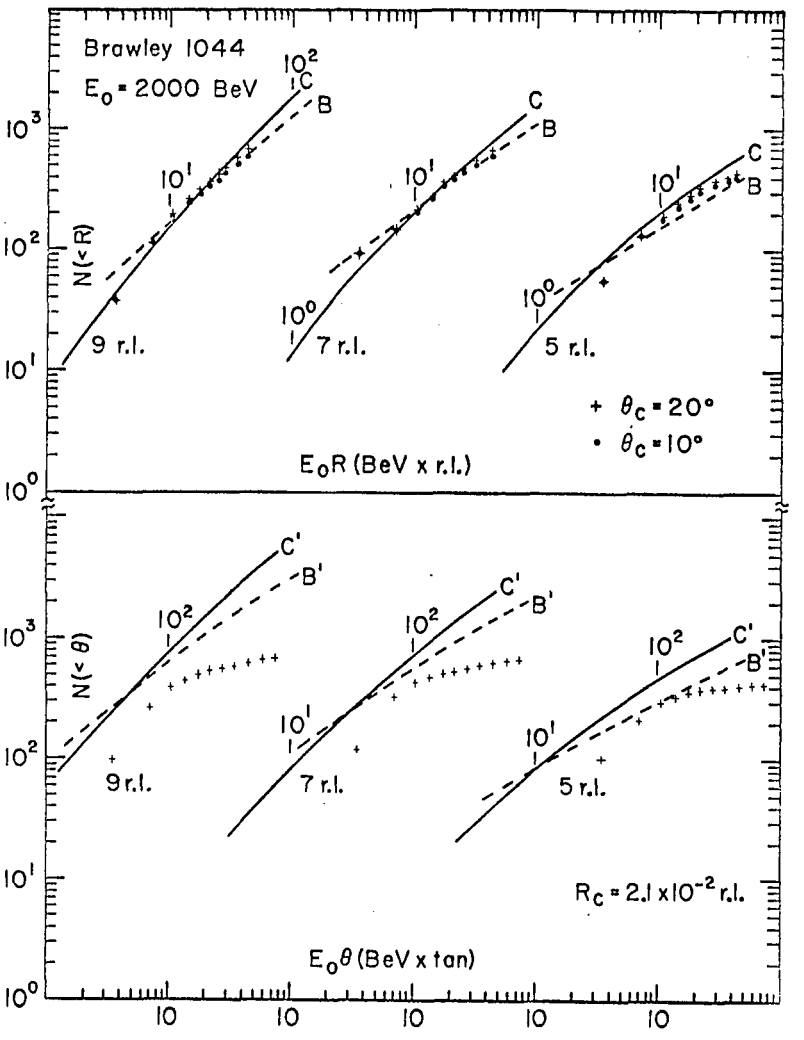

Fig. 9. Radial and angular distributions of cascade electrons for Brawley cascade 1044. Part "a" compares the integral number of electrons N(<R) with the radial core approximation (curve C) and approximation B (curve B). Experimental points are given for cutoff angles θ_c = 10 and 20°. Part "b" compares the integral number of electrons N(<θ) with the angular core approximation (curve C') and approximation B (curve B'). Experimental points are given for the radial cutoff $R_c = 2.1 \times 10^{-2}$ r.l. The distance t from the cascade origin is given below the curves.

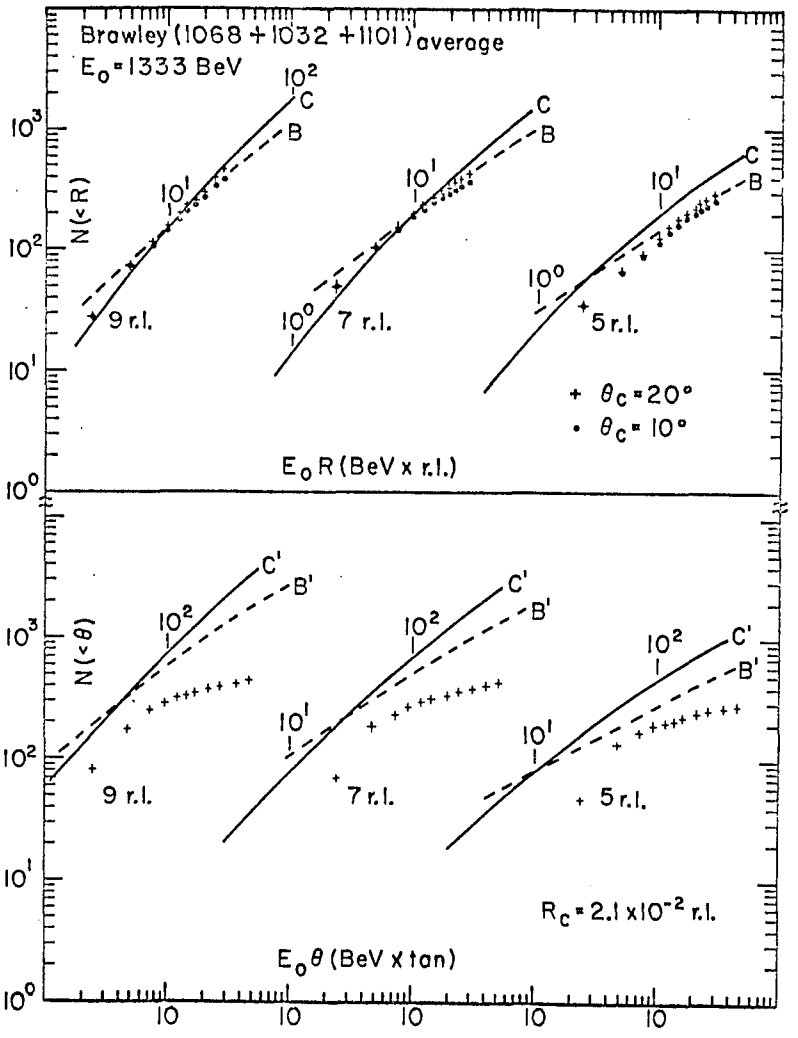

Fig. 10. Radial and angular distributions of cascade electrons for the average of Brawley cascades 1068, 1032 and 1101. Part "a" compares the integral number of electrons N(<R) with the radial core approximation (curve C) and approximation B (curve B). Experimental points are given for cutoff angles θ_c = 10 and 20°. Part "b" compares the integral number of electrons N(<θ) with the angular core approximation (curve C') and approximation B (curve B'). Experimental points are given for the radial cutoff $R_c = 2.1 \times 10^{-2}$ r.l. The distance t from the cascade origin is given below the curves.

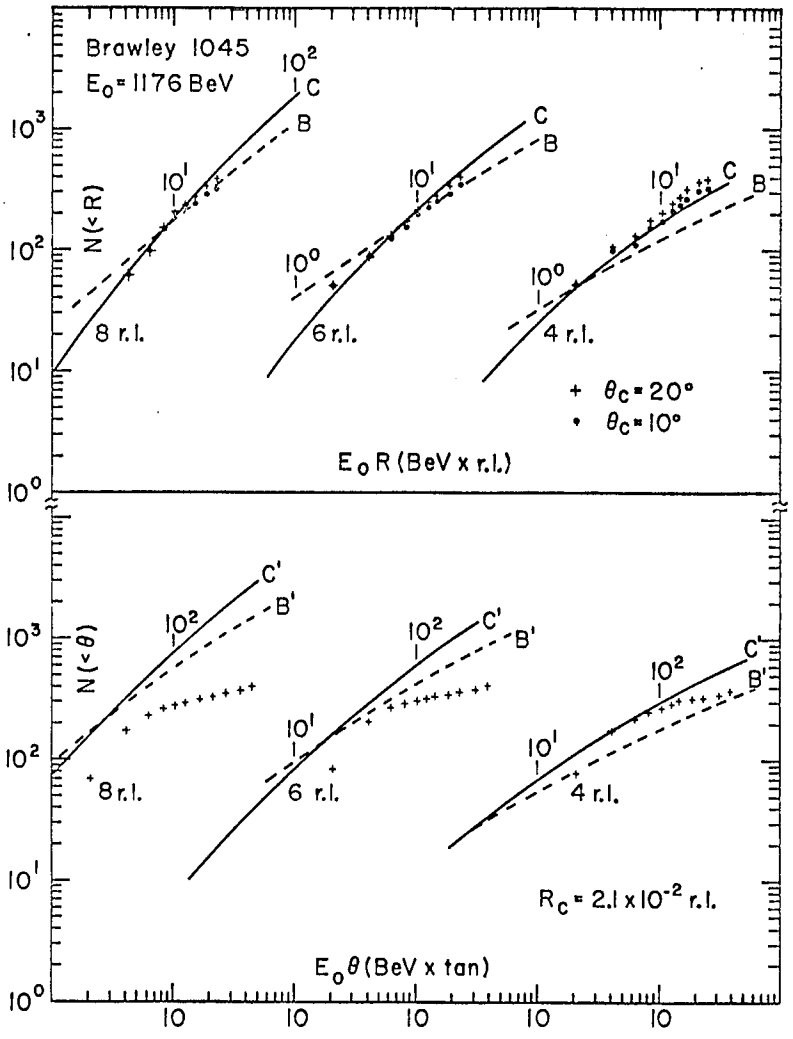

Fig. 11. Radial and angular distributions of cascade electrons for Brawley cascade 1045. Part "a" compares the integral number of electrons $N(<R)$ with the radial core approximation (curve C) and approximation B (curve B). Experimental points are given for cutoff angles θ_c = 10 and 20°. Part "b" compares the integral number of electrons $N(<\theta)$ with the angular core approximation (curve C') and approximation B (curve B'). Experimental points are given for the radial cutoff $R_c = 2.1 \times 10^{-2}$ r.l. The distance t from the cascade origin is given below the curves.

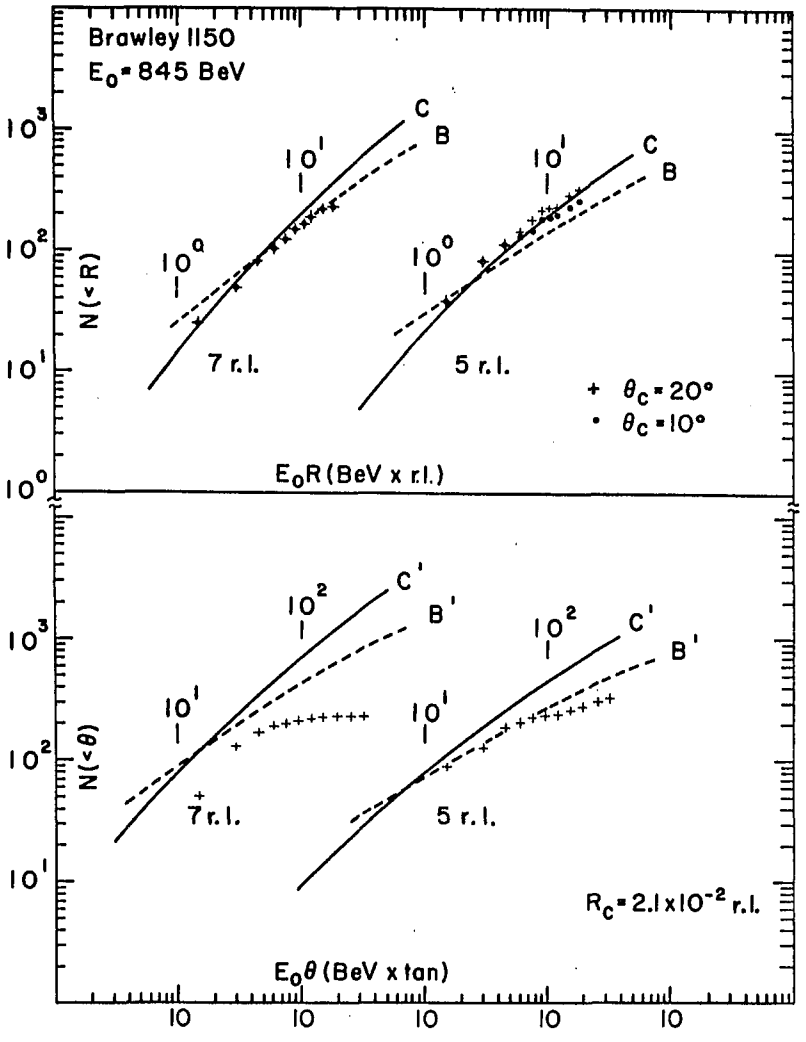

Fig. 12. Radial and angular distributions of cascade electrons for Brawley cascade 1150. Part "a" compares the integral number of electrons $N(<R)$ with the radial core approximation (curve C) and approximation B (curve B). Experimental points are given for cutoff angles θ_c = 10 and 20°. Part "b" compares the integral number of electrons $N(<\theta)$ with the angular core approximation (curve C') and approximation B (curve B'). Experimental points are given for the radial cutoff $R_c = 2.1 \times 10^{-2}$ r.l. The distance t from the cascade origin is given below the curves.

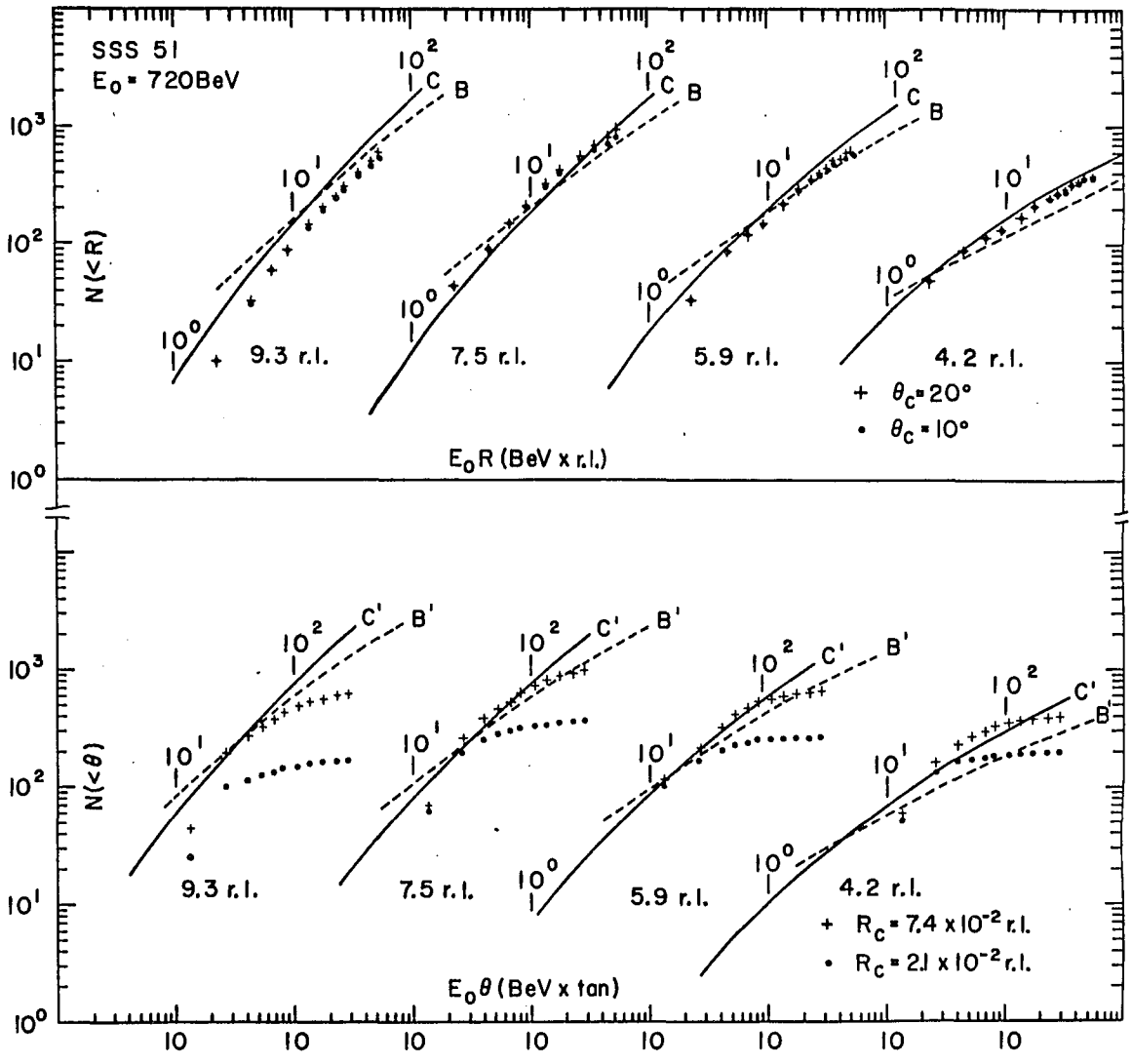

Fig. 13. Radial and angular distributions of cascade electrons for SSS cascade 51. Part "a" compares the integral number of electrons $N(<R)$ with the radial core approximation (curve C) and approximation B (curve B). Experimental points are given for cutoff angles θ_c = 10 and 20°. Part "b" compares the integral number of electrons $N(<\theta)$ with the angular core approximation (curve C') and approximation B (curve B'). Experimental points are given for the radial cutoff $R_c = 2.1 \times 10^{-2}$ and 7.4×10^{-2} r.l. The distance t from the cascade origin is given below the curves.

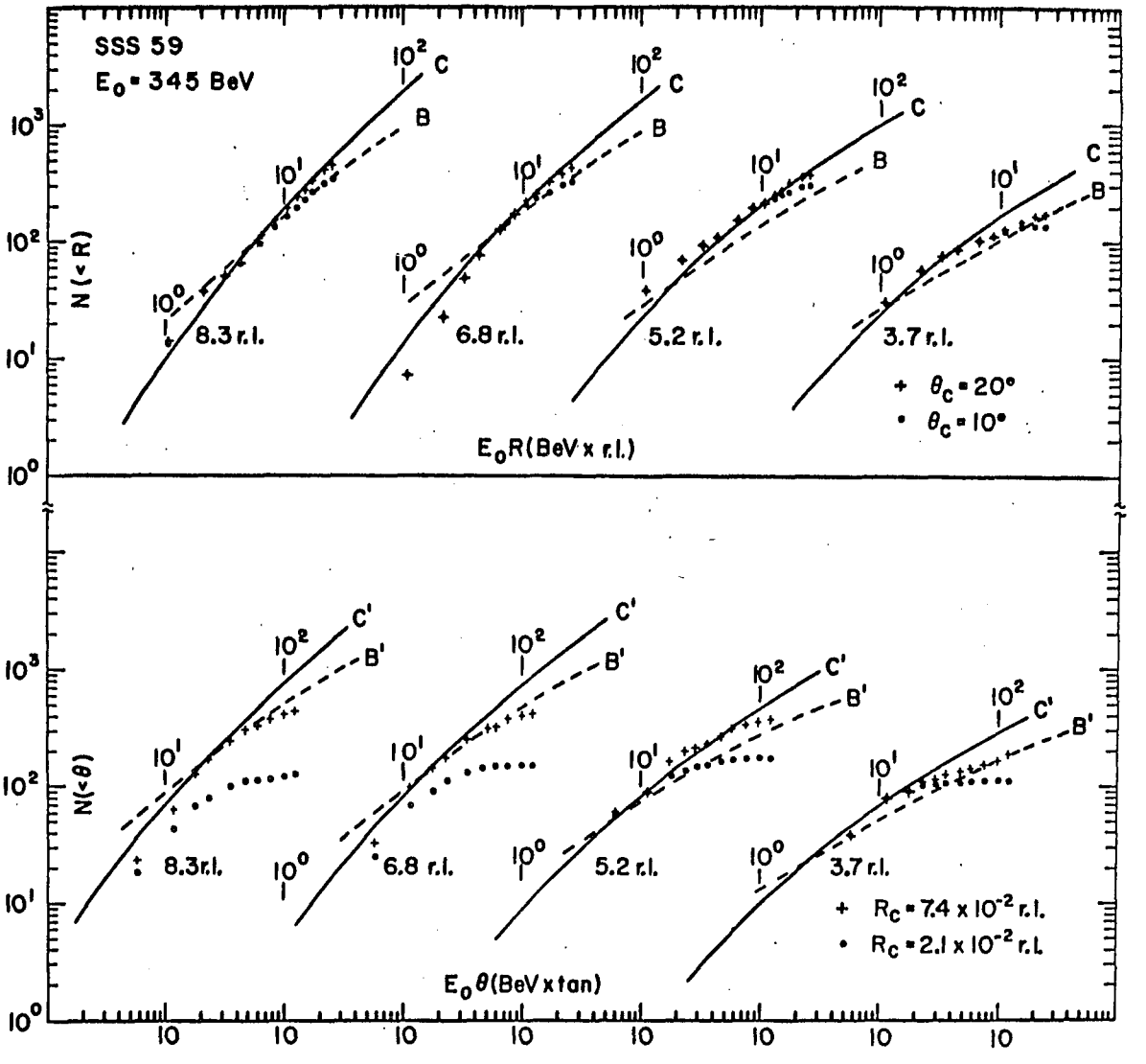

Fig. 14. Radial and angular distributions of cascade electrons for SSS cascade 59. Part "a" compares the integral number of electrons N(<R) with the radial core approximation (curve C) and approximation B (curve B). Experimental points are given for cutoff angles θ_c = 10 and 20°. Part "b" compares the integral number of electrons N(<θ) with the angular core approximation (curve C') and approximation B (curve B'). Experimental points are given for the radial cutoff R_c = 2.1 x 10^{-2} and 7.4 x 10^{-2} r.l. The distance t from the cascade origin is given below the curves.

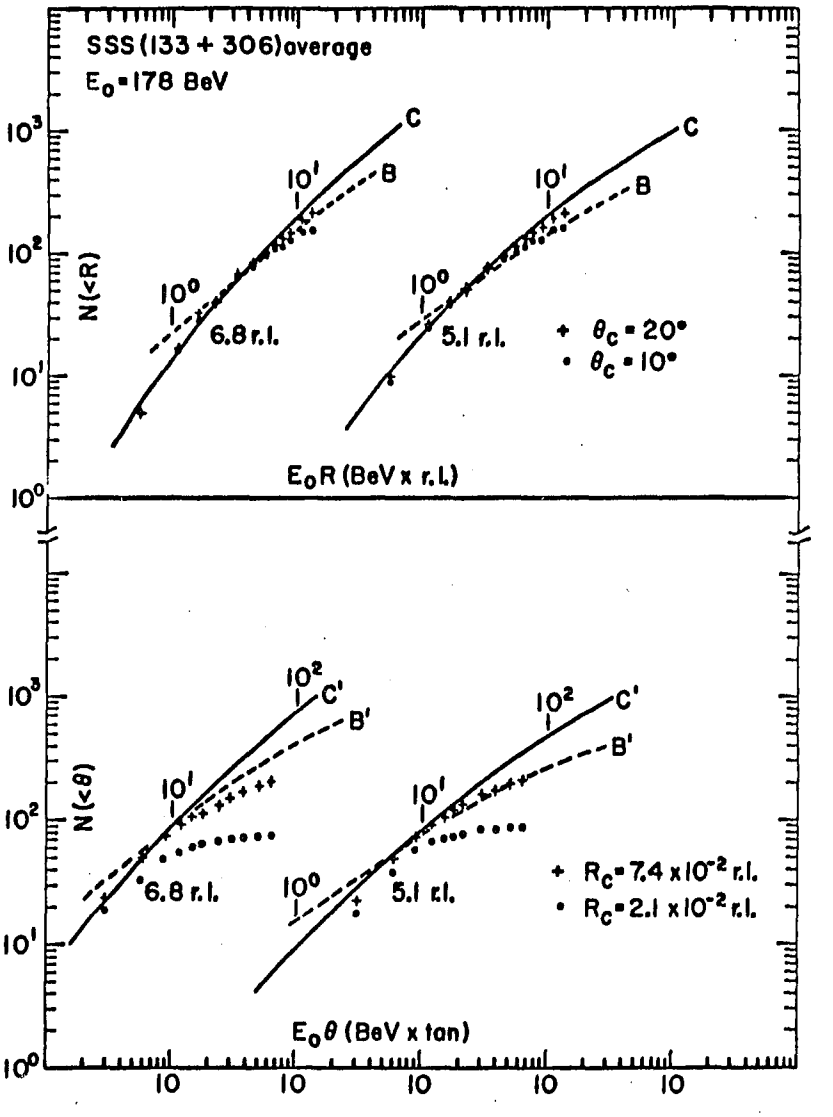

Fig. 15. Radial and angular distributions of cascade electrons for the average of SSS cascades 133 and 306. Part "a" compares the integral number of electrons $N(<R)$ with the radial core approximation (curve C) and approximation B (curve B). Experimental points are given for cutoff angles θ_c = 10 and 20°. Part "b" compares the integral number of electrons $N(<\theta)$ with the angular core approximation (curve C') and approximation B (curve B'). Experimental points are given for the radial cutoff R_c = 2.1 x 10^{-2} and 7.4 x 10^{-2} r.l. The distance t from the cascade origin is given below the curves.

TABLE III

Cascade Energies Using Core Approximation

Cascade	E_o(BeV) From Radial Distribution	E_o(BeV) From Angular Distribution
Brawley		
1044	2000	---
1068 1032 1101 Ave.	1333	---
1045	1176	---
1150	845	---
SSS		
51	720	780
59	345	333
133 306 Ave.	178	174

The illustrations in Fig. 16 are examples of photographs of scale models constructed to show the differential R-θ distributions of the particles in a cascade. The models shown are for the four positions of measurement of cascade SSS 51. The radial scale corresponds to 50 μ increments (annular rings) ranging from 0-600 μ (0-7.4 x 10^{-2} r.l.) while the angular scale is given in 2° increments from 0-20°. The radial limit of the measurements in the Brawley stack was 2.1 x 10^{-2} r.l. which corresponds to 172 μ in the SSS stack. It is quite obvious from the illustrations that a large percentage of the cascade particles lie outside the range of measurements in the Brawley stack. From the illustration one can see the correlation between R and θ at different distances t from the cascade origin.

2. Discussion of Experimental Results

The comparisons shown in part "a" of Figs. 9-15 of the experimental radial distributions with the theoretical curves of the core approximation and approximation B indicate that the experimental results are consistent with the cascade theory under the core approximation in the radial and energy range which were measured. The measurements in the Brawley stack extended up to R = 2.1 x 10^{-2} r.l. and covered an energy range of 845-2000 BeV, while in the SSS stack the radial measurements were made up to R = 7.4 x 10^{-2} r.l. and the energy range was 178-720 BeV. The apparent, small but systematic, deviation from the core approximation appears to be the result of having omitted particles with angles

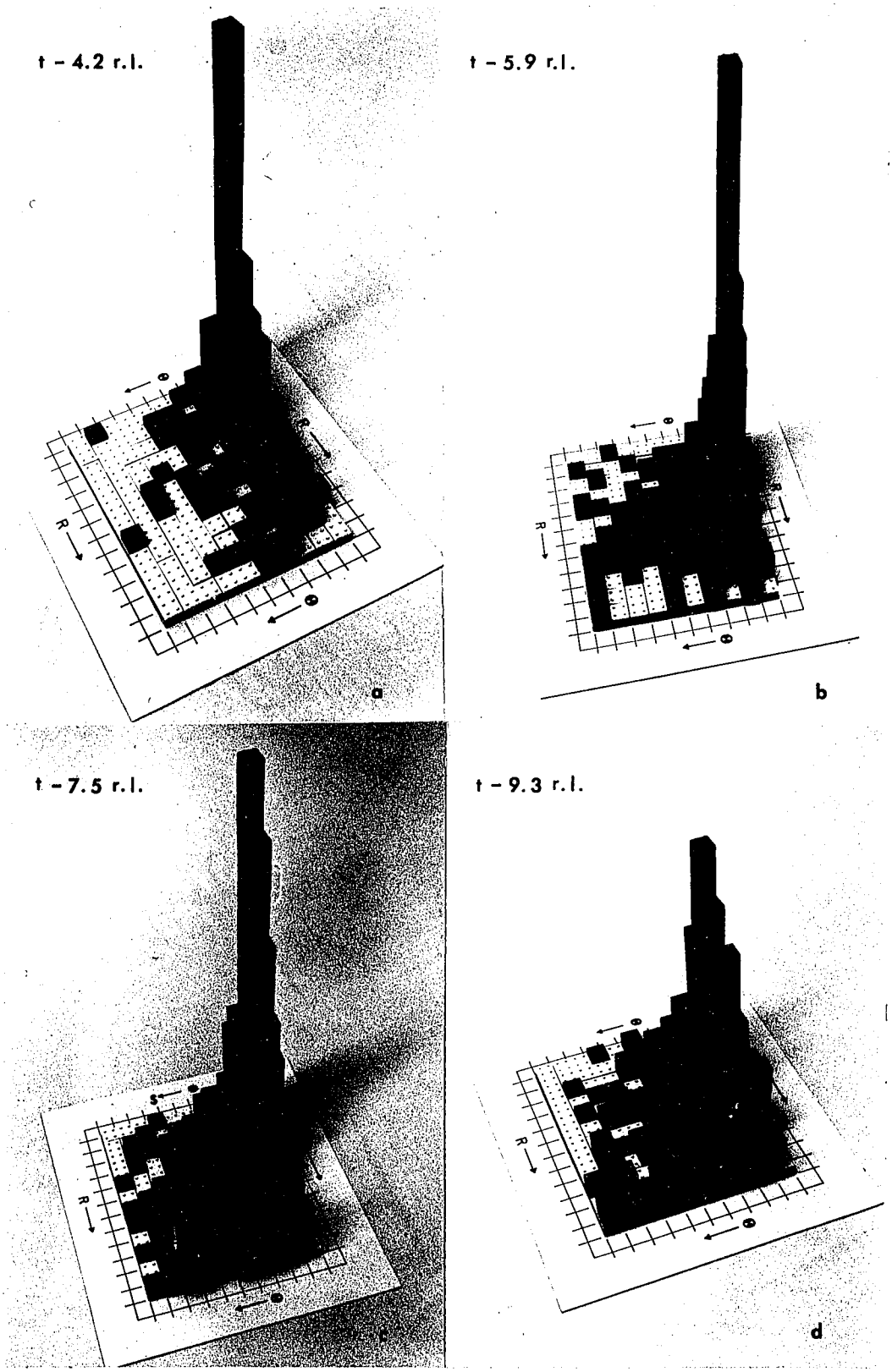

Fig. 16. Differential R vs θ distribution for SSS cascade 51.

greater than 20° in the radial distribution. This conclusion is justified by observing the increase in the total number of particles when the cutoff angle is increased from 10 to 20°.

The experimental results serve as a lower limit to the total number of particles in approximation B. Since the curves of approximation B in the radial distribution clearly demand a deviation of the results from the core approximation well within the range of measurements, the conclusion must be drawn that approximation B underestimates the total number of particles in the radial interval which was measured. This is because the only way one could get the experimental results to agree with approximation B would be to shift the curves of this approximation in the vertical direction until they agree with the experimental results i.e., to increase the total number of particles until the curves of approximation B are in agreement with the experimental results and the core approximation in the radial interval which has been measured.

As shown in part "b" of Figs. 9-12, there is an apparent discrepancy when the angular distributions of cascade particles measured in the Brawley stack are plotted as a function of $E_o\theta$ and compared with the cascade theory under the angular core approximation. It should be noted here that the value of E_o was obtained from the radial distribution as described in the previous section of this chapter. This apparent discrepancy could conceivably stem from two sources. The first source could be an internal inconsistency in the predictions of the theoretical curves while the second could be that the measurements suffered from the limited radius (2.1×10^{-2} r.l.) which was covered in the Brawley stack. From the measurements in

the SSS stack where the radial range was much larger (7.4×10^{-2} r.l.), it is clear that the latter source is the correct one. Part "b" of Figs. 13-15 show that for the SSS stack, the radial cutoff $R_c = 2.1 \times 10^{-2}$ r.l. does not allow the measurement of all particles even at 1-2°. However, for $R_c = 7.4 \times 10^{-2}$ r.l., there is complete agreement of the experimental points up to $\sim$ 4-5° with the cascade theory under the core approximation. Consequently, one must conclude that no comparison is possible between theory and experiment for the angular distributions in the Brawley stack, because the limited radial interval which could be measured did not permit the measurement of all particles even at very small angles.

It can be seen quantitatively from the integral radial and angular distributions of the SSS cascades presented in Table II that there would not be any significant increase in the total number of particles having angles less than 4-5° if the radial extent of the measurements were considerably increased. This is also qualitatively shown for SSS cascade 51 in the illustration in Fig. 16 of the differential R vs θ distributions. Therefore, in exact analogy to the use of the radial distributions, the primary energy of the SSS cascades can be determined by considering only the experimental points for the angles where all particles have been measured, and making direct comparison with the theoretical curves obtained under the angular core approximation that are given in Appendix III. The results of the energies so obtained are given in column 3 of Table III. One can see that there is very good

agreement between the energy estimates obtained from the radial and angular distributions.

Two important conclusions can be drawn from the agreement of the energy determination from the radial and the angular distributions of the cascade particles. First, the agreement shows the internal consistancy of the cascade theory as derived under the core approximation. Second, the agreement shows that the wavelength in the heavy SSS stack (See Chap. I) is sufficiently small so that the arrangement can be considered to be a homogeneous mixture of lead and emulsion as far as the determination of the effective radiation length for the radial distribution is concerned.

The deviation of the experimental angular distribution from the core approximation for angles greater than $\sim 4\text{-}5^{o}$ in the SSS stack can certainly be explained to some extent by the fact that the radial limitation of 7.4×10^{-2} r.l. was not large enough to include all particles having angles greater than 5^{o}. This appears to be the main reason for the apparent deviation. However, one cannot exclude the possibility, especially for large angles, that part of this deviation may truly be a deviation from the core approximation.

The question remains how to extend the measurements and/or the theory in order to make full use of all the available experimental material. One approach would consist of trying to derive a mixed radial-angular distribution from the theory for comparison with the experimental data. For example, one might try to fold the mixed radial-angular distribution for mono-energetic particles

given by Rossi[38] with the energy spectrum given by Pinkau[39] for the particles in a cascade, in order to obtain the density distribution of particles having zero angle. Such a distribution would be one of radius only and would actually be very similar to the integral radial distribution integrated over all angles, with the important difference being in the normalization factor. This distribution is completely known from the measurements which have been presented, because one can see from Tables I and II that practically no additional particles at zero angle are expected to be found even beyond the limited radial interval in the Brawley stack.

---

[38] B. Rossi, High Energy Particles (Prentice-Hall, Inc., Englewood Cliffs, N.J., 1952) p. 69.

[39] K. Pinkau, Phys. Rev. 139B, 1548 (1965).

V. SUMMARY AND CONCLUSIONS

The lateral and angular distributions of six electromagnetic cascades in the energy range 845 - 2000 BeV have been measured in the Brawley pure emulsion stack. The measurements covered all particles having angles less than 20^{o} up to the radial distance of $R = 2.1 \times 10^{-2}$ r.l. from the cascade axis. Four such cascades in the energy range 178 - 720 BeV were measured in the SSS lead-emulsion sandwich stack. The latter measurements covered all particles having angles less than 20^{o} up to the radial distance of $R = 7.4 \times 10^{-2}$ r.l.

From the ten cascades which have been investigated it is concluded that :

1. There is no clear deviation of the experimental results from the cascade theory under the radial core approximation within the range of distances and energies measured.
2. Approximation B underestimates the total number of cascade particles in the radial region beyond its intersection with the core approximation and up to the maximum radial distances which were measured.
3. The energy determination using only small angles from the angular distribution of the cascade particles in the SSS stack is in complete agreement with the energy determination from the radial distribution. Therefore, the cascade

theory is internally consistant under the core approximation. Also, the wavelength of the SSS stack is small enough so that the results can be interpreted as being derived from a homogeneous medium.

4. The radial range must extend up to $\sim 7 \times 10^{-3}$ r.l. in the SSS stack in order to include all particles up to $4\text{-}5^{\circ}$ in the angular distribution. Therefore, comparison between theory and experiment for the angular distributions in the Brawley pure emulsion stack was not possible.
5. The large apparent deviation of experimental results from the angular core approximation for angles greater than $\sim 5^{\circ}$ in the SSS stack is mainly caused by the limited radial distance used. However, part of this deviation may truly be a deviation from the predictions of the core approximation.

SELECTED BIBLIOGRAPHY

Books

Abramowitz, M. and Stegun, I. A. Handbook of Mathematical Functions. New York: Dover Publications, Inc., 1965. p. 255.

Fowler, P. H., Perkins, D. H. and Pinkau, K. Proceedings of the Moscow Cosmic Ray Conference, Moscow, 1960. Vol. 2, p. 302.

Pinkau, K. Proceedings of International Conference on Cosmic Rays, Jaipur, India, 1963. Bombay, India: The Commercial Printing Press, Ltd., 1964. Vol. 5, p. 555.

Rossi, B. High Energy Particles. Englewood Cliffs, N.J.: Prentice-Hall, Inc., 1952, Chap. 5, Pp. 69, 214, 296, 52, 84.

Periodicals

Akashi, M., Watanabe, Z., Misaki, A., Mito, I., Oyama, Y., Tokunaga, S., Ogata, T., Tsuneoka, Y., Dake, S., Yokoi, K., Hasegawa, S., Nishimura, J., Niu, K., Taira, T., Nishio, A., Fujimoto, Y., and Ogita, N. Supplement of Progress of Theoretical Physics (Kyoto), Vol. 32 (1964), 1.

Babecki, J., Holynski, R., Krzywdzinski, S., Peeva, A., Rybicki, K., and Wolter, W. Nukleonika, Vol. 9 (1964), 271.

Bethe, H. A. The Physical Review, Vol. 89 (1953), 1256.

Bethe, H. A. and Heitler, W. Proceedings of the Royal Society (London), Vol. A 146 (1934), 83.

Duthie, J., Fowler, P. H., Kaddoura, A., Perkins, D. H. and Pinkau, K. Nuovo Cimento, Vol. 24 (1962), 122.

Janossy, L. and Messel, H. Proceedings of the Physical Society (London), Vol. A 63 (1950), 1101.

Kamata, K. and Nishimura, J. Supplement of Progress of Theoretical Physics (Kyoto), Vol. 6 (1958), 93.

Kidd, J. M. Nuovo Cimento, Vol. 27 (1963), 57.

Lohrmann, E. The Physical Review, Vol. 122 (1961), 1908.

Malhotra, P. K., Shukla, P. G., Stephens, S. A., Vijaylakshmi, B., Boult, J., Bowler, M. G., Fowler, P. H., Hackforth, H. L., Keereetaveep, J., Mayes, V. M. and Tovey, S. N. Nuovo Cimento, Vol. 40 A (1965), 385.

Minakawa, O., Nishimura, Y., Tsuzuki, M., Yamanouchi, H., Fujimoto, Y., Hawegawa, S., Nishimura, J. and Niu, K. Supplement of Nuovo Cimento, Vol. 11 (1959), 125.

Nishimura, J. and Kamata, K. Progress of Theoretical Physics (Kyoto), Vol. 7 (1952), 185.

Nishimura, J. and Kidd, J. Supplement of Nuovo Cimento, Vol. 1 (1964), 1039.

Pinkau, K. Nuovo Cimento, Vol. 3 (1956), 1156.

_____. Nuovo Cimento, Vol. 33 (1964), 221.

_____. Philosophical Magazine, Vol. 2 (1957), 1389.

_____. The Physical Review, Vol. 139 B (1965), 1548.

Rossi, B. and Greisen, K. Reviews of Modern Physics, Vol. 13 (1941), 240.

Snyder, H. S. and Scott, W. T. The Physical Review, Vol. 76 (1949), 220.

Unpublished Papers

Abraham, F., Gierula, J., Levi Setti, R., Rybicki, K., Tsao, C. H., Wolter, W., Fricken, R. L. and Huggett, R. W. "Multiple Meson Production by Heavy Nuclei of Cosmic Origin and Their Fragmentation Products at Energies Above 10^{12} eV." (To be published in Physical Review.)

Pinkau, K. Ph.D. Thesis, Appendix I, University of Bristol, England, 1958.

APPENDIX I

Details of Experimental Measurements and Calculations

The field of view of the square "box" graticule with 100 scale divisions per side used for making the cascade measurements covered a square area of the emulsion plate having approximately 85 μ per side under the magnification used (10X eyepieces with 55X objective). This scale calibration varied slightly with the eye spacing of the person reading the microscope. Since it was desired to make measurements to about 600 μ on either side of the cascade axis, the apparent core was located in the center of one field of view and measurements were made in this field of view and in 7 fields of view on either side. See Fig. 17.

The horizontal centerline of the "box" graticule was taken to be the precise position of the cut for a particular radiation length. Each minimum track which crossed this centerline was traced to the two points where it intersected the sides of the graticule. See Fig. 18. Tracks having twice the grain density of minimum tracks were recorded as two tracks with the same coordinates.

The coordinates (x_1, y_1) and (x_2, y_2) where each electron track intersected the two sides of the graticule were obtained by recording the sides and corresponding scale readings of the sides of the graticule at the points of intersection. The corresponding z

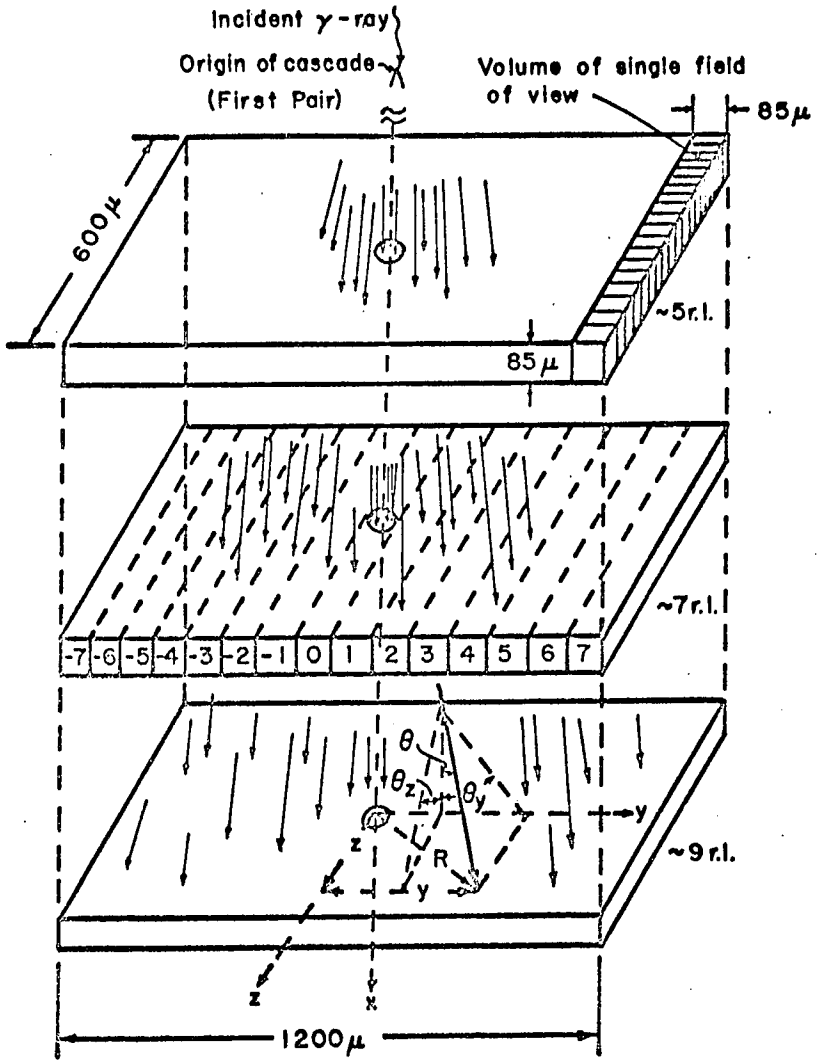

Fig. 17. Schematic diagram showing the cascade as it appears in emulsion at three positions of measurement. The numbers -7, ···, 0,···,+7 identify the various fields of view in which the measurements were made. The spatial coordinates R and θ as well as the projected coordinates y, z, θ_y and θ_z are shown for a sample track. (Diagram is not to scale.)

coordinates, z_1 and z_2, were obtained from the vernier scale of the microscope which gave the depth of the field in the emulsion, to an accuracy of 1 μ, when the track was in best focus at the sides of the graticule.

It was desired to have the y and z coordinates of each track at the centerline of the graticule which represented the position of the cut along the x axis. From Fig. 18, it is seen that these coordinates are given by

$$y_{cut} = y_1 + \tan \theta_y (50 - x_1) ,$$

$$z_{cut} = z_1 + \frac{SC}{SF} \tan \theta_z (50 - x_1) .$$

The relative projected angles, θ_y and θ_z, of each electron track were obtained from the coordinates at the intersection of the track with the sides of the graticule according to the formulas

$$\tan \theta_y = \frac{y_2 - y_1}{x_2 - x_1} ,$$

$$\tan \theta_z = \frac{z_2 - z_1}{x_2 - x_1} \cdot \frac{SF}{SC} .$$

The value of SC is the scale calibration of the graticule in microns per scale division and SF is the shrinkage factor of the emulsion plate. The shrinkage factor is defined to be the ratio of the thickness of the emulsion before processing (thickness at the time of exposure to the cascade) to the thickness after processing (thickness at the time of measurement).

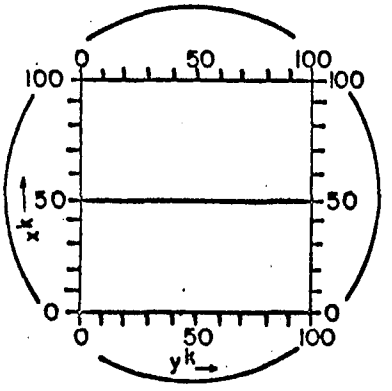

Fig. 18a. Schematic diagram of the box graticule in the field of view of the Koristka R4 microscope. Images are inverted in the vertical direction so the Koristka coordinate system (x^k,y^k,z^k) is a left handed system.

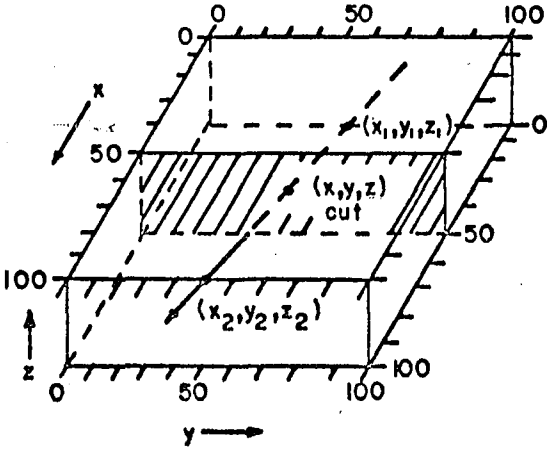

Fig. 18b. Schematic diagram showing a sample track intersecting the box graticule in two different focal planes to give the coordinates (x_1,y_1,z_1) and (x_2,y_2,z_2). The horizontal centerline of the graticule was taken to be the position of cascade measurement.

It should be noted that the x and y coordinates where the tracks intersected the sides of the graticule were recorded in "scale divisions" while the z coordinates were recorded in microns.

Besides the coordinates (x_1, y_1, z_1) and (x_2, y_2, z_2), the particular field of view in which the track was located and the exact scale calibration of the graticule were recorded for each track. The field of view in which the apparent core of the cascade was located was labeled as zero. The remaining fields of view were labeled as -1 through -7 in going away from the zero field of view in the negative y direction and +1 through +7 in the positive y direction. See Fig. 17.

The coordinates y_{cut} and z_{cut} give the position of a track in the field of view in which it was measured. It is necessary to account for the location of this field of view with respect to the cascade core to get absolute y coordinates. This can be done by setting

$$y = y_{cut} + 100\ F\ .$$

The symbol F is one of the recorded numbers, -7, . . ., -1, 0, +1, . . ., +7, which represent the field of view in which the track was located. The value of z is not dependent on the field of view and is simply given by

$$z = z_{cut}\ .$$

It is ultimately desired to know the spatial and angular coordinates of each electron track relative to the cascade axis in

the target plane. This is the plane perpendicular to the cascade axis at the position of measurement. The cascade axis is defined to be the direction of motion of the particle (γ-ray) initiating the cascade. If the radial and angular distributions are to be significant, especially for small values of these coordinates, the cascade axis must be located as accurately as possible.

The procedure usually employed in determining the cascade axis is to average over the coordinates of the particles in the cascade and choose the axis to be the position where the average values of these coordinates are zero, i.e., $\bar{y} = 0$, $\bar{z} = 0$, $\bar{\theta}_y = 0$, and $\bar{\theta}_z = 0$. This procedure assumes azimuthal symmetry of the cascade.

For the above procedure to give the best orientation of the cascade axis, it is important to use a large number of tracks so that the effect of individual track fluctuations is made as small as possible. It is obvious that this method is easily biased by the presence of a few tracks making large angles with the general direction of the cascade or being far removed from its apparent core. Also, since the cascade is superimposed on the rather uniform background tracks in the emulsion, it is advisable to use only that part of the cascade where the ratio of noise to signal is extremely low.

The results of preliminary investigations along the above lines indicated that there is only a small contribution of cascade tracks having angles greater than 5° for distances less than about 250 μ from the cascade axis. Calculations on the background which was measured far from the cascade ($\sim$ 1 cm.) indicate that the number

of background tracks having angles less than 5° with a chosen axis and located within 250 μ of that axis is $\sim$ 1 - 3% of the number of the cascade tracks.

Consideration of the above results led to the choice of tracks used in finding the cascade axis which satisfied the following criteria:

$$|\theta_y| \leq 5^{\circ}, \; |y| \leq 250\,\mu \quad ,$$

$$|\theta_z - \delta| \leq 5^{\circ}, \; |z| \leq 250\,\mu \quad .$$

The value of δ was taken to be the value of the dip angle of the cascade as measured on the microscope.

To further facilitate obtaining the most accurate value of the cascade axis, an iterative technique to obtain the average values of the coordinates by successive approximations was used. The first approximation was a simple average over the n particles satisfying the criteria given above. For example, the first approximation $\bar{y}_1$ to the average value of the coordinate y was obtained by averaging over the n values of the y coordinates for the selected tracks, i.e.,

$$\bar{y}_1 = \frac{1}{n} \sum_{j=1}^{n} y_j \quad .$$

The second approximation $\bar{y}_2$ to the value of $\bar{y}$ was obtained by averaging over 75% of the tracks closest to $\bar{y}_1$. Letting n' represent the number of tracks having y coordinates closest to $\bar{y}_1$, then

$$\bar{y}_2 = \frac{1}{n'} \sum_{j=1}^{n'} (y_j - \bar{y}_1) \quad .$$

In general, for the n' tracks having a y coordinate closest to a previous mean $\bar{y}_i$, then

$$\bar{y}_{i+1} = \frac{1}{n'} \sum_{j=1}^{n} (y_j - \bar{y}_i) \quad .$$

The iteration was stopped when

$$|\bar{y}_{i+1} - \bar{y}_i| < \epsilon_y \quad ,$$

where $\epsilon_y = 0.5\ \mu$. If this value of ϵ_y was not reached within ten iterations, the value of the mean after that number of iterations was used as the value of $\bar{y}$.

Exactly analogous iterations were used to obtain the means of the other projected coordinates, $\bar{z}$, $\bar{\theta}_y$, and $\bar{\theta}_z$. The value used for ϵ_z was also $0.5\ \mu$ while ϵ_{θ_y} and ϵ_{θ_z} were taken to be 0.001 rad.

To get the coordinates of the cascade particles in the target plane, it was necessary to transform from the (x, y, z) coordinate system in which the measurements were made to the (x*, y*, z*) system having the x* axis coincident with the cascade axis. If the cascade is assumed to be symmetric about its axis, this transformation can be performed by translation of the y and z coordinates so that $\bar{y} = \bar{z} = 0$ followed by two successive rotations.

The translations were performed by subtracting $\bar{y}$ and $\bar{z}$, respectively, from the y and z coordinates which were described earlier. After this translation one can calculate the coordinates of each track relative to a new (x', y', z') system which has the

(x', z') plane making an angle $\bar{\theta}_y$ with the old (x, z) plane. The new coordinates are given by the following formulas: (See Fig. 19.)

$$\theta_y' = \theta_y - \bar{\theta}_y \ ,$$

$$\theta_z' = \tan^{-1}\left[\frac{\tan \theta_z \cdot \cos \theta_y}{\cos \theta_y'}\right] \ ,$$

$$y' = y \frac{\cos \theta_y}{\cos \theta_y'} \ ,$$

$$z' = z - y' \cdot \sin \bar{\theta}_y \cdot \tan \theta_z \ .$$

If one now designates as (x'', y'', z'') the coordinate system which has the (x'', y'') plane making an angle $\bar{\theta}_z$ with the (x', y') plane, then the coordinates for each track in this new system are given by

$$\theta_z'' = \theta_z' - \bar{\theta}_z \ ,$$

$$\theta_y'' = \tan^{-1}\left[\frac{\tan \theta_y' \cdot \cos \theta_z'}{\cos \theta_z''}\right] \ ,$$

$$z'' = z' \frac{\cos \theta_z'}{\cos \theta_z''} \ ,$$

$$y'' = y' - z'' \sin \bar{\theta}_z \cdot \tan \theta_y' \ .$$

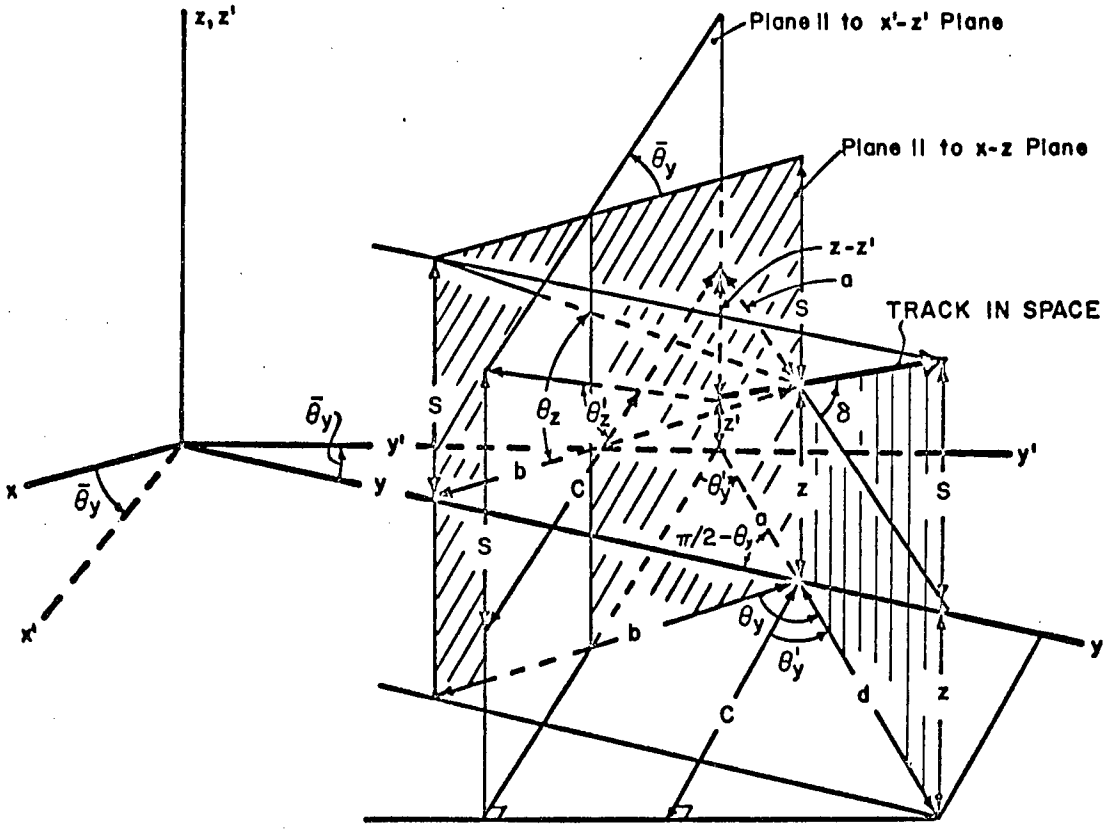

Relations:

$\theta'_y = \theta_y - \bar{\theta}_y$

$\tan \theta_z = \frac{s}{b}$

$\cos \theta_y = \frac{b}{d}$

$\cos \theta'_y = \frac{c}{d}$

$\tan \delta = \frac{s}{d} = \frac{s}{b} \times \frac{b}{d} = \tan \theta_z \cos\theta_y = \frac{z-z'}{a}$

$\tan \theta'_z = \frac{s}{c} = \frac{s}{d} \times \frac{d}{c} = \frac{\tan \theta_z \cos\theta_y}{\cos\theta'_y}$

Resulting Equations:

$$\frac{y'}{\sin(\frac{\pi}{2} - \theta_y)} = \frac{y}{\sin(\frac{\pi}{2} + \theta'_y)} = \frac{a}{\sin \bar{\theta}_y}$$

$\theta'_y = \theta_y - \bar{\theta}_y$

$\theta'_z = \tan^{-1}\left[\frac{\tan\theta_z \cos\theta_y}{\cos\theta'_y}\right]$

$y' = y \frac{\cos \theta_y}{\cos \theta'_y}$

$z' = z - y' \sin\bar{\theta}_y \tan\theta_z$

Fig. 19. Schematic diagram showing the relations among the coordinates of a track as calculated relative to the (x,y,z) system in which measurements were made and the (x',y',z') system which is rotated about the z axis of the (x,y,z) system by the angle $\bar{\theta}_y$. Exactly analogous relations are valid for the rotation about the y axis by $\bar{\theta}_z$.

Allowing that the rotations may have displaced the centroid of the tracks in the target plane, the coordinates in the (x^*, y^*, z^*) system having the x^* axis coincident with the cascade axis are given by:

$$\theta_y^* = \theta_y'' \ ,$$

$$\theta_z^* = \theta_z'' \ ,$$

$$y^* = y'' - \overline{y''} \ ,$$

$$z^* = z'' - \overline{z''} \ .$$

The space angle θ^* which a particle makes with the cascade axis and R^* its lateral displacement from that axis in the target plane were obtained from the projected coordinates according to the following formulas: (See Fig. 8.)

$$\theta^* = \tan^{-1} \left[\tan^2 \theta_y^* + \tan^2 \theta_z^*\right]^{\frac{1}{2}} \ ,$$

$$R^* = \left[y^{*2} + z^{*2}\right]^{\frac{1}{2}} \ .$$

APPENDIX II

Angular Distribution of Cascade Electrons Within Approximation B

The normalized (to unity) number of cascade electrons having angle less than θ with respect to the cascade axis is given by

$$N_o(<\theta) = \int_0^{\theta} P_{\pi_1}(E_o,0,\theta,t)\, 2\pi\theta d\theta \quad , \qquad \text{(A.II.1)}$$

where $P_{\pi_1}(E_o,0,\theta,t)$ is the normalized structure function for the angular distribution of electrons in the three-dimensional cascade theory of Kamata and Nishimura.[40] This distribution which is valid for $E_o \gg \epsilon$ can be obtained by letting $r \to \theta$ in their equation (3.54) and is given by

$$P_{\pi_1}(E_o,0,\theta,t) = [2\pi^2 i\, \Gamma(s) M_1(0,-s,s,t)]^{-1}$$

$$\int_{-i\infty}^{i\infty} dp \left(\frac{\epsilon}{E_s}\right)^2 \left(\frac{\epsilon^2\theta^2}{E_s^2}\right)^{-p-1} \Gamma(p+1)\, \Gamma(s+2p)\, M_1(p,-s-2p,s,t) \quad . \qquad \text{(A.II.2)}$$

---

[40] K. Kamata and J. Nishimura, Suppl. Progr. Theoret. Phys. (Kyoto) 6, 93 (1958).

In approximation B, the shower age parameter s is defined by

$$\ln E_o/\epsilon - \frac{1}{s} + \lambda_1'(s)t = 0 \quad . \qquad \text{(A.11.3)}$$

The integration over θ can be performed for negative values of p to obtain

$$N_o(<\theta) = [\pi i\ \Gamma(s)\ M_1(0,-s,s,t)]^{-1} \int_{-i\infty}^{+i\infty} dp \left(\frac{\epsilon\theta}{E_s}\right)^{-2p} \left(\frac{1}{-2p}\right)$$

$$\Gamma(p+1)\ \Gamma(s+2p)\ M_1(p,-s-2p,s,t) \quad . \qquad \text{(A.11.4)}$$

Using the saddle point method of solution, the integral over p gives

$$N(<\theta) = \frac{\Gamma(\bar{p}+1)\Gamma(s+2\bar{p})}{\Gamma(s)} \left(\frac{\epsilon\theta}{E_s}\right)^{-2\bar{p}} \left(\frac{1}{-\bar{p}}\right) (2\pi u''(\bar{p}))^{-\frac{1}{2}} \frac{M_1(\bar{p},-s-2\bar{p},s,t)}{M_1(0,-s,s,t)}, \qquad \text{(A.11.5)}$$

where $\bar{p}$ is the value of p at the saddle point (i.e., the value of p which maximizes the logarithm of the integrand in Eq. (A.11.4) and is defined by

$$-2 \ln \frac{\epsilon\theta}{E_s} - \frac{1}{\bar{p}} + \psi(\bar{p}+1) + 2\psi(s+2\bar{p}) = 0 \quad . \qquad \text{(A.11.6)}$$

The expression $u''(\bar{p})$ is the second order derivative with respect to p of the logarithm of the integrand in Eq. (A.11.4) and is given by

$$u''(\bar{p}) = \frac{1}{\bar{p}^2} + \psi'(\bar{p}+1) + 4\,\psi'(s+2\bar{p}) \quad . \qquad \text{(A.11.7)}$$

The functions ψ and ψ' are respectively the first and second order logarithmic derivatives of the gamma function and are tabulated in the literature.[41]

For practical application, it is sufficient to write the angular Mellin function as

$$M_1(p,q,s,t) = m_1(p,q,s)e^{\lambda_1(s)t} \quad , \qquad (A.11.9)$$

since $M_1(p,q,s,t)$ is a linear function of $e^{\lambda_1(s)t}$, $e^{\lambda_1(s+1)t}$, . . . $e^{\lambda_2(s)t}$, $e^{\lambda_2(s+1)t}$, . . . and since

$$e^{\lambda_1(s)t} \gg e^{\lambda_2(s)t}, \; e^{\lambda_1(s)t} \gg e^{\lambda_1(s+1)t} \quad . \qquad (A.11.10)$$

Therefore, the recurrence relation for the angular Mellin function given by equation (3.33) of Ref. 40 can be expressed as

$$[\lambda_1^2(s) + \{A(s+2p+q) + \sigma_0\}\lambda_1(s) + A(s+2p+q)\sigma_0 - B(s+2p+q)$$

$$c(s+2p+q)]\, m_1(p,q,s) = (\lambda_1(s)+\sigma_0)$$

$$\{p\, m_1(p-1,q,s) + (s+2p+q)q\, m_1(p,q-1,s)\} \quad , \qquad (A.11.11)$$

with the boundary condition for an electron pair primary being[42]

$$m_1(0,0,s) = \frac{B(s)\, H_1(s)}{\sigma_0} \quad . \qquad (A.11.12)$$

---

[41] Handbook of Mathematical Functions, edited by M. Abramowitz and I. A. Stegun (Dover Publications, Inc., New York, N.Y., 1965) p. 255.

[42] J. M. Kidd, Nuovo Cimento 27, 57 (1963).

The tabulated values[43] of A(s), B(s), C(s), $H_1(s)$, and $\lambda_1(s)$ can be used with this boundary condition to solve the recurrence relation for $m_1(p,q,s)$ for any positive value of p and q. However, $m_1(p,q,s)$ is needed for negative values of p since the values of θ in Eq. (A.II.5) range from 0 to ∞ as $\bar{p}$ goes from $-\frac{\bar{s}}{2}$ to 0. Using the fact that $m_1(p,0,s)$ has a pole at $p = -\frac{s}{2} - 1$ (see Ref. 40), it is possible to obtain $m_1(p,0,s)$ for negative values of p by making an extrapolation to this pole. A consistency check on this extrapolation can be made by using the recurrence relation for $m_1(p,q,s)$ for values of $q \neq 0$. In this manner, it is possible to find $m_1(p,q,s)$ for the needed values of p and q i.e., $m_1(p,q = -s-2p,s)$ can be found for $-\frac{s}{2} < p \leq 0$.

By solving Eq. (A.II.6) for various values of p for fixed values of the shower age parameter s, the normalized number of cascade particles $N_o(<\theta)$ as a function of $\epsilon\theta/E_s$ can be obtained from Eq. (A.II.5) for each value of s. This dependence is plotted in Fig. 20 for a few values of s.

To get the distribution of cascade particles in approximation B, one must determine the correct value of t, for specific values of s and the ratio E_o/ϵ, from Eq. (A.II.3). The normalized number of particles $N_o(<\theta)$ given in Fig. 20 must then be multiplied by the total number of particles at a fixed t and for a fixed ratio of E_o/ϵ which is given by Fig. 5.13.3 in Ref. 43.

---

[43] B. Rossi, High Energy Particles (Prentice-Hall, Inc., Englewood Cliffs, N.J., 1952) p. 296.

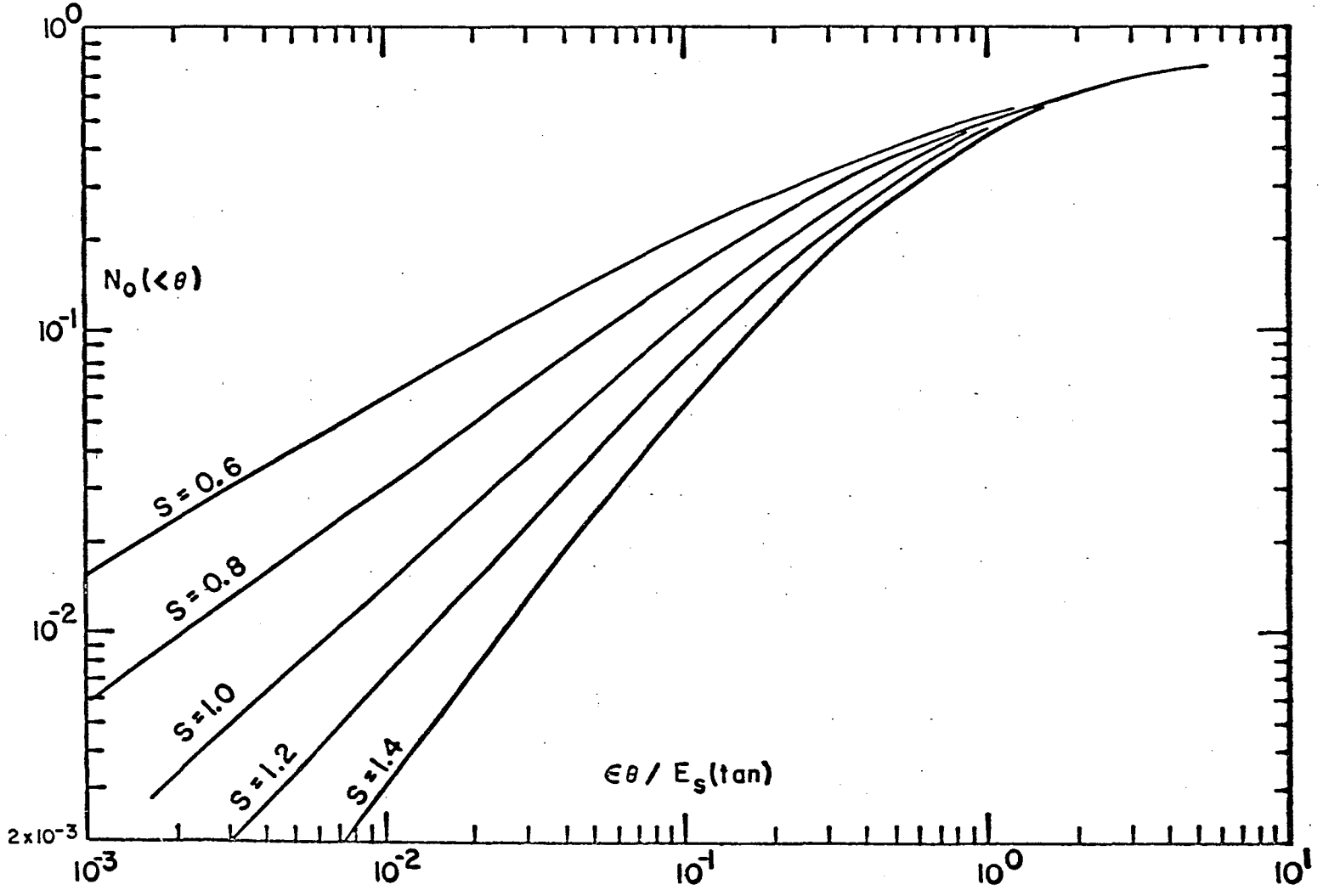

Fig. 20. Normalized integral angular distribution in approximation B. The parameter s is the shower age, ϵ is the critical energy, and E_s = 21 MeV is the scattering energy.

APPENDIX III

Angular Distribution of Cascade Electrons Within the Core Approximation

The expressions to be evaluated in obtaining the angular distribution within the core approximation are obtained by letting $r \rightarrow \theta$ in Eqs. (6.1) and (6.2) of Kamata and Nishimura.[44] These equations are the series solution to the three-dimensional cascade theory without the Landau approximation. The first term in the series represents the spread caused by multiple scattering of electrons when they are traversing matter and in fact is quite similar to the solution derived under the Landau approximation. The second term of the series gives the contribution of single scattering and some of the plural scattering. Thus, this second term gives little contribution to the structure function near the shower axis but is predominant at the tail of the structure function.

Comparison of the experimental angular distributions obtained in this experiment, where measurements have been restricted to high energy cascade particles, show good agreement with numerical calculations considering only the first term of the series.*

---

[44] See Ref. 40, Appendix II.

* See Chap. IV.

This was not true in the case of the radial distribution where it was necessary to include the second term of the series in order to get agreement with experimental data.* The physical explanation for this difference is that one must make measurements to relatively large radii in order to measure all particles even at very small angles.

The total number of particles $N(<\theta)$ which make angles less than θ with respect to the cascade axis for the approximation $\epsilon\theta/k \ll 1$ (core approximation) is expressed by

$$N(<\theta) = \frac{1}{2\pi i}\int_{-i\infty}^{+i\infty} ds \left(\frac{E_0\theta}{k}\right)^s \left(\frac{1}{s}\right)\Gamma(1-s/2)\, m_1(-s/2,0,s)e^{\lambda_1(s)t}, \quad (A.III.1)$$

if only the first term of the series solution is considered. The parameter k is proportional to the scattering parameter E_s, and the other symbols used are the same as those described in Appendix II. This equation can be solved by the saddle point method to give

$$N(<\theta) = [2\pi u''(\bar{s})]^{-1/2} \left(\frac{E_0\theta}{k}\right)^{\bar{s}} \left(\frac{1}{\bar{s}}\right)\Gamma\left(1-\frac{\bar{s}}{2}\right) m_1\left(-\frac{\bar{s}}{2},0,\bar{s}\right)e^{\lambda_1(\bar{s})t}, \quad (A.III.2)$$

where

$$\ln \frac{E_0\theta}{k} - \frac{1}{\bar{s}} - \frac{1}{2}\psi\left(1-\frac{\bar{s}}{2}\right) + \lambda_1'(\bar{s})t = 0, \quad (A.III.3)$$

*See Sec. II.2.

and

$$u''(\bar{s}) = \frac{1}{\bar{s}^2} + \frac{1}{4}\psi'(1-\frac{\bar{s}}{2}) + \lambda_1''(\bar{s})t \quad . \qquad \text{(A.III.4)}$$

The solutions of these equations for an electron pair primary are given in Table IV and in Fig. 21 at a few values of t for k = 19.3 MeV. The details of obtaining the Mellin function $m_1(-s/2,0,s)$ are given in Appendix II.

TABLE IV

Number of Electrons Having Angle Less Than θ

For Electron Pair Primary

$E_o\theta$ (BeV·tan) \ t(r.l.)	4	5	6	7	8	9
5×10^{-1}	5.1	4.0	2.8	-	-	-
1×10^{0}	10.2	9.2	7.2	4.5	-	-
2×10^{0}	19.5	19.2	16.5	13.0	9.4	5.4
5×10^{0}	42	46	44	40	34	23
1×10^{1}	72	85	88	83	73	58
2×10^{1}	130	146	165	169	155	132
5×10^{1}	202	281	360	398	392	370
1×10^{2}	440	439	620	722	762	758
2×10^{2}	-	-	1015	1290	1425	1460
5×10^{2}	-	-	-	2590	3070	3400

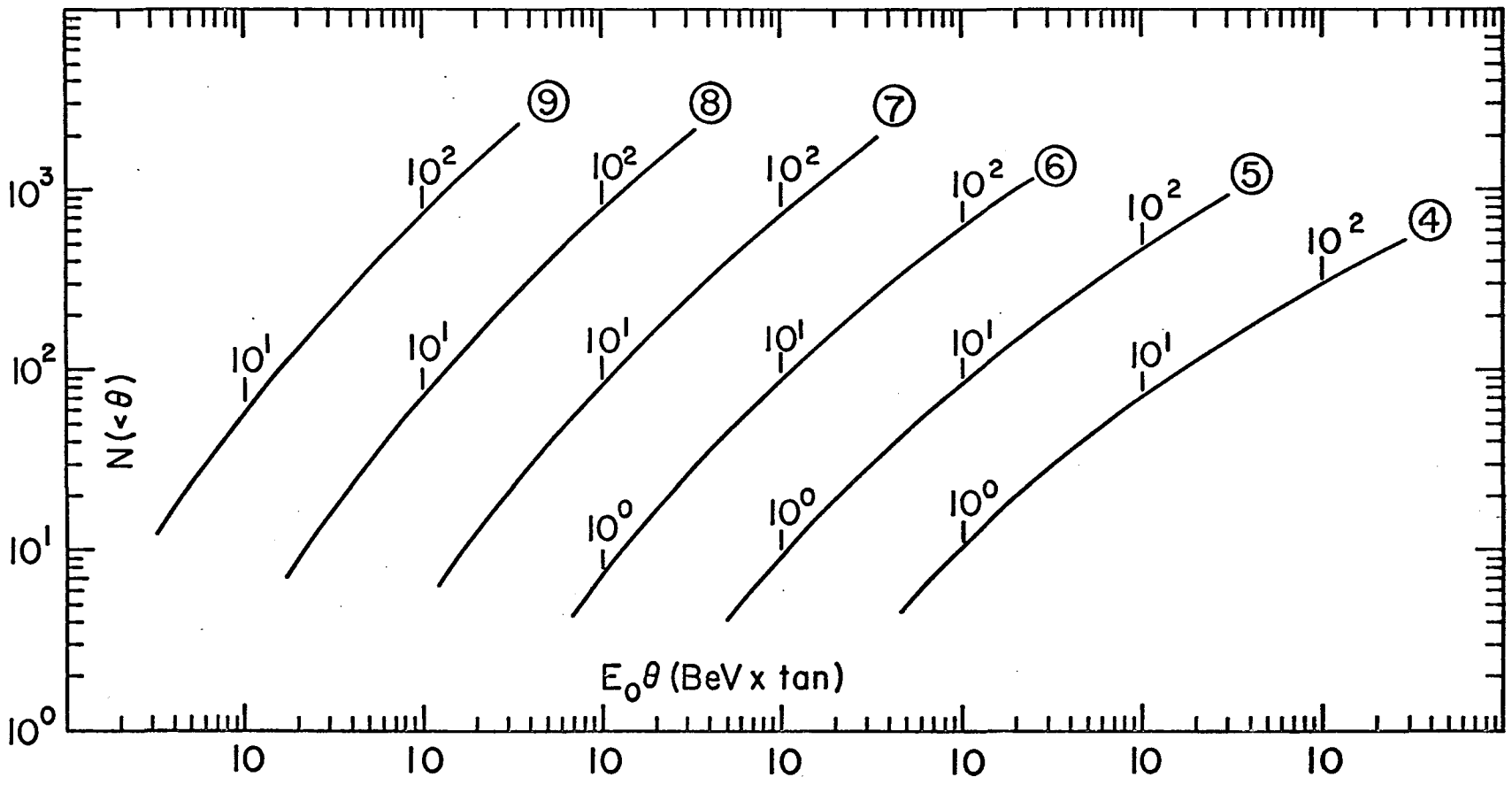

Fig. 21. The angular distribution of cascade electrons $N(<\theta)$ vs $E_o\theta$ within the core approximation. The primary energy E_o is in units of BeV and the angle θ is in units of the tangent. The circles attached to the curves give the distance from the origin in radiation lengths.

VITA

William Vernon Jones was born in Yellville, Arkansas on January 25, 1935. He attended public school in Yellville and was graduated from Yellville-Summit High School in May 1952. He was married to Freda Claudine Daniel in May 1955. After being enrolled in the Evening Division of the University of Tulsa in Tulsa, Oklahoma for four years, he became a full time student at that University in 1961, where he received a Bachelor of Science degree in Engineering Physics in 1963. He enrolled as a graduate student in the Department of Physics and Astronomy at Louisiana State University the same year where he is presently a candidate for the Doctor of Philosophy degree.

EXAMINATION AND THESIS REPORT

Candidate: William Vernon Jones

Major Field: Physics

Title of Thesis: Lateral and Angular Structure of Electromagnetic Cascades

Approved:

Major Professor and Chairman

Dean of the Graduate School

EXAMINING COMMITTEE:

Richard C. Keen

M. H. Salamon

B. B. Townsend

Chong Oh Kim

Date of Examination:

January 10, 1967